**FZR-224**

~~Juni 1998~~

# Archiv-Ex.:

*A. Schaffrath, H.-M. Prasser*

# Theoretical support to the NOKO Experiments

Final report of Workpackage 2 of the
**"BWR Physics and Thermohydraulic
Complementary Action (BWR-CA)"**

# Contents

# List of figures

# List of tables

# 1 Introduction

The safety concept of the new innovative boiling water reactor SWR1000 [BRW-961, BRW-962], which is developed by Siemens AG, is aiming at the increase of safety margins and of the grace period for operator actions during accidents by increasing the water inventory inside the pressure vessel, by the arranging large water pools in- (core flooding pool) and outside of the containment (dryer-separator storage pool), simplifying the (emergency) cooling systems and further decreasing the failure probabilities of safety systems. Therefore, active safety systems are substituted by passive ones or combined with passive safety systems in cases where a replacement is not possible. The function of passive systems is directly based on the physical phenomena: gravity, natural convection and/or evaporation. Their effectiveness is independent of operator actions. Therefore, smaller failure rates are assigned to passive safety systems. The probability of severe accidents of the new SWR1000 is reduced significantly [BRW-962].

Several approaches have been undertaken in a number of European countries to study and demonstrate the feasibility and characteristics of innovative passive safety systems. The European BWR R&D Cluster combines those experimental and analytical efforts that mainly directed to the introduction of passive safety systems into boiling water reactor technology. The main objectives of the EU BWR R&D Cluster are to use the large scale European test facilities NOKO (Jülich, Germany), PANDA, LINX (Villingen, Switzerland), PANTHERS (Piacenza, Italy) as well as the demonstration power plant Dodewaard (Netherlands) for a synergistic experimental R&D program. The project should additionally contribute to validating and improving thermalhydraulic computer codes with regard to natural convection of the coolant and passive decay heat removal both from the core region and from the containment [HIE-96].

In 1997 a *"BWR Physics and Thermohydraulic Complementary Action (BWR-CA)"* was established to further assist and broaden the objectives of the EU BWR R&D Cluster. The partners are: CEA (Commissariat a l'Energie Atomique, France), CIEMAT (Centro de Investigaciones Energeticas, Medioambientables Tecnologicas, Spain), ENEA (Ente per le Nuove Tecnologie l'Energia e'Ambiente, ITALY), FZR

(Forschungszentrum Rossendorf e.V., Germany), Siemens AG (Germany) and TU Delft (Netherlands). The activities are divided into 4 work packages (WP).

The work presented in this report is performed in WP2: *Theoretical support to the NOKO experiments*, where two different decay heat removal systems were investigated. These are isolation condensers (e.g. as operated in Gundremmingen A, Dodewaard or in the PANDA facility) or emergency condensers (e.g. as foreseen on the SWR1000 and tested in the NOKO facility). For the experimental investigation of the operation mode and the effectiveness of these passive safety systems the multipurpose thermohydraulic test facility NOKO was constructed at the Forschungszentrum Jülich (FZJ) within a German collaboration sponsored by the German Federal Ministry of Education, Sciences, Research and Technology (BMBF) and German Utilities (EVU) [SCA-961]. The facility has a maximum power of 4 MW for steam production and a maximum operating pressure of 10 MPa.

The work which was performed by FZR within the BWR-CA is divided into three tasks: Implementation of two phase flow instrumentation, ATHLET calculations of NOKO experiments and approach for the optimization of passive components.

Chapter two contains a description of the two phase flow measurement instrumentation developed by FZR in general and especially of the instrumentation of the single emergency condenser tube, which is installed in parallel to the emergency condenser test bundle. The experimental data should be used for the validation of the improved ATHLET condensation model. Because the evaluation of these experiments shows an undesired accumulation of non-condensable gases in front of the water level, some of the goals of the single tube measurements can't be met. Therefore there is a need for further single tube experiments with an improved instrumentation. On the other hand the results give valuable insights to the phenomena caused by non-condensables. In the second part of chapter two an improved two-phase flow instrumentation is suggested based on the collected experience and taking into account the detected problems.

In chapter three ATHLET calculations of NOKO experiments are presented. Within the BWR-CA FZR had performed 10 post test calculations and an additional blind test calculation of NOKO experiments. The tests were selected by FZJ. The results of

these calculations are presented and discussed. Basis of the comparison between computational and experimental data is the evaluation and the uncertainty analysis of the NOKO experiments, which were performed by FZR with the computer code CASH-(Computergestützte Auswertung und Unsicherheitsanalyse von NOKO Experimenten) Graphics.

The fourth chapter deals with the optimization of the emergency condenser. This is desirable because this allows to decrease of the pressurized BWR surface and the possibility of leakages. An ATHLET calculation is performed for an optimized emergency condenser tube of a new material (Remanit). A detailed discussion of the thermal hydraulic yield proves the advantages for the suggested design.

At least in chapter five the main results of the theoretical support to the NOKO experiments are summarized.

# 2 Implementation of two phase flow instrumentation

The second chapter is divided into four topics. The first one describes selected two phase flow instrumentation (needle probes, wire mesh sensors, conductivity tomography) in general. Then an overview on the special two-phase instrumentation (needle probes), which was installed in a single heat exchanger tube at the NOKO test facility in Jülich, is given. This instrumentation consists of needle probe arrays and thermocouples. The third topic of chapter two describes the performed single tube experiments, which were aimed at the clarification of flow regimes occurring inside the NOKO tubes during the start-up and steady state operation. The results of these experiments were presented and discussed in detail. At least, the fourth part of chapter two contains a proposal for an improved two phase flow instrumentation and is based on the experience of the performed tests.

## 2.1 Description of two phase flow instrumentation

Afterwards an overview on special two-phase flow instrumentation for the study of passive safety systems developed or being under development by Forschungszentrum Rossendorf (FZR) e.V. is given. The methods are based on conductivity measurement techniques. FZR has great experience in applying needle shaped conductivity probes to thermal hydraulic experiments concerning the safety of nuclear reactors. These probes were used and are in use in numerous integral and separate test facilities, such as PMK-II [REN-96], ISB [GAM-95, PRP-95], PKL [WEP-94], PHDR (contact condensation experiments) [PRM-92], UPTF (pressurizer tests), Bubble Condenser Test Facility in Bechovice, NOKO test facility Jülich (see chapter 2.2) and other [PRM-951, PRM-952, PRM-953, LUD-96, PRM-96].

After the description of the physical basis, which is the different electrical conductivity of gas and water, needle probes and wire mesh sensors are described in detail. This is done by taking into account different goals such as determination of flow regimes or velocity measurements. At least few ideas concerning conductivity tomography are discussed.

## 2.1.1  Physical basis

Gas and liquid have very different electrical conductivities. In the range of thermodynamic parameters interesting for nuclear safety research, the conductivity of the gas phase is neglectible (independently on the composition, i.e. steam plus non-condensables, such as nitrogen, radiolysis gases) while the water disposes of a significant conductivity. The conductivity of the water depends on the concentration of impurities (e.g. corrosion products) and of additives (in case of PWR boron acid). It also strongly increases with growing temperature. The conductivity of very pure water at room temperature is about 0.05 $\mu$S/cm, a value that does not appear in practice. The best quality water produced by technical purifying systems has about 0.5 $\mu$S/cm. At reactor temperature, the conductivity is approximately 20-50 times higher.

The different conductivity of gas or steam on the one hand and water on the other is used to detect the local appearance of gas particles inside the liquid flow. All sensors described below have in common, that the conductivity is measured in control volumes of different size, and the result is interpreted as an instantaneous volumetric void fraction inside the control volume.

## 2.1.2  Needle shaped conductivity probes for local void detection

The description of the needle probes includes a general overview with several technical background and several details. Afterwards the arrangement of several needle probes in a cross section area for the determination of flow patterns and in a double wire design for velocity measurements follows.

### 2.1.2.1   Single wire probes

The probes consist of a needle shaped metallic electrode that is surrounded by an insulation tube of low diameter (Fig. 2.1). The material used for the electrical insulation is sintered $Al_2O_3$. It has proved to be satisfactorily stable in water of reactor parameters. For protection and mounting, the arrangement of electrode and insulation tube is placed into a bearing tube of stainless austenitic steel. The sealing is located at the cold end of the probe, which is outside the test facility the probe is mounted on.
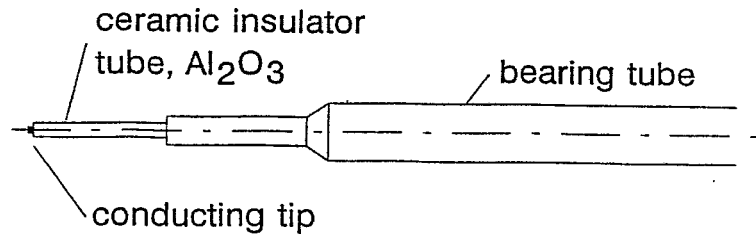
**Fig. 2.1:** Scheme of a needle shaped conductivity probe (single wire probe) for local void fraction measurements.

The electrode is electrical accessible from outside, while it is in contact with the fluid at the tip of the probe. It is supplied with a small alternating voltage that causes an electrical current flowing from the tip of the probe via the fluid towards the grounded bearing tube or the wall of the test facility. This current is analysed by a signal acquisition unit. The current is being interrupted when a gas particle is covering the sensitive tip of the probe. Bubbles moving on a certain distance from the probe do not influence the signal significantly, as long as the liquid phase represents a continuum.



$$alpha = \frac{\sum T_c}{T_{meas}}$$
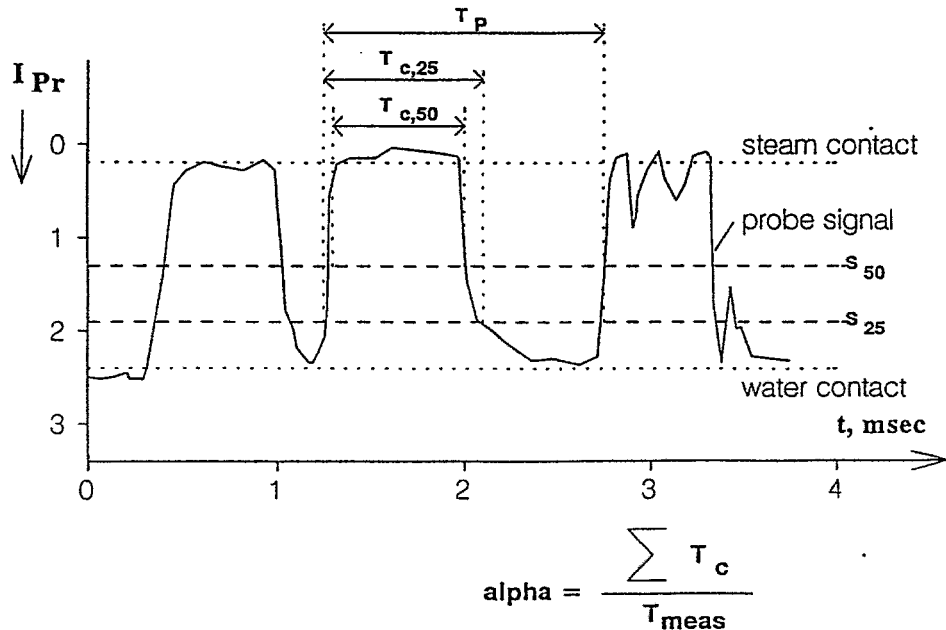
**Fig. 2.2:** Probe signal and determination of contact periods, calculation of the local void fraction.

The current is transformed into a voltage signal (Fig. 2.2) and led to an analogue-digital converter (ADC), connected to a microcomputer inside the signal acquisition unit. The typical sampling frequency is in the range of 4-16 kHz. The digital signal is compared to a discriminating level ($S_{25}$ or $S_{50}$) In the result, a binary information is obtained that characterizes the instantaneous phase state at the tip of the probe (0 - liquid, 1 - gas or steam). By counting the number of samples that indicate gas belonging to one gas particle, the so-called contact time $\Delta t_C$ is acquired (Fig. 2.2). It is defined as the time of presence of the detected gas particle. The contact periods are summed up over a certain measuring period. The result, related to the measuring period, is interpreted as the probability to meet gas/steam at the tip of the probe, and is assumed to be equal to the local instantaneous void fraction $\alpha$ averaged over the measuring period:

$$\alpha = \frac{\sum \Delta t_c}{t_{meas}}$$

Additionally, the number of phase changes per unit time is recorded. For more detailed analyses, it is possible to obtain probability density distributions of the contact periods and the periods between the appearance of gas particles. It is also possible to record the raw signal of the probes. The evaluation procedure can be easily adapted to different evaluation methods. The discrimination level is automatically adapted to the instantaneous level of the liquid conductivity. This is also performed by the software of the microcomputers inside the modules.

In the present, probes for high pressure and temperature are available as follows:

| | |
|---|---|
| pressure: | max. 25 MPa |
| temperature: | max. 350 °C (saturation at 25 MPa) |
| diameter of the sensitive tip: | down to 0.5 mm |
| diameter of the bearing tube: | down to 3 mm |
| length: | max. 400-500 mm |
| required conductivity of liquid: | min. 0.5 μS/cm [1] |

[1] the pre-amplifiers can be adjusted to lower conductivity by special measures

High pressure probes have to be strait ones. They cannot be bended and must be can be hermetically connected to metallic cable. This was done in case of the application of probes to the NOKO facility. The probes were mounted to one of the NOKO tubes, and the connecting cable was laid through the secondary side (pressure up to 1 MPa, temperature 180 °C).

The following signal acquisition systems are available:

*System A with 8-bit microcomputers* (s. Fig. 2.3)

| | |
|---|---|
| channels per unit: | 2 |
| sampling rate per channel: | 3.84 kHz |
| microcomputer: | zilog Z8, 4 MHz |
| memory: | 1 kByte ROM, 128 Byte RAM |
| probe supply voltage: | 3V /3.84 kHz AG (square wave) |
| pre-amplifiers: | digitally controlled, 9 ampl. ranges (steps of 6 dB) |
| ADC (2 units): | 10 bit (8 bit used) |
| output: | RS232c (20 mA current loop, optically coupled insulators) |
| interface performance: | 57.6 kBaud |
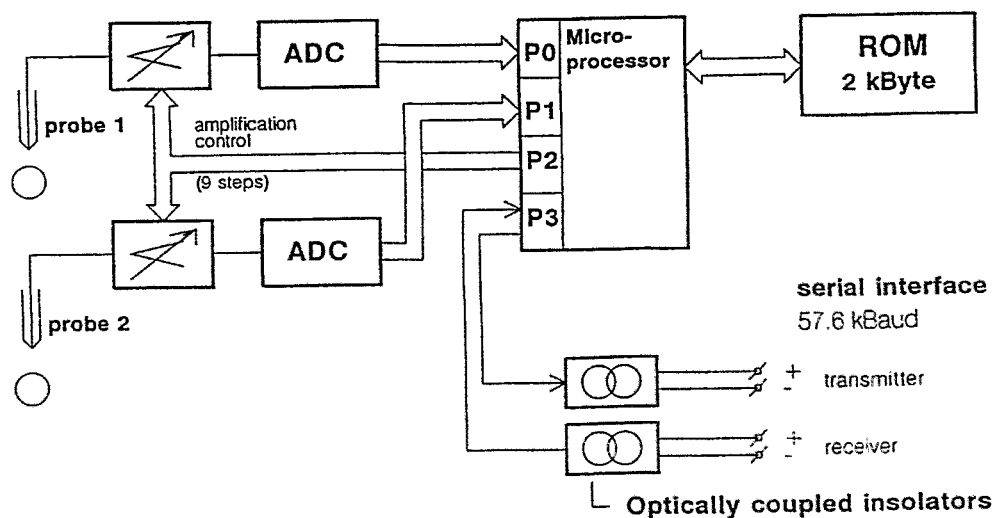


Fig. 2.3: Block scheme of the signal acquisition module type A (8 bit microcontroller).

| | |
|---|---|
| results: | void fraction, gas particle frequency |
| measuring period: | 1 - 5 s (usual value 1 s) |
| Aluminium casing: | 180 x 150 x 100 mm, splash protected |
| power supply: | 220 V AC |
| data acquisition: | IBM-PC (min. AT 286) |

The units can be cascaded up to 8. The resulting system has 16 channels (Fig. 2.4).

**probe inputs (1-16) :**
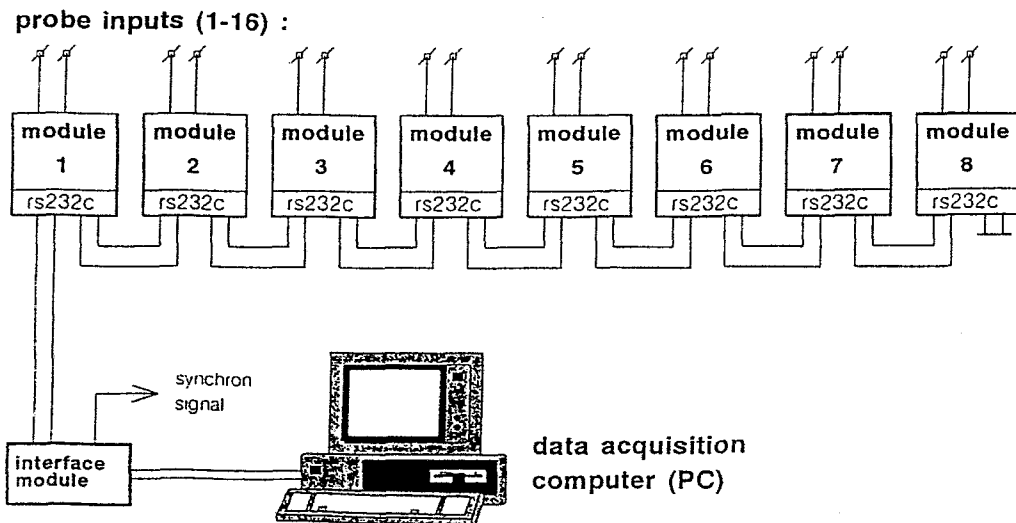


**Fig. 2.4:** Cascade of signal acquisition units (Type A)

*System B with 16-bit microcomputers*

| | |
|---|---|
| channels per unit: | 1-4 |
| sampling rate per channel: | 4.096 (4 channels) /16.384 kHz (1 channel) |
| microcomputer: | motorola 68340, 25 MHz |
| memory probe supply voltage: | 5 V AG (square wave) |
| pre-amplifiers: | logarithmic |
| ADC: | 12 bit |
| output: | RS232c (20 mA current coupled insulators) |
| interface performance: | up to 115.2 kBaud |

| | |
|---|---|
| results: | void fraction, gas particle frequency, raw probe signal, individual gas particle characterization, probability density distributions a.s.o.[1] |
| measuring period: | variable |
| Aluminium casing: | 260 x 225 x 130 mm, splash protected |
| power supply: | 220 V AG |
| data acquisition: | IBM-PC (min. AT 486 /66 MHz) |

1) The software of the units can be easily adapted to special measurement tasks.

The units can be cascaded in the same manner as the 8-bit ones.

Beside the void fraction measurement the detection of the interface surface can be carried out. The thickness of liquid films, for example, can be supervised. For this purpose the tip of the probe has to be allocated at the required distance from the wall of the tube. A measurement of film thickness would require a movable probe. This is possible in principle, but technically not yet solved.

### 2.1.2.2    Arrays of needle probes

Needle shaped conductivity probes can be complected to sensor arrays. This was done in experiments on a special single heat exchanger tube at the NOKO facility. The probe assembly is displayed in Fig. 2.5. Seven probes were allocated in a hexagonal grid, so that the cross section is almost covered by equally distributed probes. The grid was rotated by an angle of 19.1 deg. In this way an equal distribution of sensitive points over the height was achieved, too. This construction was chosen, because the equal distribution over the cross section allows to observe and distinguish the flow patterns stratified flow, wavy stratified flow, bubble flow and slug flow. In case of a stratified flow, the vertical graduation of about 5-6 mm allows to measure the height of the liquid layer.
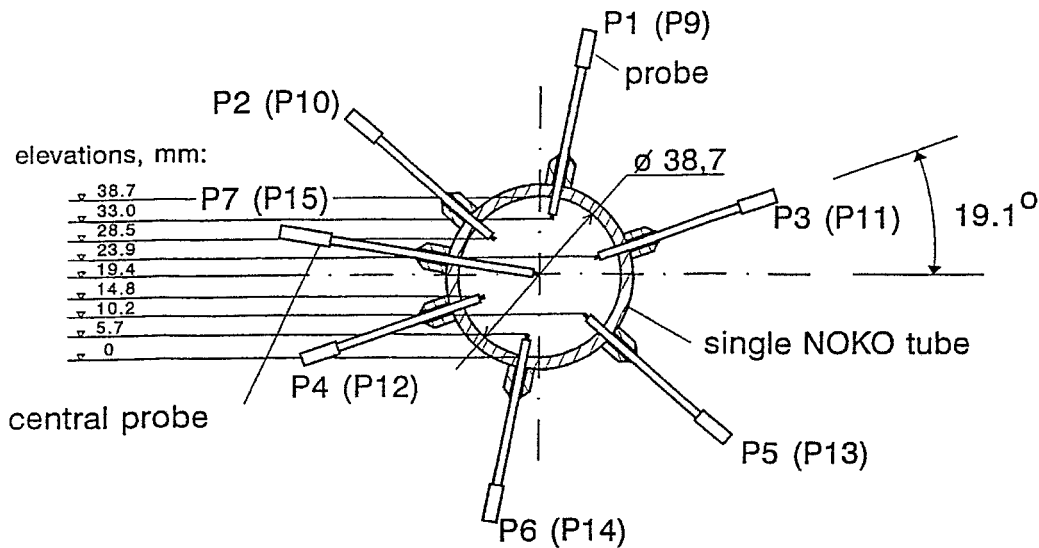
**Fig. 2.5:** Probe array used in the single tube of the NOKO test facility in Jülich. The probe number 1 – 8 are arranged in the upper probe assembly, the probe numbers 9 – 15 in the lower probe assembly.

Probe arrays were mounted into the upper and the lower leg of the single NOKO tube. As an example of the capability of such a probe array, Fig. 2.6 presents a plot of the probe signals during the level decrease when NOKO starts to operate. The signals are represented by horizontal bars. A black bar means that water is at the probe position instantaneously. The bars are stacked in the same order as the probes are distributed over the height. In all experiments it was found that the flow pattern during the level drop is wavy stratified. Neither slugs nor bubble flow were observed. More detailed results are presented in chapter 2.3.

## 2.1.2.3 Double wire probes for velocity measurements

Needle probes for high pressure and temperature are also available in double wire design. A special ceramics tube with two orifices is applied. The tip of the probe has an oval cross section (Fig. 2.7). When the probe is placed into the flow in a direction perpendicular to the flow direction, the velocity of gas particles can be estimated. The gas particle interrupts the current of the electrodes successively. The distance divided by the time-of-flight equals the velocity.
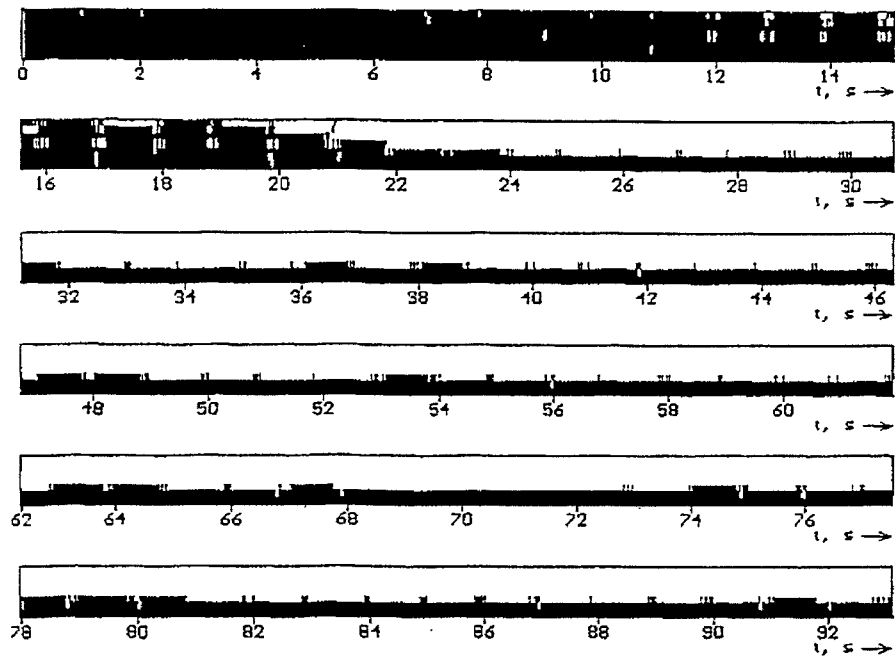
**Fig. 2.6:** Passing of the liquid level during start of operation of NOKO in the lower leg of the single tube.
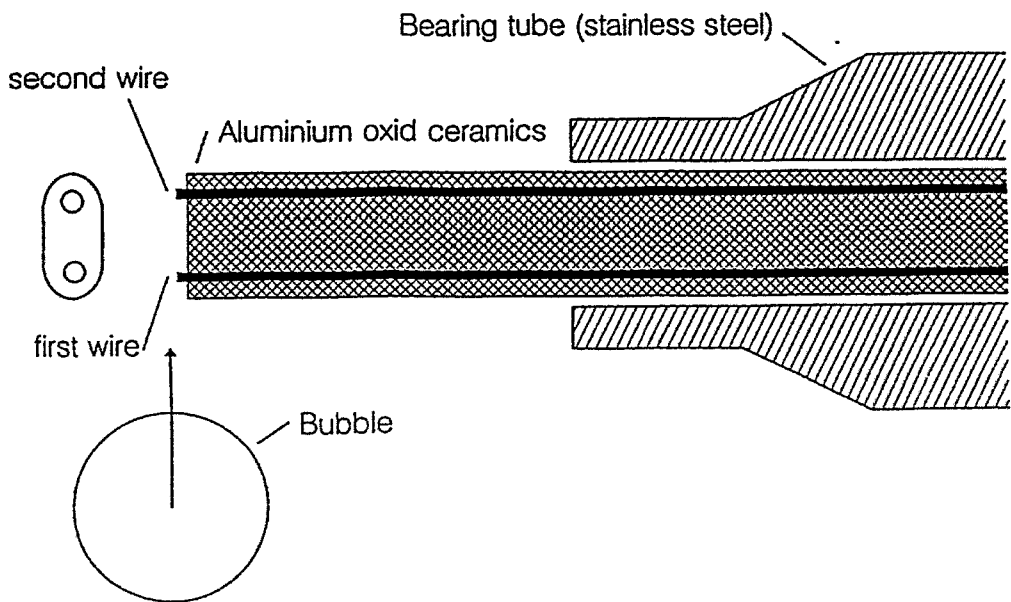


**Fig. 2.7:** Scheme of a double wire probe for bubble velocity measurements

The dimensions of the probe were chosen as a compromise between stability in pressurized water and time respond. The distance between the two wires of the

probe in Fig. 2.7 is 50.8 mm. In this case, the accuracy of the velocity measurement is about 10 % at a velocity of 1 m/s, if a sampling rate of 8 kHz is applied. This does not take into account the influence of the probe on the bubble. The bubble will obviously be braked down, so that it has to be expected that the probe underestimates the bubble velocity. The error is increasing with growing velocity. Nevertheless this kind of probe was successfully used for indicating the flow direction and estimating the velocity.

The signal acquisition systems presented in chapter 2.1.2.1 are prepared for the application of double wire probes. This was already done at PMK-II, PKL and some separate test facilities.

In certain applications two single wire probes placed one after the other in the direction of the flow were used for the velocity measurement (Fig. 2.8). Depending on the distance, the direct time-of-flight method or a cross-correlation technique has to be used.
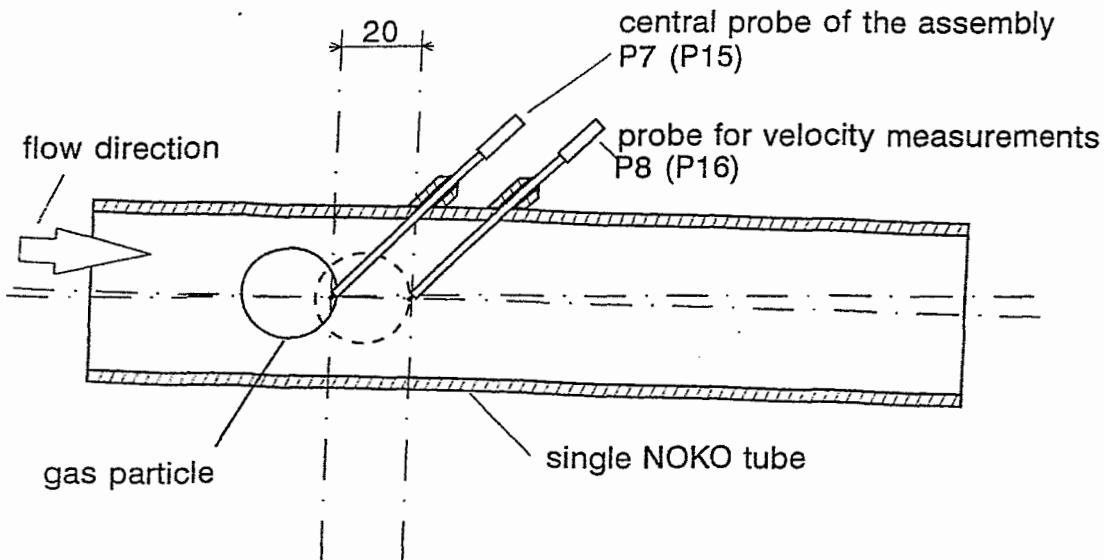


**Fig. 2.8:** Use of two single wire probes for the purpose of bubble velocity measurements (probe array for the single NOKO tube).

## 2.1.3 Wire-mesh sensors

A wire-mesh tomograph for gas-liquid two-phase flows is presented. It is based on the measurement of the conductivity distribution over the cross section of the flow.

Two planes of wire grids are placed into the flow in a short distance from each other. The angle between the wires of both grids is 90°. The conductivity is measured at all cross points of the wires of the two planes An imaging rate of 1000 frames per second was achieved, the measured data is directly transformed into local volumetric gas fractions without image reconstruction efforts.

The starting point was an existing wire mesh system published in [REN-96]. The device consists of three planes of 29 thin wires each (diameter 0.1 mm). The wires of the different planes are forming an angle of 60°. By measuring the impedance between all pairs of adjacent wires belonging to one and the same plane, a projection of the conductivity distribution along the direction of the wires is recorded. The impedance measurement is carried out with alternating current of high frequency (1 MHz). This operation is performed for all three planes. In the result, three independent projections are obtained, which are afterwards transformed into the conductivity distribution within the cross section the sensor is allocated in. The distribution is interpreted as the void fraction distribution. The system disposes of a imaging rate of about 112 frames per second. The spatial resolution of the images equals the distance between two adjacent wires. Related to the cross section, this means 1000 pixels.

The transformation into the image has to be performed by applying tomographic image reconstruction algorithms. The conductivity measurement provides a total of 3 x (29-1) = 84 linearly independent values of average conductivity along the projecting lines. In the same time, images of the mentioned 1000 pixels are reconstructed. The system of equations to be solved for the image reconstruction is therefore highly underdetermined. The solution is stabilized by additional a-priory knowledge, for example: the local conductivity must be in the interval between the conductivities of the gas and the liquid. Nevertheless, the image reconstruction cannot apriorily taken for free of artefacts. Another disadvantage is the necessity of high numerical efforts for the iterative reproduction algorithm. The presented work aimed at the increase of the time resolution, the decrease of numerical efforts, and a simplification of the sensor. It was sought for a method that excludes the potential appearance of artefacts.

The main idea of the FZR sensor development was to measure the impedance not between adjacent parallel wires but between crossing wires of two adjacent planes. In this case, the number of wire-mesh planes can be reduced to two, which prefer-

ably include an angle of 90°. The conductivity distribution is then been obtained by a successive polling procedure. One plane of wires is used as transmitter, the other as receiver plane. Each wire of the transmitter plane is supplied with a measuring voltage for a short period. In the same time, the electrical current arriving at the wires of the second plane is measured. In this way, the conductivity distribution is obtained row by row. After the last transmitter wire was activated, a two-dimensional matrix of values of current is competed that reflects the conductivities between all crossing points of the wires of the two perpendicular planes.

Two types of sensors have been developed: the first sensor consists of two planes of wire grids with 16 wires of a diameter 0.15 mm each. The wires are equally distributed over the diameter. The distance between the two planes is 1.5 mm. In total the sensor disposes of 16 x 16 = 256 cross points.

Due to the limited mechanical stability of the thin wires a second type of sensor was developed. It is built of metallic rods of stainless steel instead of the wires. The rods have lentil shaped cross sections to avoid high hydraulic resistance (Fig. 2.9). This sensor can be applied in situations where large mechanical loads have to be expected. It was constructed in two versions: with 8 (8 x 8 = 64 cross points) and with 16 (256 cross points) electrodes in each plane. The sensors will be applied for investigations of shock waves in two-phase flows. The recent specimens were built for pipes of 50 and 100 mm inner diameter. The maximum fluid pressure is 7 MPa at a temperature up to 80° C.
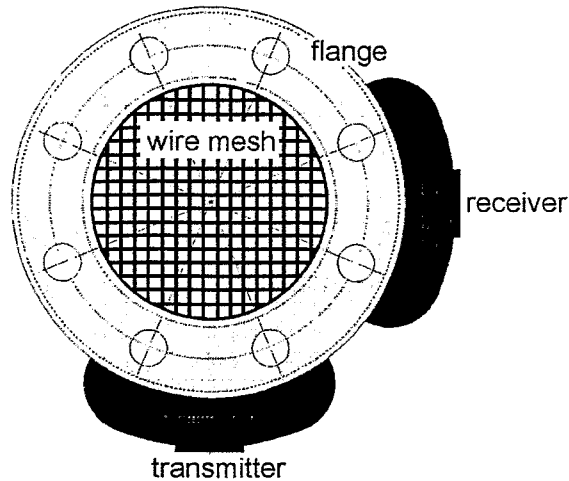
**Fig. 2.9:** Mesh sensor with lentil shaped electrodes for applications with high mechanical loads.

The data acquisition unit consists of four microcontrollers with motorola 68340 disposing of 1 MByte RAM and 25 MHz clock rate. Each microcomputer is equipped with a four channel ADC of 12 bit resolution. One of the microcomputers controls the transmitter driver. The maximum imaging speed of 1 kHz requires a total sampling rate of 256 kHz, which is achieved by the transverting time of 10 μs of the applied four ADC. The data acquisition unit is connected to a PC for storing and visualizing of the data.

Two working modes are available: direct mode (on-line) and storing mode (off-line). The high imaging rate of 1 kHz is achieved in storing mode. The capacity of the RAM allows to capture a sequence of a bit less than 8 s. This can be increased by compressing the data. In this case, the imaging rate is lower due to the numeric efforts for compressing.

In on-line mode 20 samples of images (taken at 385 Hz) are averaged and displayed immediately after capturing. The number of images per second is additionally limited by the capacity of the interface between the data acquisition unit and the PC. A rate of 8 images per second was achieved, applying an RS232c interface of 38.4 kBaud and an IBM AT 486 PC. The pre-amplifiers are digitally controlled. The amplification can be changed in steps of 1:2. It is adjusted to the conductivity of the liquid during calibration.

The physical capabilities are not yet expired. It is possible to reach about 10000 images per second, if flash ADC and direct coupling with the computer bus system is applied. This is under development. The spatial resolution can also potentially be increased by adding wires.

The raw data is obtained as a matrix of AD conversion results for each image. In case of a 12 bit ADC, these are integer numbers between 0 and 4095. The matrix has the dimensions of 16 x 16 elements, if the 2 x 16 wire sensor is applied, i.e. 256 linearly independent values are recorded. Each component $u_{i,j}$ characterizes the conductivity in the vicinity of the related cross point of transmitting wire i and receiving wire j. During a calibration procedure, measurements for the situations ,,tube completely filled with liquid" and ,,tube completely filled with gas" are performed and the resulting matrices $u_l$ and $u_g$ are stored. The matrices acquired during the measuring of the two-phase flow are transformed into void fraction distributions by relating the individual measured components to the calibration values:

$$\alpha_{i,j} = 1 - \frac{u_{ij} - u_{g,ij}}{u_{l,ij} - u_{g,ij}}$$
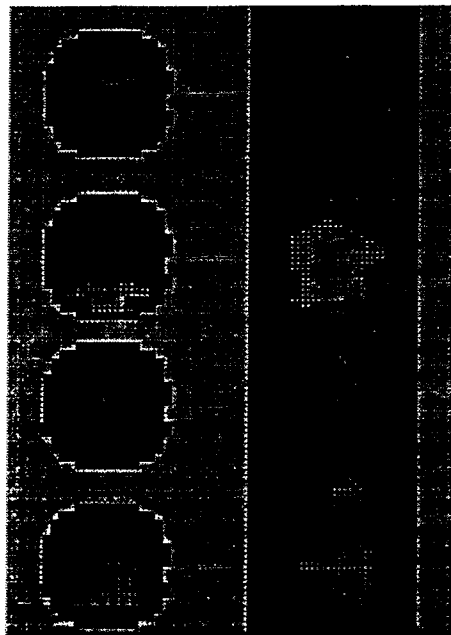


**Fig. 2.10:** Application of the wire-mesh sensor to a bubble flow in an air-water column (left side phase distribution in several cross section areas, right side reconstructed side view).

The sensors were tested in air-water flow (Fig. 2.10). Both types of sensors are available for experimental investigations at low temperatures (up to 80° C). A sensor for high pressure and temperature (nuclear reactor conditions, 16 MPa / 350° C) is under development.

## 2.1.4. Conductivity tomography

It is planned to use the data acquisition unit of the wire mesh tomograph for driving a tomographic sensor with electrodes at the inner wall of the pipe. For this purpose, it is not necessary to change or adapt neither the electronic circuitry nor the software. A scheme of such a sensor is given in Fig. 2.11.



parallel
sampling
by ADC

Voltage supply
1 of 16 electrodes)
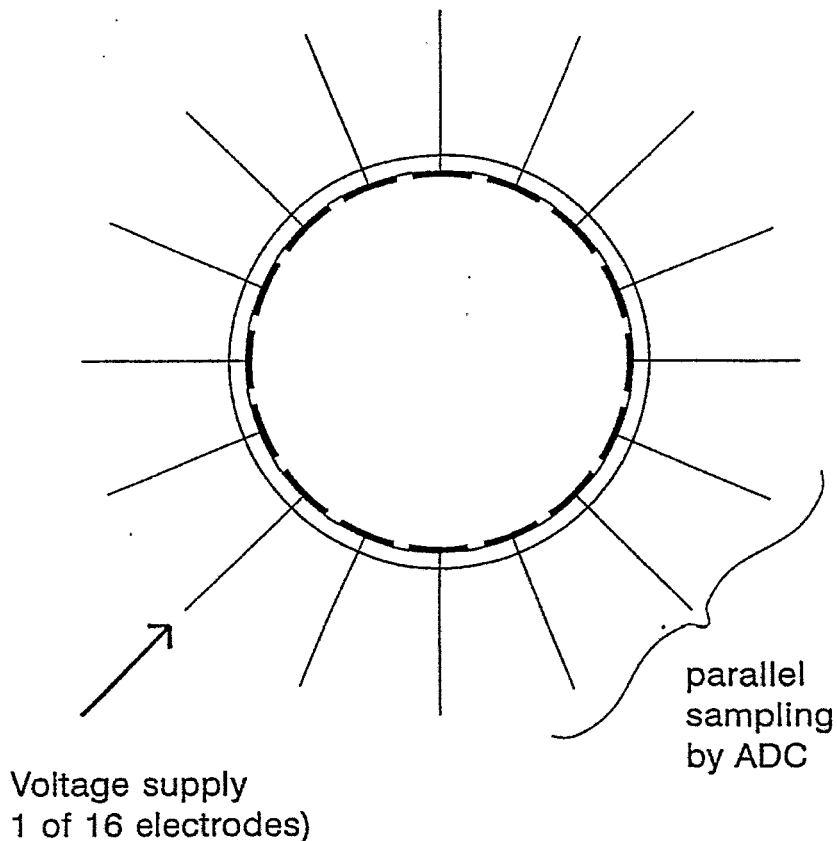
Fig. 2.11: Working principle of a conductivity tomography system.

The resistance between all independent combinations of electrodes is measured. The conversion into a void fraction distribution inside the measuring volume has to be performed by applying image reconstruction algorithms typical for tomography. The method was not yet tested in FZR.

## 2.2    Investigation of two phase flow patterns

The investigation of the flow patterns were carried out in the frame of a project for code validation and code improvement sponsored by BMBF. The instrumentation consists of needle probes and thermocouples. The signals of the needle probes indicate the moment of the appearance of the water level at the probe location very accurately. The comparison of the signals of the probe arrays allow to distinguish between steam or non-condensable gas. As shown, this comparison will hint at the presence of non-condensable gases.

### 2.2.1    Needle shaped conductivity probes

The detailed description of needle probes is given in [PRM-96]. Therefore in this report the interest is focussed in the arrangement of probes for the measuring task. The probes were arranged to sensor arrays, which were installed into the single tube of the NOKO facility. The probe assembly is displayed in Fig. 2.5. Seven probes were allocated in a hexagonal grid, so that the cross section is almost covered by equally distributed probes. The grid was rotated by an angle of 19.1 degree. In this way an equal distribution of sensitive points over the height was achieved, too.

This construction was chosen, because the equal distribution over the height allows to observe and distinguish the flow patterns stratified flow, wavy stratified flow, bubble flow and slug flow. In case of a stratified flow, the vertical graduation of about 5-6 mm allows to measure the thickness of the flume.

An additional probe was placed at the central position in a distance of 20 mm behind the central probe of the probe assembly (Fig. 2.8). This probe was aimed at a velocity measurement. The number of events of gas particles that caused correlating signals at the two probes was very low, and for that matter, an evaluation of the velocity data was not performed.

Probe arrays were mounted into the upper and the lower leg of the single NOKO tube. The axial position was in both cases in the middle of the overall length of the upper and lower legs (Fig. 2.12). The single tube had the dimensions of the smallest (inner) tube of the NOKO bundle.
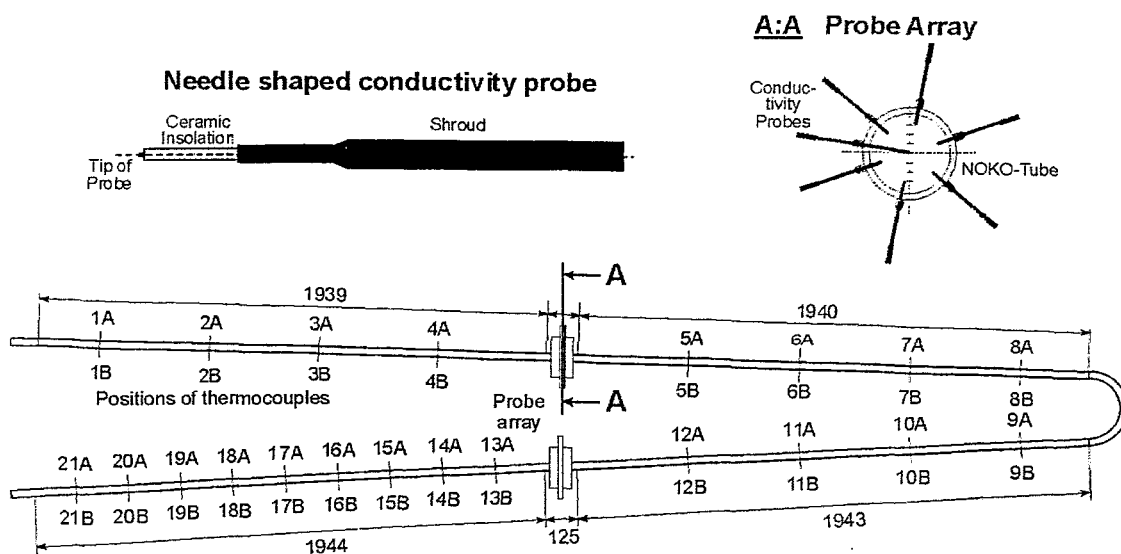
**Fig. 2.12:** Single NOKO tube with thermocouples and probe assemblies.

The probes were constructed and manufactured by FZR. A special solution was developed that allowed to operate the probes inside the NOKO tank. The data acquisition was done by a 16 channel computerized signal acquisition unit. The sampling rate was 4096 Hz for each probe, i.e. the appearance of steam-water or water-steam changes is recorded with an accuracy of 0.25 ms. The measured information was stored in a PC on hard disc.

## 2.2.2 Thermocouples

The single tube was equipped with thermocouples (see Fig. 2.12). They were introduced into the tube, both from the top and the bottom. The sensitive tip of the thermocouples was allocated in a distance of 6 mm from the inner wall of the tube, i.e. the fluid temperature was measured. During the experiments, 28 thermocouples were operated. The allocation of the thermocouples and the needle probe assemblies is shown in Fig. 2.12. The thermocouples were provided and mounted by FZJ.

## 2.3 Results

Afterwards the results of the measurements of the needle probes and the thermocouples are presented and compared, discussed and assessed.

## 2.3.1  Flow patterns in the single NOKO tube

Measurements with the needle probes were performed at the primary pressure levels of 1, 3, 5 and 7 MPa. The secondary side was on atmospheric pressure. It was planned to setup a constant drainage from the reactor vessel in order to decrease the level slowly by 2-3 cm/min. This was not achieved. In most of the cases, the level decreased faster, and occasionally, additional actions with the drainage valve were necessary. In the result, the level decrease was not uniform in time and not identical in the individual tests.

When the level in the single NOKO tube arrived at the positions of the probe assembly, the probes successively changed from water to steam. At the upper probe assembly, the level has shown to be almost calm and well stratified. The probes change to steam within a few seconds (Fig. 2.13). In none of the experiments slugs or similar phenomena were found. The time delay between the individual probes corresponds to the velocity of the level decrease calculated from the pressure drop over the primary side. The level can be considered as a horizontal water surface inside the inclined tube.

After the level passage, the lower probes of the assembly remain in water. This indicates the condensate layer at the bottom of the tube. Probe 1, which was located at a very low depth (by mounting problems) indicated the water film, when annular flow was established. The level passage at the lower probe assembly is characterized by more events of phase changes. The transition from water to steam lasts much longer, than at the upper assembly (Fig. 2.14). When looking at the probe signals in more detail, it can be observed that the water surface is more wavy and excited (Fig. 2.15). This is due to the larger amount of condensate flow and the fluctuations of the pressure drop caused by the higher power level.
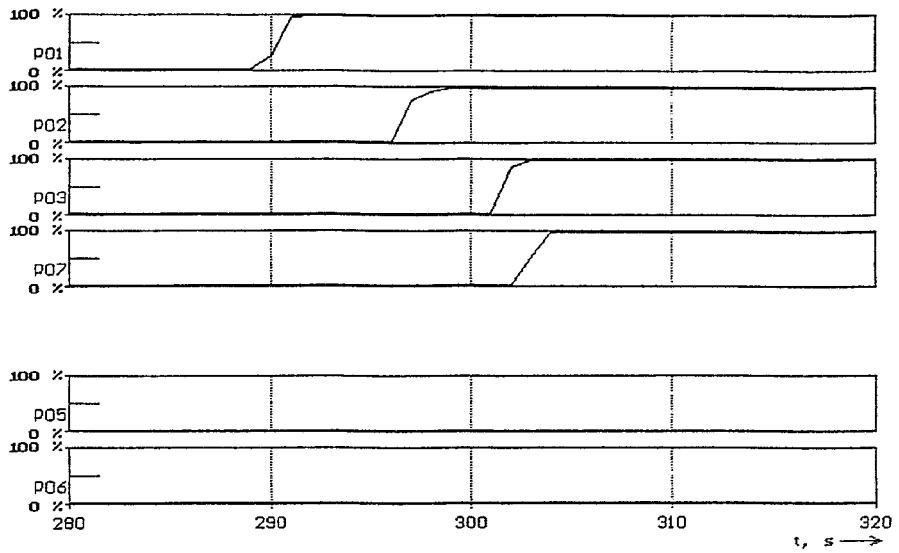
**Fig. 2.13:** Passage of the water level through the upper probe assembly (test E3). The local void fractions are plotted versus time. The pressure inside the tubes is 5 MPa, the pressure in the condenser 0.1 MPa. The water level in the pressure vessel is decreased approximately by 1.1 mm/s.
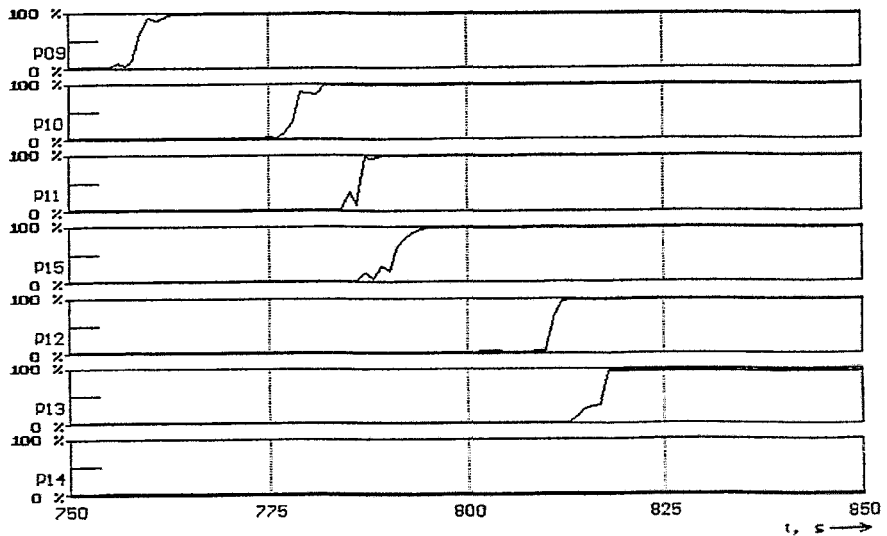


**Fig. 2.14:** Passage of the water level through the lower probe assembly (test E3). The local void fractions are plotted versus time. The pressure inside the tubes is 5 MPa, the pressure in the condenser 0.1 MPa. The water level in the pressure vessel is decreased approximately by 0.9 mm/s.
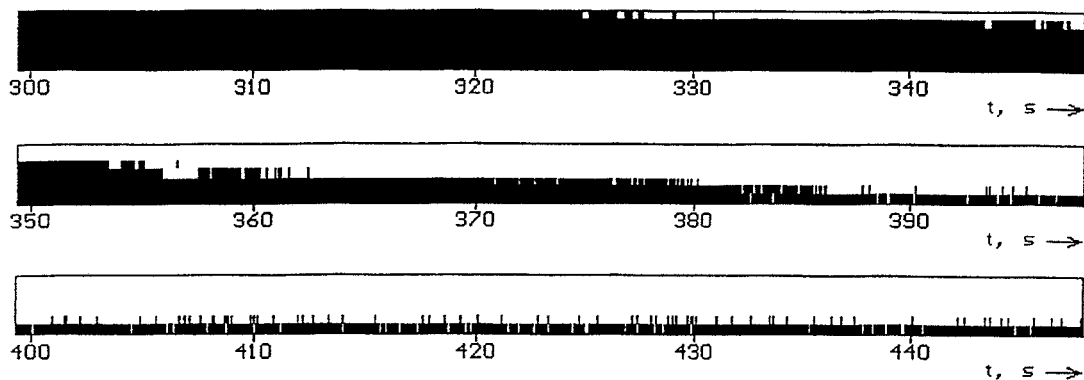
**Fig. 2.15:** Plot of the probe signals during the water level passage through the lower probe assembly. The black bars represent time intervals, when water is present at the individual probes. The probes plotted are from top to bottom: P9, P10, P11, P15, P12, P13, P14, i.e. the probes are plotted in their geometric order. In this plot t = 0 s corresponds to t = 432 s in Fig. 2.5.

In two experiments, gas bubbles were indicated by the upper probe (P9) of the lower array, a long time before the water level arrived at the probe location (Fig. 2.16). They were interpreted as bubbles of non-condensable gases, dragged by the water flow down the inclined tube. The presence of non-condensables is caused by the feed water supply system of the NOKO facility. In fact the temperature measurements inside the single NOKO tube have shown that in all tests a large plug of non-condensable gas (air) was formed in front of the water level. This can be seen on the plots of the temperature measured at the top of the tube (Fig. 2.17). The temperatures in front and behind the probe assembly remain well below saturation for a long period after the level has passed the probes. This effect was observed for the upper as well as the lower probe assembly.

Single tube measurements are more sensible to a given amount of non-condensables in the system than experiments with the bundle. In case of the bundle, the gases are distributed over several heat exchanger tubes, so that their influence on the thermal power is hardly observed. On the contrary, the concentration of the gases in the single NOKO tube leads to gas plugs of significant volumes. During the single NOKO tube tests, the non-condensables have dominated the process. Gas plugs were observed with a length of several meters. The gas covered the liquid surface in the region of the water level location in the inclined tube. Condensation was possible only

2-20

in the part of the tube far above the water level. As result, the steam/gas velocity above the water level was almost zero and there was no driving shear force on the surface that could change the flow pattern (e.g. create slugs).
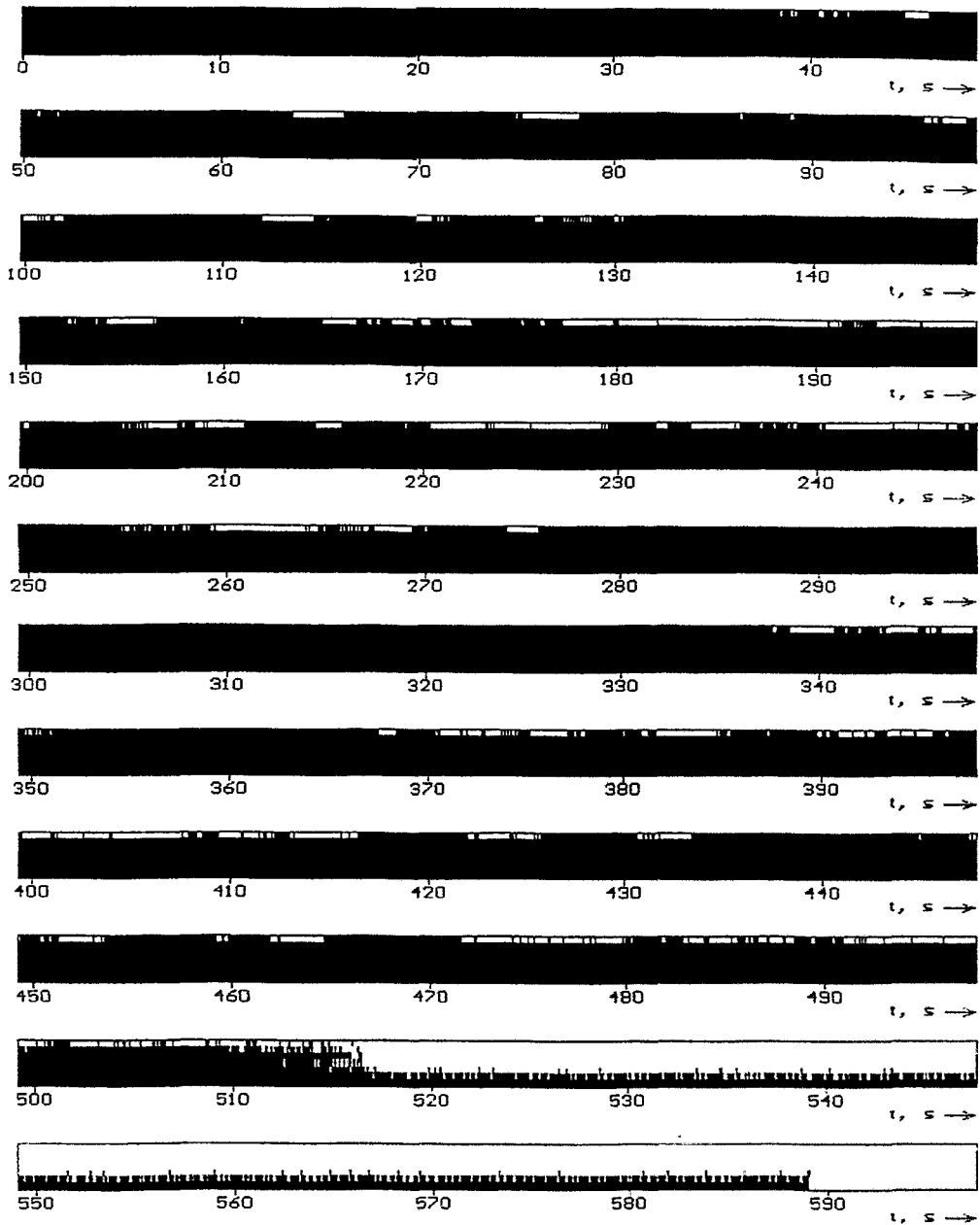


**Fig. 2.16:** Water level passage through the lower probe assembly, indication of non-condensable bubbles at probe P9 (test E9, 3 MPa). The black bars represent time intervals, when water is present at the individual probes (see Fig. 2.6).
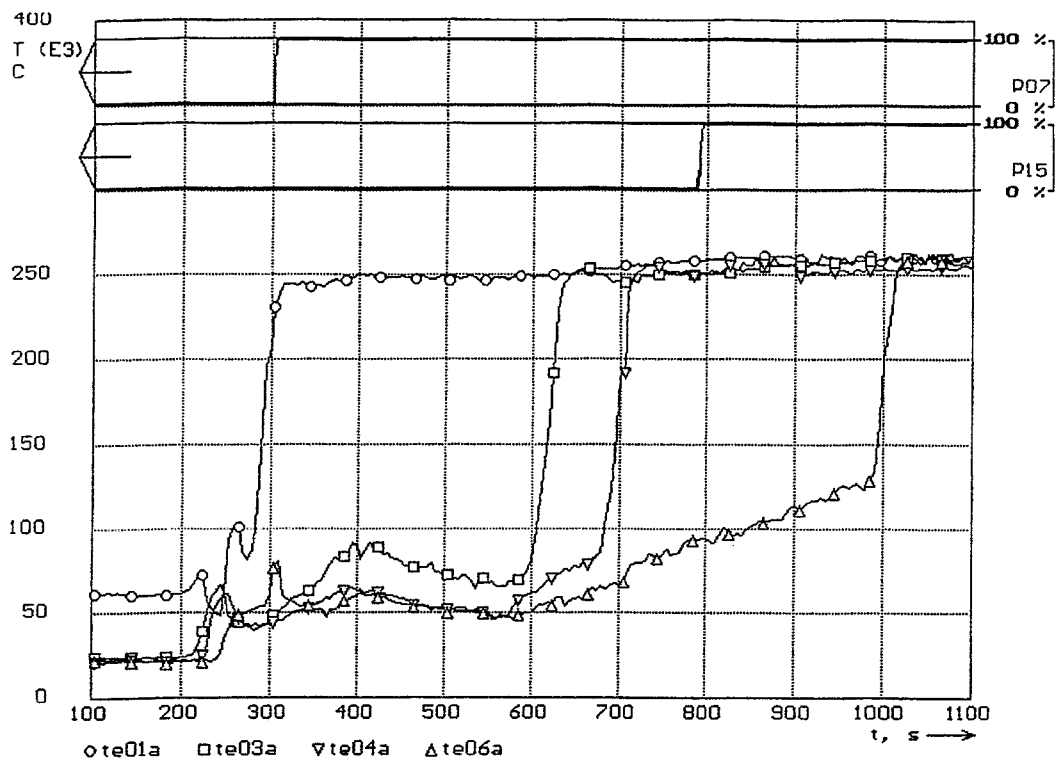
**Fig. 2.17:** Temperatures at top of the single NOKO tube in the upper leg (test E3, pressure 5 MPa). Probe P07 indicates the level passage through the upper probe assembly, probe P15 indicates the level passage through the lower probe assembly. The thermocouples te01a – te04a are arranged upstream of P07, thermocouple te06a is arranged downstream of P07.

It has to be concluded that the observed calm or slightly wavy water levels may be not typical for the situation, when NOKO is operated with pure steam. Then, the steam velocity above the water level may cause a change in the flow pattern that has to be considered in the computational modeling. Further, in certain situations, even void collapses cannot be apriorily excluded.

## 2.3.2   Interpretation of the temperature distributions

The results of the thermocouple measurements represent valuable information about the influence of non-condensables in condenser tubes. Fig. 2.18 presents a comparison between the thermocouple readings in the upper leg of the single NOKO tube. Only those thermocouple positions are plotted, which are in the neighbourhood of the upper probe assembly, and for which thermocouples at the top and the bottom of the tube were available.
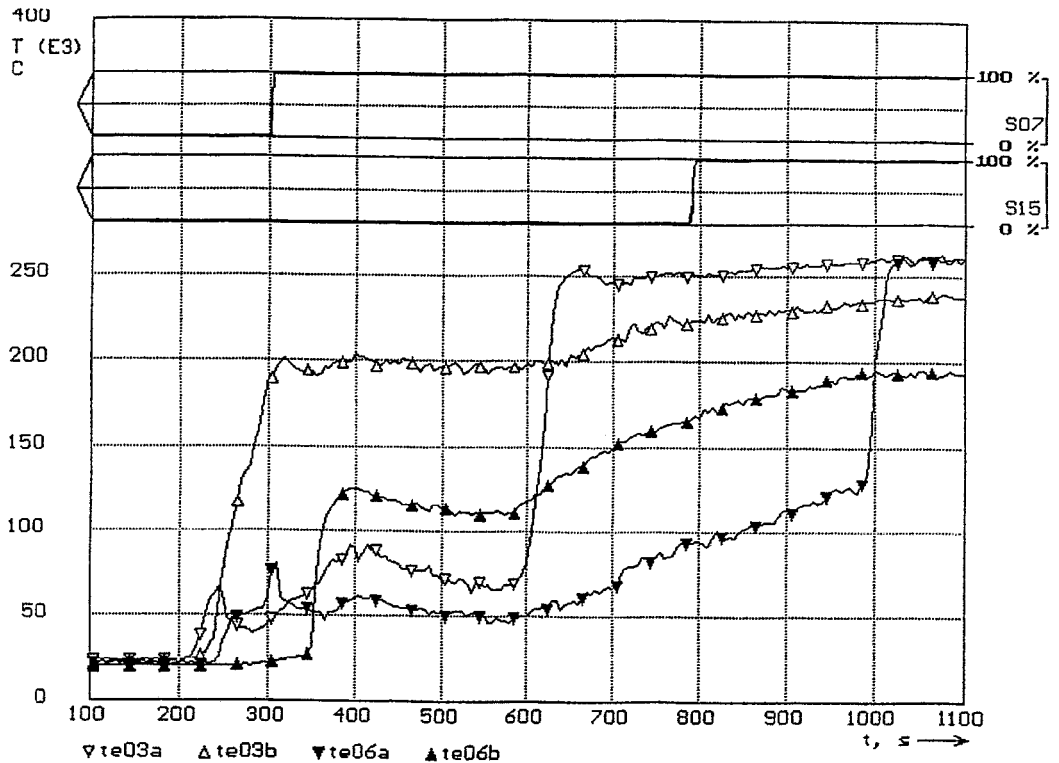
**Fig. 2.18:** Temperatures at the top and the bottom of the single NOKO tube in the upper leg (test E3, pressure 5 MPa). The probe P07 indicates the level passage through the upper probe assembly, the probe P15 indicates the level passage through the lower probe assembly. The thermocouples te03a is arranged at the top of tube upstream of P07, te06a at top of tube downstream of P07 and te03b at bottom of tube upstream of P07 and te06b at the bottom of tube downstream of P07.

The temperature at position te03a at the top of the tube reaches the saturation temperature only 300 s after the water level passed the conductivity probe. It has to be kept in mind, that te03a was located approximately 450 mm upstream of the probe assembly. The thermocouple te06a downstream of the conductivity probes indicated saturation temperature only after the lower probe assembly was uncovered. From the thermocouple data it was concluded, that the plug of non-condensables was approximately 4 m long, in this particular experiment.

The readings of the thermocouples at the bottom of the tube (te03b and te06b) show significant increases, when the level is in the region of the upper probe assembly. The temperature, however, remains well below saturation, but becomes significantly higher than the temperatures at the top of the tube. The reason is the liquid layer at the bottom of the tube which has a higher temperature, because the water was

generated by condensing steam near the inlet of NOKO, while the non-condensable at the top is rapidly cooled down to the secondary temperature. When the temperature at the top reaches the saturation level, the temperature at the bottom starts to increase slightly because the condensation of steam at the water surface, but the temperature nevertheless becomes lower than the temperature at the top of the tube.

Another effect was observed in the lower leg of the single NOKO tube (Fig. 2.19). Here, in the single phase flow before the uncovery of the probe assembly, the temperature at the top was slightly higher than on the bottom. This is the result of a stratification effect in the single phase flow, caused by the cooling from the secondary side. The cold liquid in the boundary layer collects on the bottom of the tube. When the le-
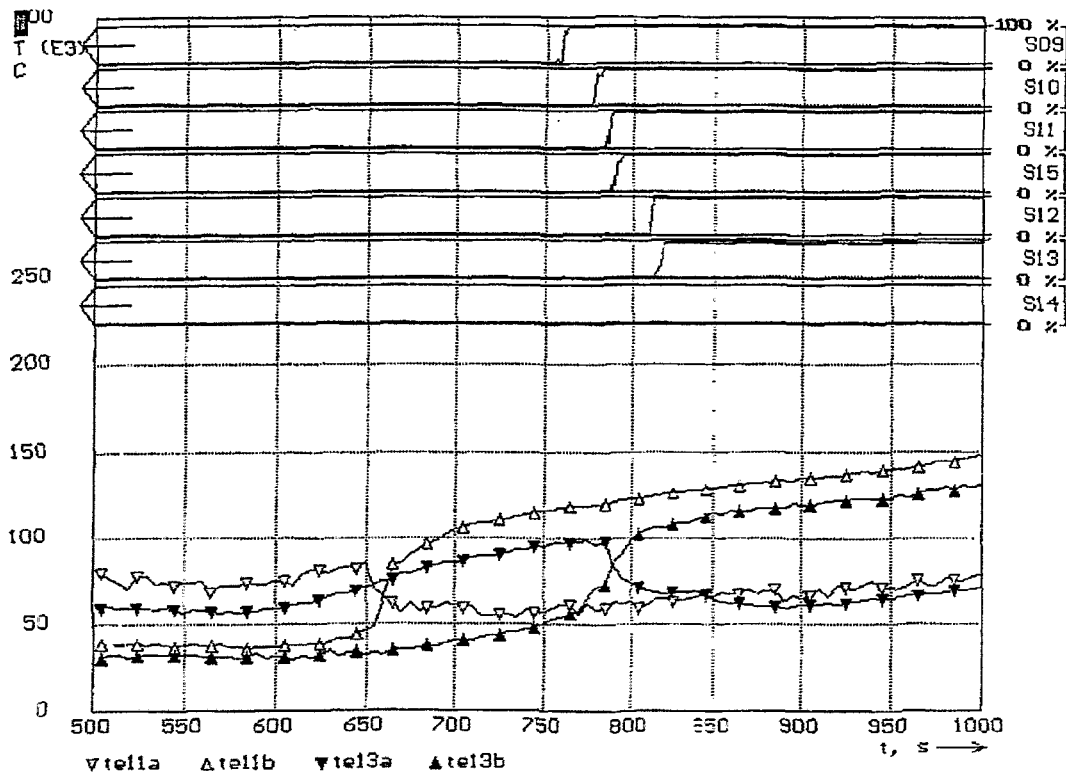


**Fig. 2.19:** Plot of the temperatures at the top and the bottom of the single NOKO tube in the lower leg (test E3, pressure 5 MPa). The plot of the probes P09 - P15, which are arranged in the lower probe array is arranged in geometric order. The temperatures plotted are the thermocouple at top of tube (te11a) and at the bottom (te11b) upstream of probe assembly (te11a) and bottom of tube, upstream of probe assembly (te13b).

vel passes the position of the thermocouples, the readings exchange place: the temperature at the top decreases because of the arrival of the non-condensable, while the temperature on the bottom increases, because condensate of slightly higher temperature arrives.

### 2.3.3 Non-condensable injection into the single NOKO tube

During the single tube experiments numerous injections of non-condensable gas were performed. The gas was oxygen. It was injected into either the upper or the lower leg of the tube. The condensation is blocked almost immediately. This was indicated by the thermocouples at the top of the tube (Fig. 2.20). The injected gas was found to form a plug in front of the water level, as expected (Fig. 2.21). After several minutes, the gas was removed from the NOKO tube through a sampling tube. The evaluation and interpretation of the results has not yet been finished.
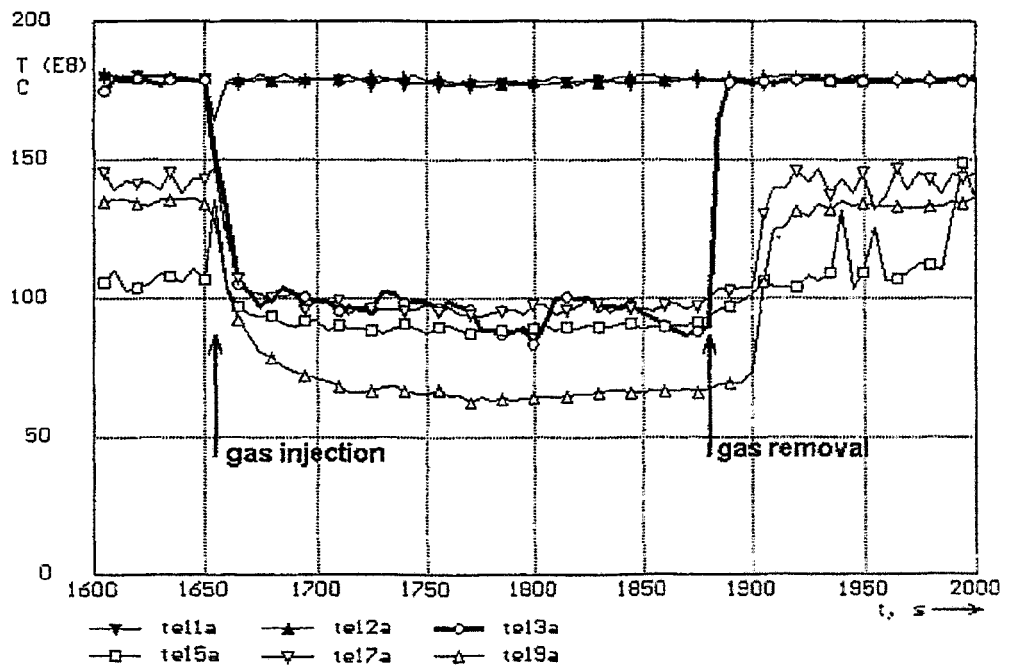


**Fig. 2.20:** Example for a non-condensable injection (test E8, pressure 1MPa). The water level is at the location of lower probe assembly (confirmed by the probes). The injected volume of oxygen is 1.5 l (at 1 MPa)

## 2.3.4 Conclusions of the experiments

The needle probes have proved to provide the information necessary for the identification of the flow patterns. Single tube experiments are much more sensible to the amounts of non-condensables, which are present in the NOKO facility by technical reasons. The calm or wavy stratified flow patterns found were caused by the suppression of the condensation in front of the water level. Non conclusion can be done concerning the flow patterns that have to be expected in the actual case, i.e. when NOKO is supplied with pure steam. For this purpose, the experiments have to be repeated after the necessary improvements of the NOKO facility. On the other hand, the tests have delivered valuable information about the behaviour of slightly inclined condenser tubes in the presence of non-condensables. This is important for code validation with respect to the extension of the thermal hydraulics with non-condensables. Here the NOKO facility can play a valuable role. It is suggested to use single tube experiments for this purpose, too, in the future.
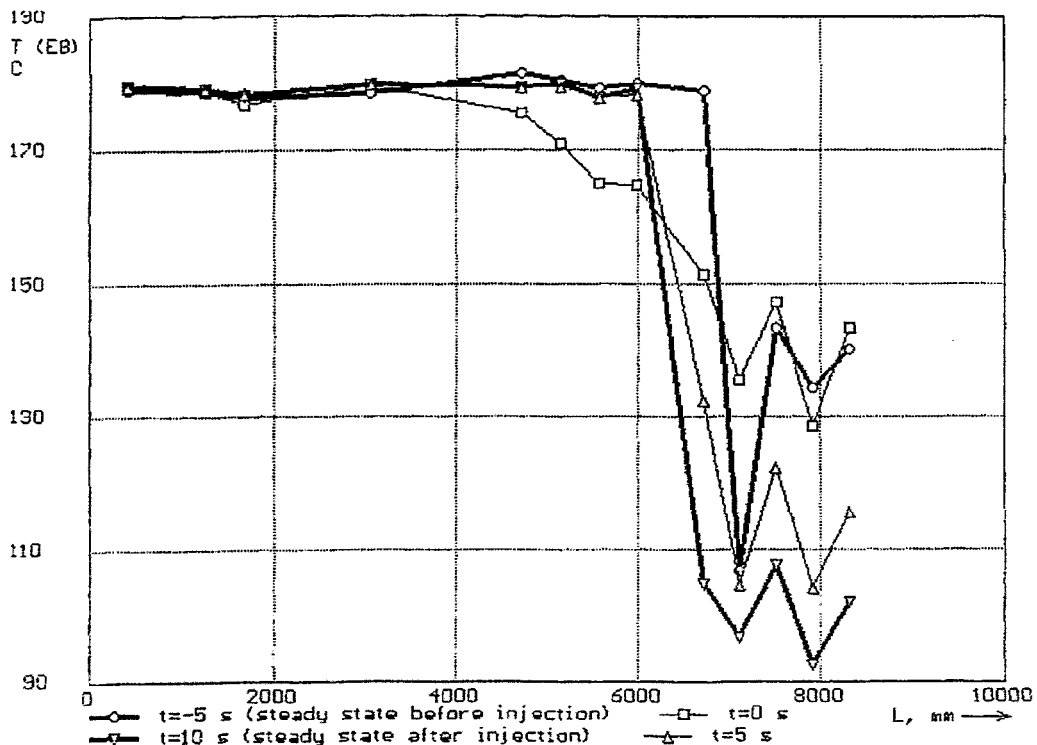


**Fig. 2.21:** Change of the temperature distribution over the length of the single NOKO tube during the gas injection (test E8, pressure 1MPa).

## 2.4 Proposal for an improved two phase flow instrumentation

The proposal for an improved two phase flow instrumentation is based on the experience obtained during several single tube experiments at the NOKO test facility in Jülich (see Chap. 2.2). It includes suggestions for the implementation of certain kinds of additional instrumentation for future single tube experiments. The proposed instrumentation can also be used for other passive safety systems. After a discussion of the general goals the improvements were described in detail, and a general scheme of the instrumentation is presented.

### 2.4.1 General goals of an improvement

Experience has shown that it is difficult to achieve good experiment quality at the single tube using the standard instrumentation of the NOKO test facility, because most of the measuring ranges are designed for bundle operation and do not fit the parameters of the single tube operation. On the other hand, the additional two-phase instrumentation by needle probes has provided new detailed insights into the flow regime inside the heat exchanger tube and also at the secondary side.

Non-condensables, desired and not desired during the experiments, play an important role. For example, signals of thermocouples are difficult to understand, when the local instantaneous phase state at the end of the thermocouple is not known. In the presence of non-condensables, it is not possible to distinguish between subcooled condensate and plugs of non-condensables also subcooled compared to the saturation temperature.

The present method of measuring the non-condensable concentration by taking samples and an off-line gas analysis is not sufficient. In the process of sampling the flow inside the tube is disturbed. The accumulation and displacement of non-condensables is an unsteady process, so that a continuous measurement with a time resolution of about 1 - 10 s would be needed instead.

In particular, the need of improvements can be summarized as follows:

- A precise correlation between the local phase detection and the temperature measurement is desirable.

- More local void probes along the z-axis of the single tube could help to characterise the instantaneous water level.

- A continuous measurement of non-condensable concentration is needed, it should not disturb the flow inside the single tube.

- An increase in accuracy of the differential pressure measurement is necessary in order to determine the hydraulic characteristics of the single tube.

- An increase of accuracy in measuring the steam and water flow rates is necessary.

Local flow pattern investigations should make use of methods of higher spatial resolution than the probe arrays used in previous work.

In the following chapters the necessary special instrumentation will be described briefly. It will be pointed out the availability or the needs of development activities.

### 2.4.1.1    Advanced Measuring systems

Afterwards the measuring systems, the proposal is based on, are introduced. New developements for the instrumentation are advanced needle probes and wire mesh sensors. Modifications or replacement of existing measurement systems are planned for the measurement of non-condensables, the differential pressure over the collectors and the mass flow rate.

### 2.4.1.2    Advanced needle probes

Advanced needle probes can deliver precise information about the appearance of gas particles or of the arrival of an liquid level (phase change). In the previous measurements the comparison between the signals of the probes and the thermocouples was very helpful to understand the behaviour of the single tube in case of the presence of non-condensables.

Unfortunately, the probes and the thermocouples were not at the same positions. For future experiments, we propose a new type of needle probes (Fig. 2.22), which is equipped with a micro thermocouple substituting the traditional electrode. These probes combine a local phase indication with a fast temperature measurement, so that the temperature can be correctly related to the instantaneous phase state.

These so-called advanced probes have not yet been manufactured nor tested. The electronic circuitry has also to be developed.



electrode =
thermocouple

$Al_2O_3$ insulation
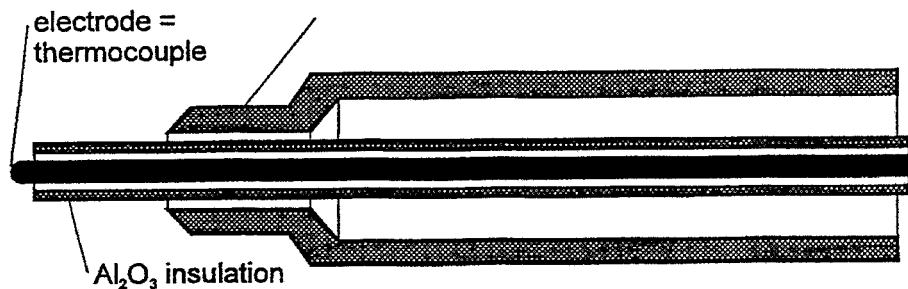
**Fig. 2.22:** Combined needle probe with thermocouple (tip).

## 2.4.2   Wire-mesh sensor

The wire-mesh sensor described in Chapter 2.1.3 is now available for a pressure up to 7 MPa, but the maximum temperature is still limited to 150 °C. This sensor provides an excellent resolution of 1024 frames/s with 16 x 16, i.e. it should replace the needle probe array used up to now.

The application under primary side conditions require a working temperature of about 250 - 290 °C. A sensor for such parameters was designed, but not yet constructed. The main material is sintered $Al_2O_3$ ceramics. The efforts for manufacturing and testing are also in the range of 1 man-year.

### 2.4.3 Sensor for non-condensables

FZR proposes to use acoustic sensors for measuring the gas content of the steam inside the heat exchanger tube. A small gas sample of less 100 $cm^3$/min (normal) is taken from the primary side, heated up to a temperature above 100 °C to avoid steam condensation and led to a fluidic oscillator, the frequency of which depends on the speed of sound. From a frequency measurement, the mass ratio between $H_2O$ and the applied non-condensable (e.g. $N_2$) is calculated. The small sampling flow does not influence the conditions in the heat exchanger tube significantly. Samples should be taken from the heat exchanger tube inlet and outlet as well as from several intermediate positions along the tube.

This kind of measuring device is available at the Hochschule für Technik und Wirtschaft Dresden (FH). The developer and manufacturer is the department of Prof. L. Zipser [ZIL-93]. It costs about 5 kECU per channel.

### 2.4.4 Differential pressure transducer

For the determination of the hydraulic characteristic a differential pressure transducer is proposed. This pressure transducer should be connected directly to the heat exchanger tube at the inlet and outlet bushings. In this way, the accuracy can be significantly increased compared to a DP measurement between the inlet and outlet collectors. This technology is available.

### 2.4.5 Mass flow rate

A striking disadvantage of the existing NOKO instrumentation with regard to single tube experiments is the measuring range of the mass flow meters, which was adjusted to bundle tests. In case of single tube operation, the low flow rate causes high measuring errors. For the determination of exact hydraulic characteristics of the heat exchanger tube, we propose individual mass flow meters for the steam at the inlet and the condensate at the outlet of the single tube. Diaphragms, but also other kinds of instrumentation, can be applied. Additional thermocouples for the determination of the physical properties of the fluid have to be envisioned.

## 2.4.6 General scheme of the single tube instrumentation

The general scheme of the single tube instrumentation is shown in Fig. 2.23. The advanced needle probes are allocated at several positions along the z-axis. There is always one probe from above and another from below. In this way, the level movement, appearing non-condensable plugs as well as the condensate flow can be observed.

The best location for the wire mesh sensor is somewhere in the second half of the overall length, because there the condensate flow is significant and the steam flow is still high and there is a real chance of detecting different flow patterns.

The proposed positions of the flow meters, the non-condensable sensors and the differential pressure transducer are also shown in Fig. 2.23. FZR suggests to use the same approach of instrumentation for a vertical, inclined or horizontal orientation of the tube bend.

The proposed instrumentation is capable to deliver necessary insights into the processes at he primary side of the tubing of the emergency condenser. The different kinds of measuring devices are subject to certain development efforts.
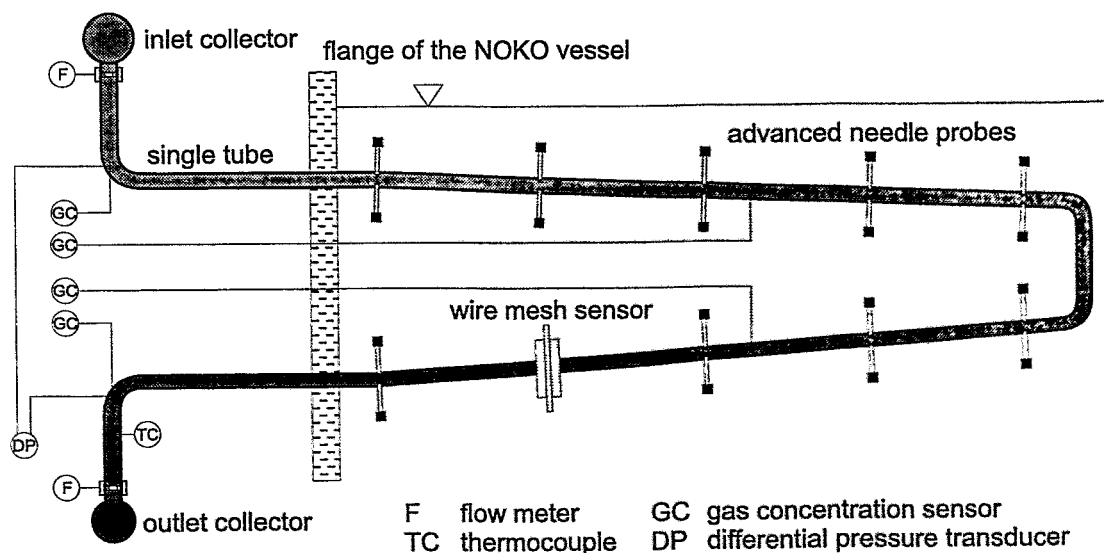
Fig. 2.23: Scheme of the proposed special instrumentation for a future single tube for NOKO.

# 3   ATHLET calculations of NOKO experiments

In chapter three the results of the ATHLET calculations of NOKO experiments are presented. The chapter starts with a description of the NOKO test facility and test performance, the transfer of the available experimental data and the evaluation of the NOKO experiments. Then follows an overview on the ATHLET code and the necessary improvements of the condensation model for the NOKO post test calculations. After the presentation of the nodalisation of the NOKO loop results of the post test calculations of selected NOKO experiments and the blind test calculation were presented.

## 3.1   NOKO Test Facility and Test Performance

The general design of the NOKO test facility is shown in Fig. 3.1. Main components of the facility are the pressure vessel (height 12.6 m, diameter 0.448 m) simulating the reactor pressure vessel of the SWR1000 and the laterally connected emergency condenser bundle. In NOKO, the steam (maximum mass flow 2.5 kg/s) is produced by an electrical heater with a maximum power of 4 MW. The heater produces a two phase flow mixture which is afterwards separated. Because the heater power during the experiments can only be adjusted in steps more steam than needed for the experiments is produced continuously. The surplus steam is blown off and the system pressure is controlled by a valve [SCA-961].

The condenser (see Fig. 3.1) represents the core flooding pool of the SWR1000. The main dimensions of this pool are: length 6 m, diameter 2 m, volume 20 m³. The relief tank is the heat sink of the test facility. There, the surplus steam and the steam built inside the condenser is blown off.

The design of the test facility provides the possibility of adjusting the same pressure and temperature conditions as in the SWR1000. Additionally, the geodetic heights, water levels, the dimensions and the material of the heat exchanger tubes are the same as in the original reactor design. The number of tubes of the test bundle is chosen corresponding to the available electrical heater power. Eight tubes of the test bundle were used optionally in the test.
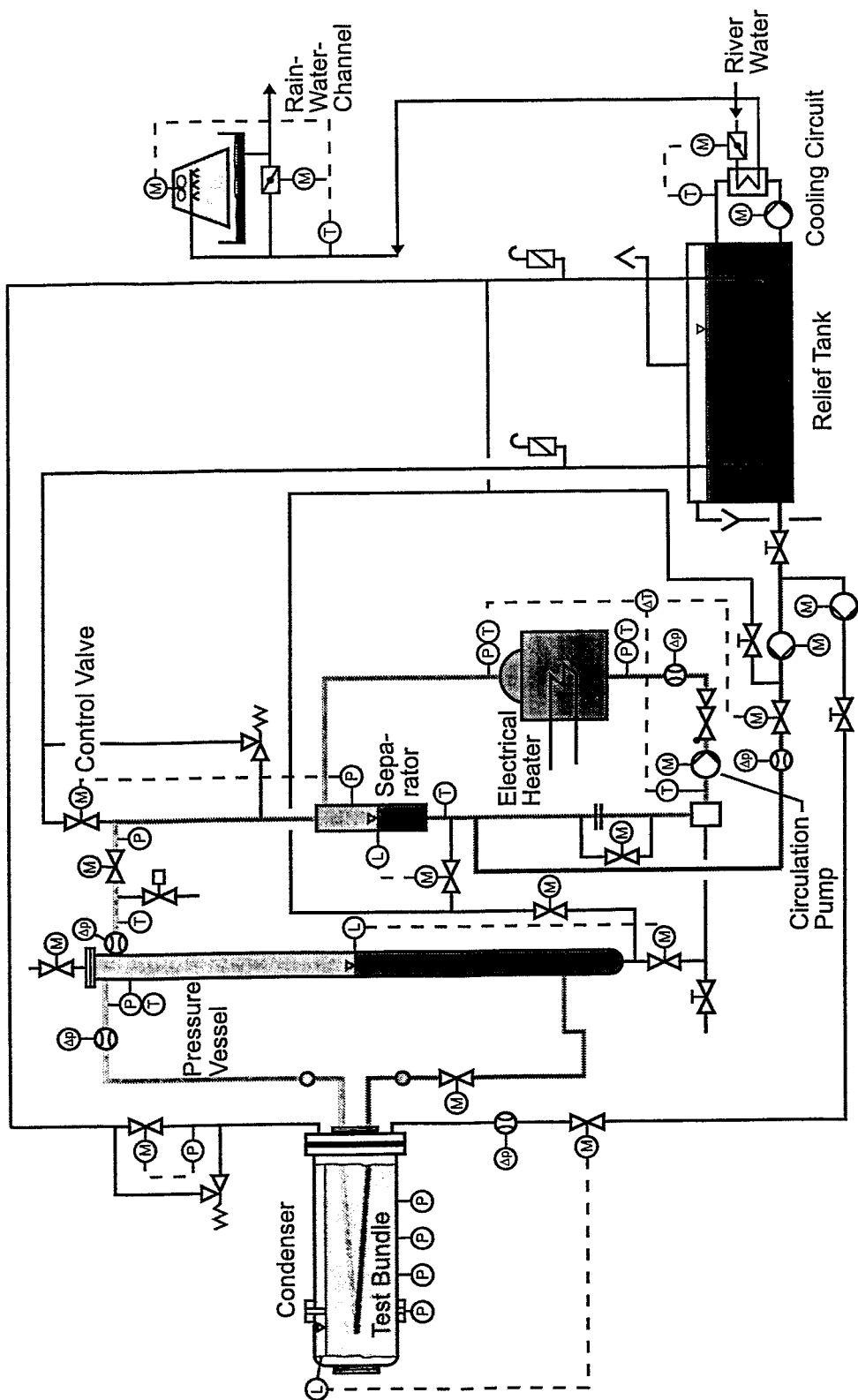
**Fig. 3.1:** NOKO test facility [SCA-961].

The bundle tests are so called steady state tests. After adjusting the initial and boundary conditions, initiating the experiment and the adjustment of steady state conditions the data acquisition is started and runs approximately 20 minutes. During this period every 5 seconds a complete set of measurement data is stored. In CASH-Graphics for each time point the NOKO capacity is determined.

A description of the single tube test is missing, because up to now there are no data for the single tube tests available (see Tab. 3.1).

## 3.2    Transfer of Available Data

Table 3.1 gives an overview of the test matrix and the number of the experiments within the BWR Cluster and the BWR/CA. The experiments EU1 - EU6 were each performed with a test bundle consisting of four tubes. Up to now, no measurement data for the single tube test experiments (EU7 - EU10) are available. The data of the NOKO experiments, which are available in the BWR/CA were transferred to FZR via Internet and evaluated as described in Chap. 3.3.

**Tab. 3.1:** Available experimental and evaluated NOKO data.

| No. | Date | $p_{DRU}$ [bar] | $h_{DRU}$ [m] |
|---|---|---|---|
| EU-1 | 30.09.1996 | 10 | 6,1 – 4,9 – *3,7* – *2,5* – 1,3 |
| EU-2 | 01.10.1996 | 10 | 6,1 – 4,9 – 3,7 – 2,5 – 1,3 |
| EU-3 | 08.10.1996 | 30 | 6,1 – *4,9* – *3,7* – *2,5* – 1,3 |
| EU-4 | 09.10.1996 | 30 | 6,1 – *4,9* – 3,7 – 2,5 – 1,3 |
| EU-5 | 21.10.1996 | 70 | 7,3 - *6,1* – 4,9 – *3,7* – 2,5 – *1,3* |
| EU-6 | 22.10.1996 | 70 | 7,3 - *6,1* – 4,9 – 3,7 – 2,5 – 1,3 |
| EU-7 | 13.11.1996 | 30 | Variable |
| EU-8 | 13.11.1996 | 70 | Variable |
| EU-9 | 14.11.1996 | 30 | Variable |
| EU-10 | 14.11.1996 | 30 | Variable / Non-condensible |

Data available and transferred via Internet
Data not yet available
*X.X*    Test selected by FZJ for post test calculation

## 3.3  Evaluation of the NOKO Experiments

The emergency condenser tests were to assess the emergency condenser capacity as a function of the parameters given in Table 3.1. The evaluation of the experiments is performed with the code system CASH-Graphics. CASH is the German abbreviation for evaluation and uncertainty analysis of NOKO experiments and was developed at the DEC workstation cluster of FZJ during a PhD thesis [SCA-962]. Within the actual framework CASH was implemented on the SUN workstation Cluster of the FZR. Additionally an IBM/RISC Version of CASH is now available.

The main features of CASH-Graphics are the:

- plotting of the measured data,

- logical checking, if the measured data are within the measuring range of the measurement systems,

- determination of the emergency condenser capacity by using three independent energy balances,

- determination of the uncertainty balances of the three energy balances

and

- the output of the results as diagrams and tables.

The emergency condenser capacity is determined by three independent energy balances (see Fig 3.2). The first one is the balance of the emergency condenser bundle ($L_{NOKO,1}$), the second for the condenser ($L_{NOKO,2}$) and the third for the whole primary circuit containing the electrical heater loop, the pressure vessel and the emergency condenser system ($L_{NOKO,3}$). For the second energy balance it must be distinguished between the heat up and the blow off phase. Heat up phase means, that the water in the condenser is subcooled and the produced steam is totally condensed. In this period the emergency condenser capacity is determined as the product of the water inventory and the temperature gradient of the condenser. After the water in the condenser reaches saturation conditions the produced steam is blown off into the relief
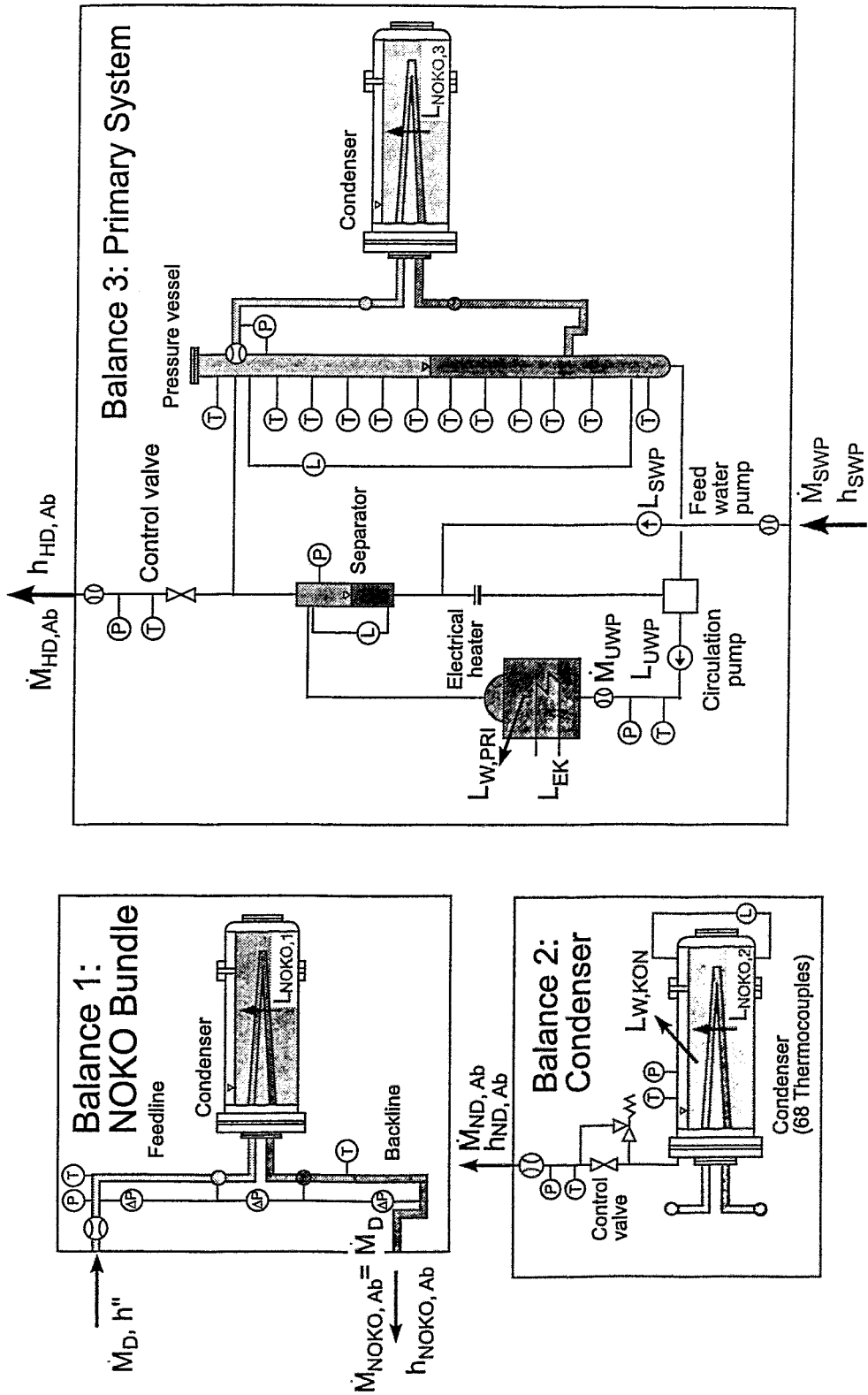
**Fig. 3.2:** Energy balances for the determination of the emergency condenser capacity [SCA-962].

tank. In this case the condenser capacity is determined by the product of the blow off steam flow rate and the evaporation enthalpy. During the experiments a strong inhomogeneous temperature distribution was observed. Therefore it is not possible to associate water volumes of the condenser to the thermocouples and the evaluation of the second energy balance was only performed for the blow off phase.

The results are presented in terms of the water level in the pressure vessel. Reference point is the inlet of the emergency condenser outlet line at the pressure vessel. The bars in the capacity curves show the fluctuations of the capacity during the measurement time period. For each energy balance a detailed uncertainty analysis was performed.

Fig. 3.3 shows the results of the above described evaluation of the tests EU1 - EU2, Fig. 3.4 of the tests EU3 - EU4 and Fig. 3.5 of the tests EU5 - EU6. Additionally in appendix A tables with the measured and from measured data determined values (e.g. mass flows, water level), capacities and uncertainties are presented. The capacity curves in the Fig. 3.3 - 3.5 show fluctuations up to ± 150 kW for one experiment and the same energy balance over the measurement time period and up to ± 250 kW between the different energy balances for the same time period. One reason for these fluctuations is, that during some experiments the pressure outside the bundle increases during the test series (e.g. in EU6-6 from 0.14 MPa up to 0.185 MPa).

Further on in two cases big differences in the specified pressure vessel water level in the test matrix and the adjusted water level in the experiments were observed (see. Tab. 3.2). In the first case, that means for the experiment EU4-2, the first and second measurement data set are mixed up. The right data of EU4-2 are stored at the file "eu4m1.asc". In the second case, that means the experiment EU6-2, there are no data available for a pressure vessel water level of 6.1 m. Therefore the calculations will be performed with the water level of 4.4 m. Therefore the comparison of tests EU5-2 and EU6-2 is not possible. To avoid trouble the test matrix should be corrected by FZJ.
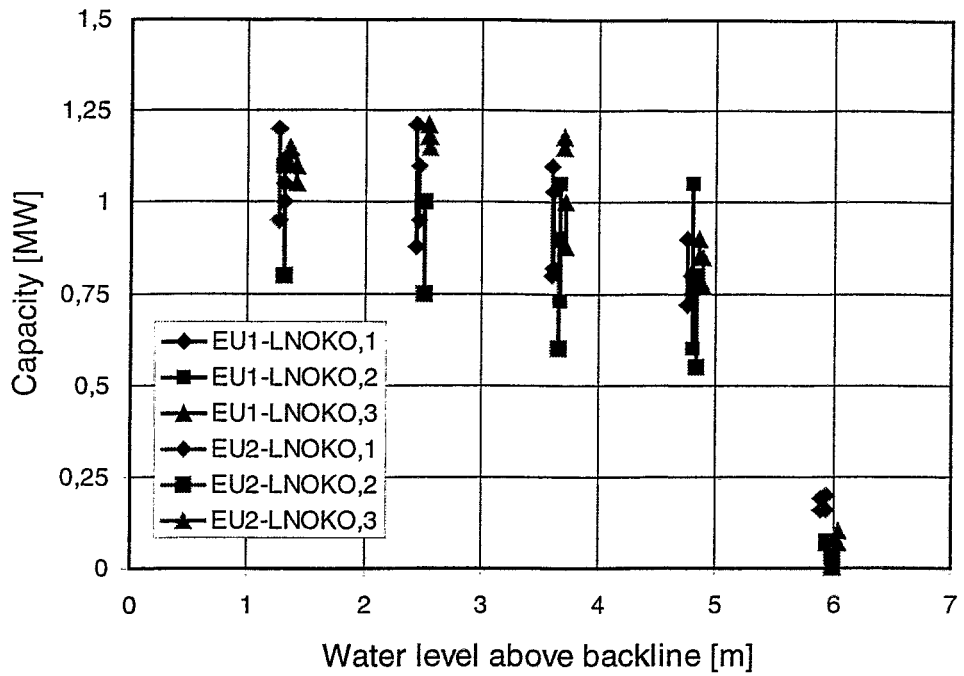
**Fig. 3.3:** NOKO capacity of the EU experiments EU1 and EU2.
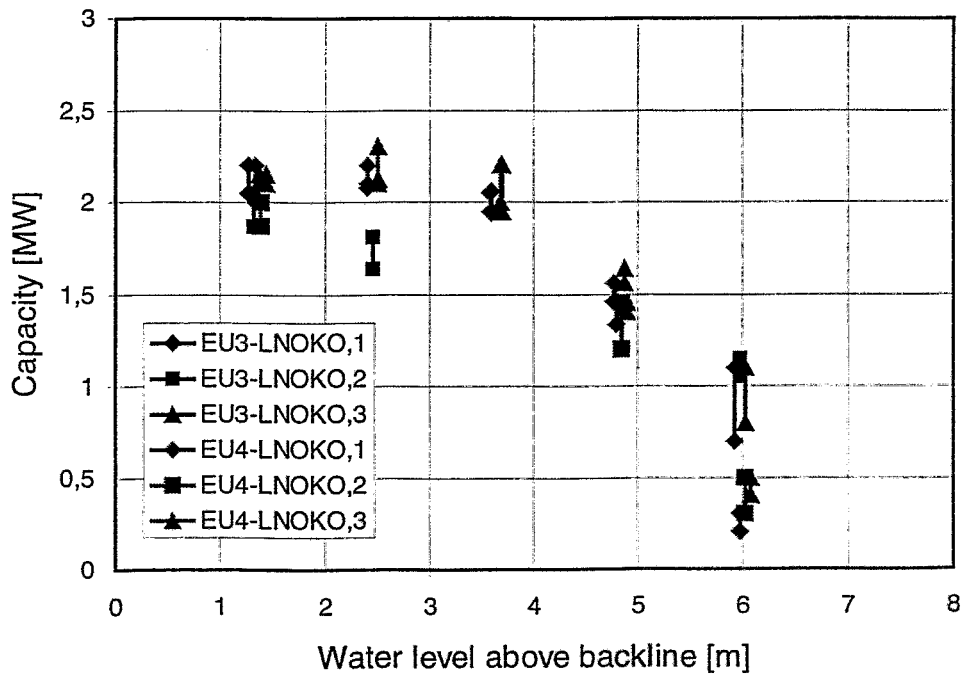


**Fig. 3.4:** NOKO capacity of the EU experiments EU3 and EU4.
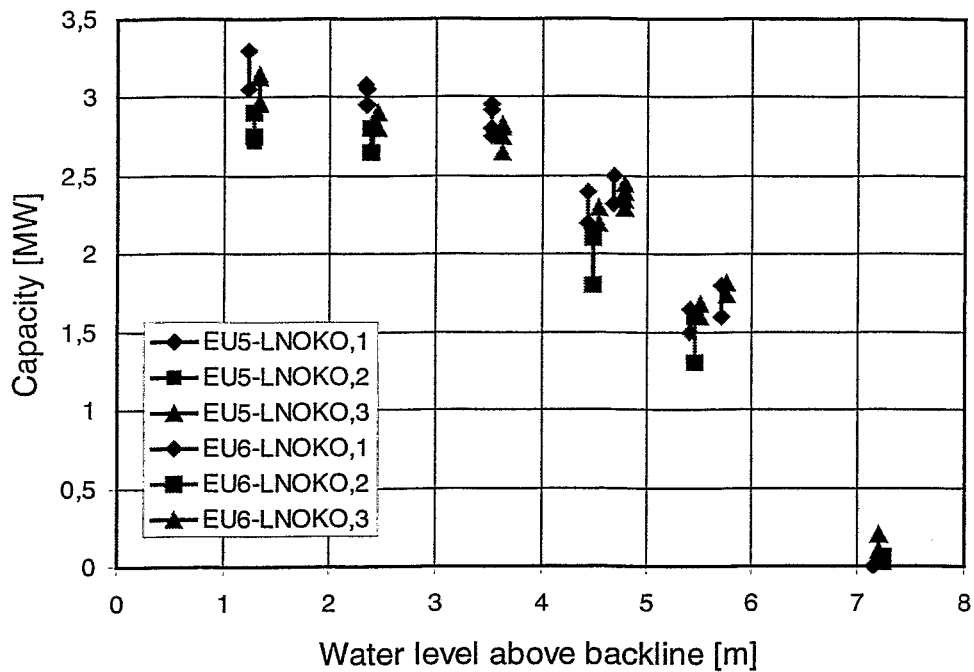
**Fig. 3.5:** NOKO capacity of the EU experiments EU5 and EU6.

**Table 3.2:** Comparison between the foreseen and the adjusted values of the pressure vessel water level.

| Test | Pressure vessel water level above the backline [m] | |
|---|---|---|
| | foreseen value | adjusted value |
| EU1 - 3 | 3.7 | 3.66 |
| EU1 - 4 | 2.5 | 2.49 |
| EU3 - 2 | 4.9 | 4.83 |
| EU3 - 3 | 3.7 | 3.64 |
| EU3 - 4 | 2.5 | 2.47 |
| EU4 - 2*) | 4.9 | 4.85 |
| EU5 - 2 | 6.1 | 5.89 |
| EU5 - 4 | 3.7 | 3.58 |
| EU5 - 6 | 1.3 | 1.29 |
| EU6 - 2 | 6.1 | 4.42 |

*) stored in data file eu4m1.asc

The uncertainties for the different energy balances are shown in the Fig. 3.6 – 3.8. The uncertainties for the second energy balance are only determined for the blow off phase.
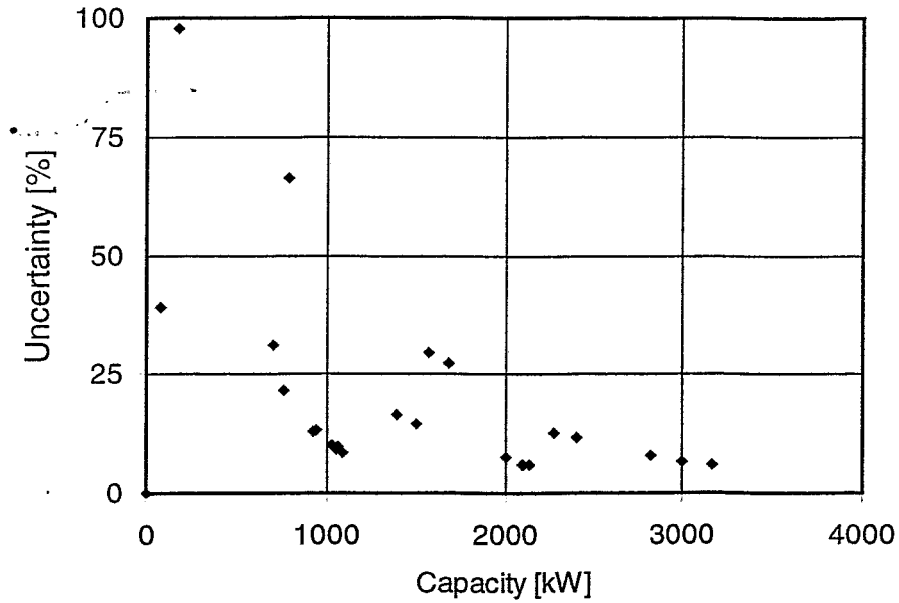


**Fig. 3.6:** Calculated uncertainty of $L_{NOKO,1}$.
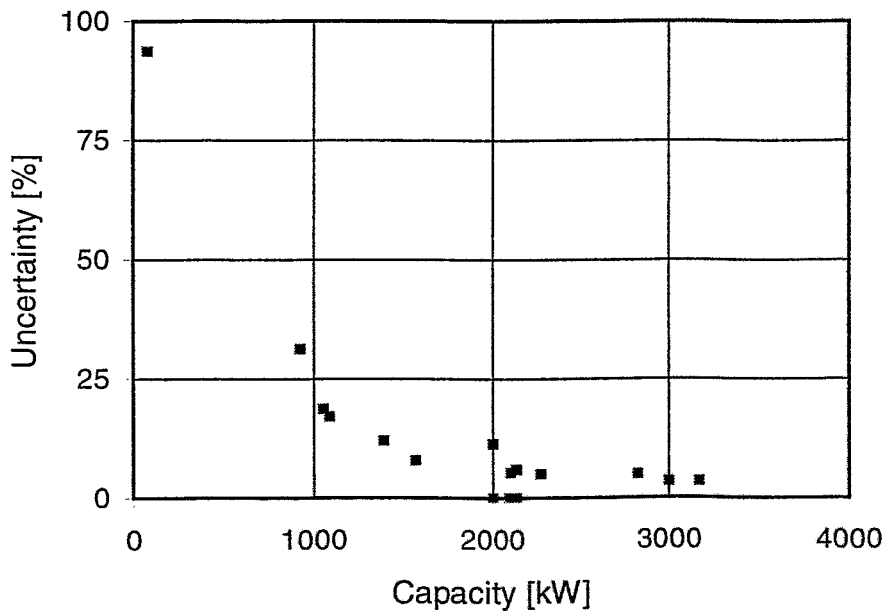


**Fig. 3.7:** Calculated uncertainty of $L_{NOKO,2}$ (only determined for the blow off phase).
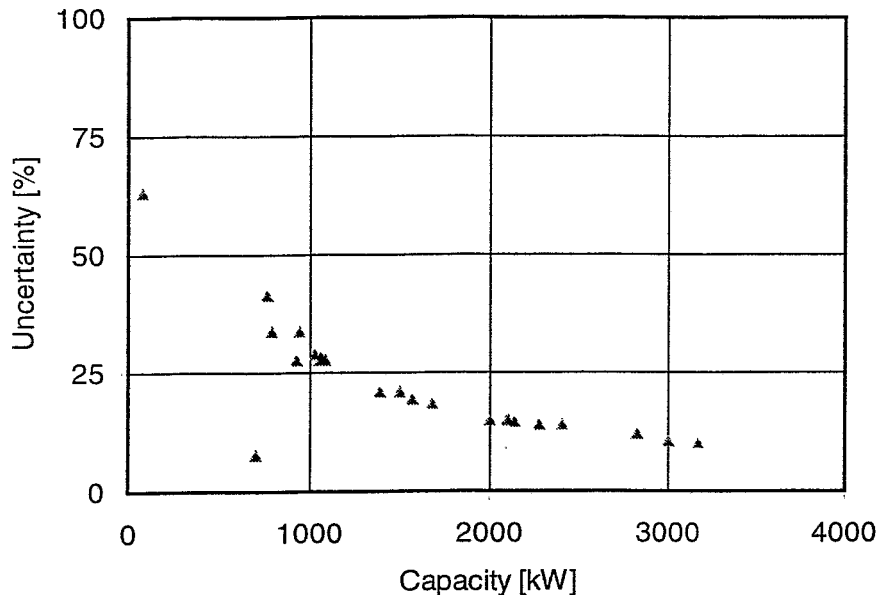
**Fig. 3.8:** Calculated uncertainty of $L_{NOKO,3}$.

## 3.4 ATHLET Code

The post test calculations of NOKO experiments have been performed with an impro-
ved version of the ATHLET (Analysis of the thermohydraulics of leaks and transients)
code [TEV-88, LEG-96]. ATHLET which is being developed by the Gesellschaft für
Anlagen- und Reaktorsicherheit (GRS) mbH is intended to cover in a single code the
entire spectrum of loss-of-coolant and transient accidents in Light Water Reactors
(LWR). For determination of the heat transfer coefficients during condensation in ho-
rizontal und slightly inclined tubes the module KONWAR (Kondensation in waage-
rechten und leicht geneigten Rohren) has been developed and implemented in
ATHLET Mod. Cycle C [SCA-971].

In Fig. 3.9 the different options for the calculation of heat transfer coefficients (HTC's)
inside tubes of the original and the improved version of ATHLET are compared. The
condensation model of ATHLET (see left side of Fig. 3.9) was developed for the
calculation of HTC's in vertical tubes. The condensation process is characterized by
symmetrical condensate films with equal layer thickness over the cross section area.
The HTC's are calculated by using the correlations of CHEN, NUSSELT, CARPEN-

**Fig. 3.9:** Calculation of heat transfer coefficients in ATHLET and ATHLET - coupled with KONWAR [SCA-971].

annular film

laminar wavy film

transition regime laminar - turbulent

turbulent film

single phase flow

inlet

outlet

$\alpha$ = maximum (Chen, Nusselt, Carpenter-Colburn, 20 W/m²K)

ATHLET MOD1.1 - Cycle C

inlet

annular flow | transition regime | stratified flow | slug flow | plug flow

outlet

$j_D^*$

10 — spray flow — Soliman | bubbly flow

annular flow — Kosky & Staub, Nusselt

inlet

1 — Palen | Breber

transition range | slug flow

0,1 — Jaster & Kosky

0,01 — Breber outlet | plug flow

0,001 — stratified flow (wavy) | Breber

0,0001  0,001  0,01  0,1  0,5 1   10

$\dfrac{1-\varepsilon}{\varepsilon}$

flow regime map for condensation (see Tandon)

ATHLET - KONWAR (condensation in horizontal tubes)

TER-COLBURN or a minimum of 20 W/(m²K). For further calculations the maximum of these values is used.

The condensation process in horizontal tubes is much more complicated than in vertical tubes. Over the tube length the flow regimes (e.g. spray, plug, slug, bubble and stratified flow) are changing (see right sight of Fig. 3.9). For the calculation of HTC's it is necessary to identify the flow regimes in the concerned cross section area.

For this KONWAR uses the flow map of TANDON where the dimensionless steam velocity of Wallis $j_D^*$ is given as a function of the quotient of the condensate and void fraction $(1-\varepsilon)/\varepsilon$. According to PALEN a transition regime between annular and stratified flow has to be considered in the flow map [STK-88]. The HTC's are calculated by the correlations of SOLIMAN (spray flow), NUSSELT (laminar annular flow), KOSKY and STAUB (turbulent annular flow), RUFER and KEZIOS (stratified flow) and BREBER (bubble, slug and plug flow) (see Fig. 3.9).

## 3.5 Nodalisation of the NOKO Loop

For the post test calculations of the NOKO experiments two different nodalization schemes were developed. The first nodalization is used for the bundle tests EU1 - EU6 (see Tab. 3.2), the second for the single tube tests (EU6 – EU10).

The model of the NOKO test facility, which is used for the bundle post test calculations, is shown in Fig. 3.10 and consists of the pressure vessel and the emergency condenser system (containing in- and outlet line, bundle, inlet and outlet collector and the flooding pool). The steam supply, the water level and the pressure control of the pressure vessel and the pressure control of the flooding pool are simulated with the general control simulation module (GCSM) of ATHLET [AUH-90].
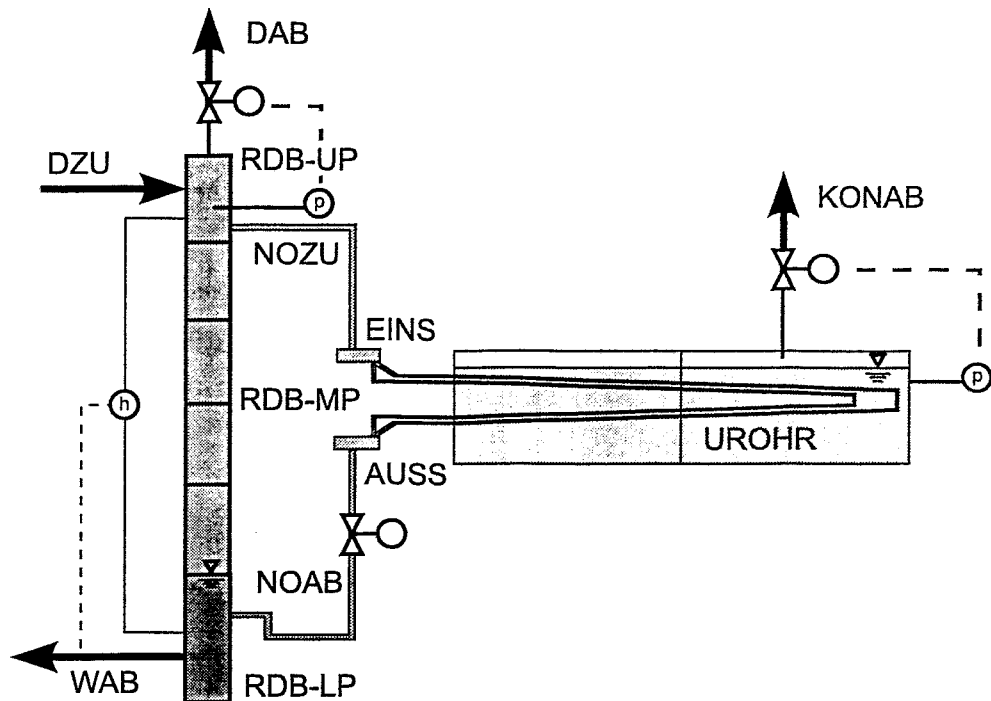
**Fig. 3.10:** Nodalisation scheme for post test calculations of the NOKO experiments.

The pressure vessel is divided into three objects. The upper plenum (RDB-UP) and the lower plenum (RDB-LP) are specified as branches, the middle plenum (RDB-MP) as a pipe. The abbreviations given in brackets are the names of the ATHLET objects (compare Fig. 3.10). The upper plenum is additionally used for the input of the initial and boundary conditions and connected with two so called single junction pipes. These are used for modeling the steam supply (DZU) and the control of the system pressure (DAB). During the experiments the electrical heater produces more steam than the emergency condenser condenses. The surplus steam is blown off into the blow off tank (see Fig. 3.1).

The bundle (UROHR) is coupled via the inlet line (NOZU) and the inlet collector (EINS) at the upper plenum. The collector is specified as a branch and the feed line as a pipe. The bundle consists of four levels each with one tube, which are divided into 9 control volumes. Only two of the four tubes are sketched in Fig. 3.10.

The condensate flows back to the pressure vessel through the outlet collector (AUSS) and the back line (NOAB) - only driven by gravity forces. In the back line a valve is located, which is closed at the beginning of the experiments. Therefore it is

possible to adjust a mixture level in the pressure vessel independent from the mixture level in the NOKO system. By opening this valve the test is initiated. Via the outlet line the outlet collector is connected to the lower part of the pressure vessel (RDB-LP). The single junction pipe WAB is coupled at the lower plenum for the controlling of the pressure vessel water level. The control is modeled with GCSM.

Because the experiments show that there is only a negligible influence of the sub-cooling in the flooding pool on the emergency condenser capacity, the flooding pool is modeled as one big branch (KONDEN). The single junction pipe KONAB is coupled to the pool for pressure control.

A problem for the modeling of the test facility is that there are no control system data available. Therefore the range of adjustment is determined from the experimental data.

All objects of the input data set are coupled with so called heat structures. These allow the determination of the one dimensional heat conduction in solid materials. The material properties of the stainless steal and isolation material is taken from data sheets of the manufacturer [SCA-962].

## 3.6 Post Test Calculations of selected NOKO Experiments

Ten post test calculations of NOKO tests were performed by FZR with an improved version of ATHLET Mod. 1.1 Cycle C (ATHLET coupled with KONWAR [SCA-971]). The tests were selected by FZJ [JAH-97]. The results of these post test calculations are presented here and are compared with the experimental data.

The initial and boundary conditions (see Fig. 3.11) of the post test calculations are given in Tab. 3.3. These tests are so called steady state NOKO tests. In the first phase the initial and boundary conditions (e.g. pressure $p_{DRU}$ and water level above connecting point of the outlet line $h_{DRU}$ in the pressure vessel and initial water temperature $T_{KON}$, pressure $p_{KON}$ and water level $h_{KON}$ of the condenser) were adjusted. For that, the valve in the outlet line of the emergency condenser was closed. By opening this valve the experiment was initiated. After reaching steady-state
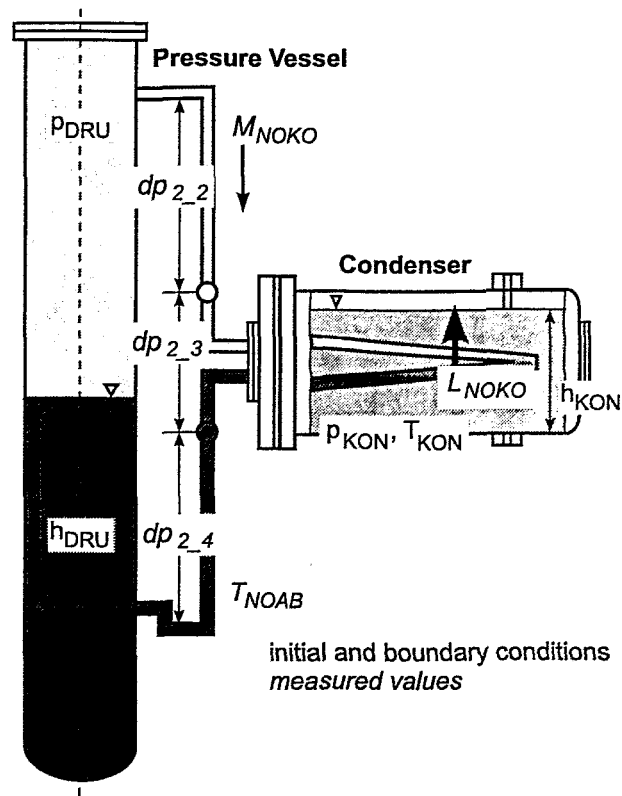
**Fig. 3.11:** Initial and boundary conditions for the NOKO calculations.

conditions the data acquisition was started and runs approximately 20 minutes.

During the evaluation of the experiments it was mentioned that the measured steam temperature in the inlet line was up to 4 K lower than the saturation temperature of the pressure in the pressure vessel. This phenomena was observed for all experiments. Because the uncertainties of the pressure measurement are greater than the uncertainties of the temperature measurement the primary side pressure boundary conditions are determined from the temperature measurements in the inlet line.

**Table 3.3:** Initial and boundary conditions for the NOKO post test calculations [JAH-97].

| No. | Test | Primary Conditions | | | Secundary Conditions | | |
|---|---|---|---|---|---|---|---|
| | | pressure $p_{DRU}$ [MPa] | water level $h_{DRU}$ [m] | mass flow $M_{NOKO}$ [kg/s] | water level $h_{KON}$ [m] | temperature $T_{KON}$ [°C] | pressure $p_{KON}$ [MPa] |
| 1 | EU1-3 | 0.98 | 3.66 | 0.42 | 1.33 | 66.1 | 0.11 |
| 2 | EU1-4 | 1.00 | 2.49 | 0.50 | 1.33 | 88.0 | 0.11 |
| 3 | EU3-2 | 3.02 | 4.83 | 0.69 | 1.40 | 63.2 | 0.11 |
| 4 | EU3-3 | 3.01 | 3.64 | 1.01 | 1.43 | 101.7 | 0.11 |
| 5 | EU3-4 | 3.01 | 2.47 | 1.17 | 1.37 | 111.0 | 0.14 |
| 6 | EU4-1 | 3.01 | 4.85 | 0.65 | 1.41 | 105.1 | 0.12 |
| 7 | EU5-2 | 7.07 | 5.89 | 0.78 | 1.37 | 44.6 | 0.11 |
| 8 | EU5-4 | 7.07 | 3.58 | 1.60 | 1.39 | 111.0 | 0.14 |
| 9 | EU5-6 | 7.06 | 1.29 | 2.08 | 1.34 | 117.0 | 0.17 |
| 10 | EU6-2 | 7.07 | 4.42 | 1.19 | 1.38 | 113.5 | 0.15 |

A detailed discussion of a post test calculation is given in Chap. 3.7. The NOKO tests are steady state tests. The fluctuations of the measured values should be low per definition. During steady state the magnitude of these fluctuations are documented in Table 3.4. Here for each measured value the minimum and the maximum of the measure time period are given: These values are compared with the computational data (characterized by the abbreviation ATH). This comparison is performed for the condensate mass flow $M_{NOKO}$, the temperature at the outlet $T_{NOAB}$, the capacity of the emergency condenser and the pressure drops in the emergency condenser system $dp_{2\_2}$, $dp_{2\_3}$ and $dp_{2\_4}$ (see Fig. 3.11). The three values of the capacity of the bundle are determined by the three independent energy balances described in Chap. 3.3. The upper values give $L_{NOKO,1}$, the middle value $L_{NOKO,2}$ and the lower value $L_{NOKO,3}$.

In Tab. 3.4 a very good agreement for mass flow and emergency condenser capacity and a good or acceptable agreement for outlet temperatures and pressure drops in the emergency condenser system can be observed. For the comparison of the experimental and computational pressure drops it has to be recognized that no zero point corrections were available. For comparable NOKO experiments these corrections lay in the magnitude of up to 0.6 kPa for $dp_{2\_2}$, up to 1.4 kPa for $dp_{2\_3}$ and up to 1.9 kPa for $dp_{2\_4}$ [PRM-97]. Assuming the corrections the calculated data are quite good. All computational data can be released on request.

Additionally in the Fig 3.12 - 3.14 the bundle capacity is plotted versus water level for the primary side pressures of 1, 3 and 7 MPa. As shown in Tab. 3.4 there is a good agreement between computational and experimental results.

Table 3.4:  Comparison of the experimental and computational data of EU experiments which were selected for post test calculations.

| Test | Mass Flow [kg/s] | | Temperature in outlet line [°C] | | Capacity [MW] | | Pressure drop in inlet line [kPa] | | bundle [kPa] | | outlet line [kPa] | |
|---|---|---|---|---|---|---|---|---|---|---|---|---|
| | measure | ATH | measure | ATH | measure | ATH | measure | ATH | measure | ATH | measure | ATH |
| EU1-3 | 0.36 - 0.46 | 0.57 | 118 - 130 | 170 | 0.82 - 1.03<br>0.73 - 1.05<br>0.88 - 1.00 | 1.17 | 1.75 - 1.8 | 2.7 | 1.0 - 1.7 | -2.4 | -36 - -35 | -36 |
| EU1-4 | 0.44 - 0.57 | 0.61 | 156 - 161 | 178 | 0.88 - 1.21<br>1.18 - 1.21 | 1.19 | 2.8 - 3.1 | 3.1 | 2.6 - 3.0 | 3.9 | -29 - -28 | -32 |
| EU3-2 | 0.66 - 0.72 | 0.66 | 141 - 148 | 157 | 1.46 - 1.56<br>-<br>1,56 - 1.64 | 1.38 | 1.5 - 1.8 | 0.7 | -6.4 - -6.0 | -7 | -36 - -34 | -36 |
| EU3-3 | 0.98 - 1.04 | 1.02 | 185 - 192 | 203 | 1.56 - 1.64<br>1.94 - 2.06<br>1.95 - 2.20 | 1.99 | 3.2 - 3.6 | 2.5 | -1.6 - -1.0 | -2.9 | -33 - -32 | -33 |
| EU3-4 | 1.14 - 1.21 | 1.21 | 224 - 228 | 229 | 2.08 . 2.20<br>1.64 - 1.81<br>2.12 - 2.30 | 2.21 | 4.5 - 4.8 | 3.9 | 3.8 - 5.0 | 2.8 | -32 - -30 | -31 |

**Tab. 3.4:** Comparison of the experimental and computational data of EU experiments which were selected for post test calculations (continued).

| Test | Mass Flow [kg/s] | | Temperature in outlet line [°C] | | Capacity [MW] | | Pressure drop in | | | | | |
|------|---------|-----|---------|-----|---------|-----|---------|-----|---------|-----|---------|-----|
| | | | | | | | inlet line [kPa] | | bundle [kPa] | | outlet line [kPa] | |
| | measure | ATH | measure | ATH | measure | ATH | measure | ATH | measure | ATH | measure | ATH |
| EU4-1 | 0.63 - 0.68 | 0.59 | 151 - 155 | 178 | 1.34 - 1.47 1.20 - 1.45 1.40 - 1,45 | 1.18 | 1.4 - 1.7 | 0.4 | -6.8 - -6.2 | -6.5 | -35 - -34 | -35.2 |
| EU5-2 | 0.73 - 0.83 | 0.75 | 141 - 146 | 164 | 1.60 - 1.80 - -1.74 - 1.82 | 1.55 | -0.15 - 0.05 | -0.8 | -9.5 - -9.0 | -1.03 | -35 - -34.7 | -35.7 |
| EU5-4 | 1.57 - 1.67 | 1.56 | 227 - 235 | 245 | 2.80 - 2.92 - 2.75 - 2.81 | 2.68 | 2.2 - 2.9 | 1.4 | -2.4 - -1.8 | -3.1 | -31 - - 28.5 | -28.6 |
| EU5-6 | 2.05 - 2.16 | 2.11 | 277 - 282 | 276 | 3.05 - 3.30 2.72 - 2.90 2.96 - 3.13 | 3.29 | 4.9 - 5.5 | 3.9 | 5.0 - 6.0 | 3.1 | -24.8 - -23 | -22.9 |
| EU6-2 | 1.16 – 1.26 | 1.24 | 198 - 203 | 219 | 2.21 - 2.42 - 2.22 - 2.33 | 2.27 | 0.1 -1.0 | 4.2 | -5.5 - -5.8 | -5.7 | -32 - - 31.6 | -31.6 |
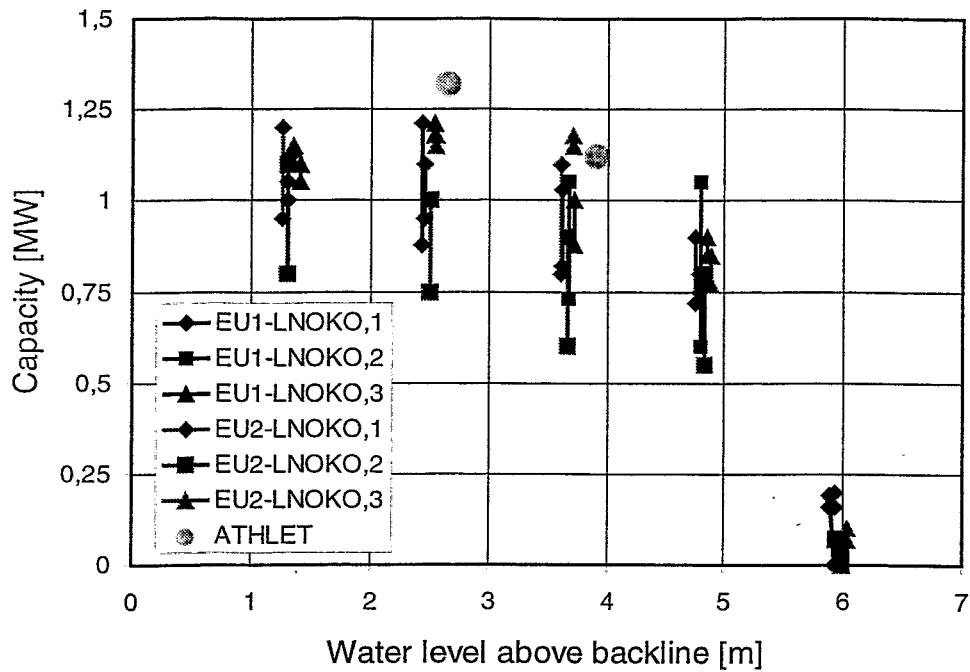
**Fig. 3.12:** Comparison of the experimental and computational values of the bundle capacity for a primary side pressure of 1 MPa.
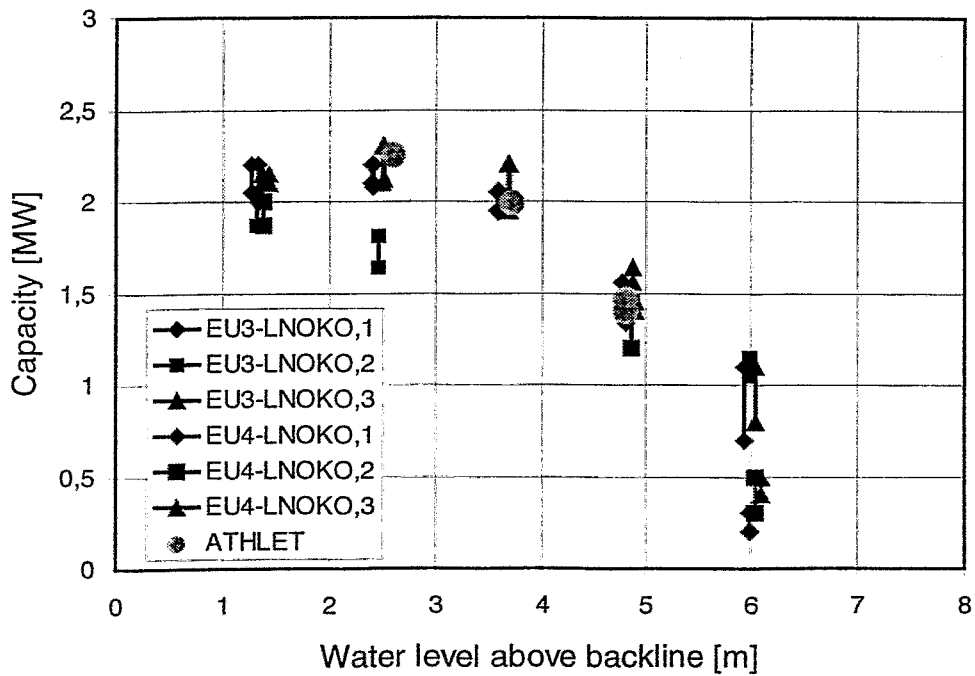


**Fig. 3.13:** Comparison of the experimental and computational values of the bundle capacity for a primary side pressure of 3 MPa.
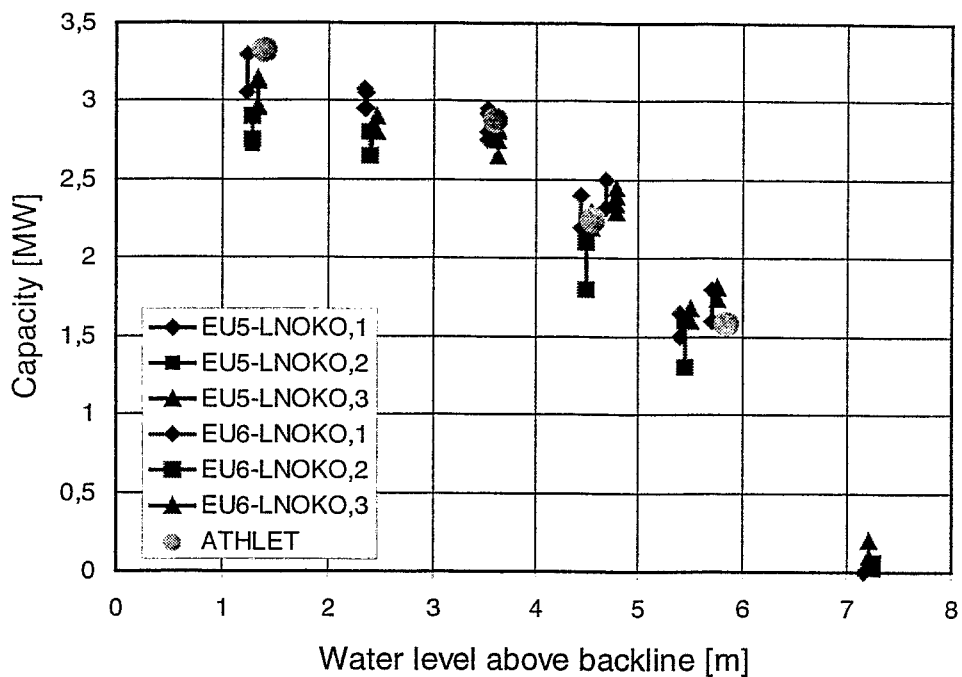
**Fig. 3.14:** Comparison of the experimental and computational values of the bundle capacity for a primary side pressure of 7 MPa.

The general problems of the post test calculations are that for each test only few experimental data are available. These are as described the temperature at the outlet, the pressure drops in the emergency condenser system and the capacity. For a code validation it would be beneficial to have more experimental data, e.g. the history of the temperature distribution in the different cross section areas, steam and condensate velocities, heat transfer coefficients and at least the heat flux density. In the single tube experiments the condensate temperature along the tubes was measured at 21 positions. But these data are not available up to now. Therefore in the last BWR/CA meeting the partners make the suggestion to compare the computational data of these values.

For understanding the different physical phenomena the histories of steam and condensate velocities, heat transfer coefficients, temperature distribution along the tube and heat flux density are plotted versus tube length for a pressure in the pressure vessel of 7 MPa. Additionally the flow map of TANDON was used for the determination of the flow regimes. Here the dimensionless steam velocity of Wallis $j_D^*$ is given as a function of the quotient of the condensate and void fraction $(1-\varepsilon)/\varepsilon$ (compare Chap. 3.3).

Fig. 3.15 shows the changing of the flow regimes in an emergency condenser tube for the tests EU5-2 and EU5-6. In both tests the pressure in the pressure vessel was about 7 MPa. In the test EU5-2 a water level in the pressure vessel of 5.9 m was adjusted and in EU5-6 a water level of 1.3 m. In the test EU5-2 at the inlet of the tube a transition regime between annular and stratified flow establishes. After nearly 3 m stratification dominates. Slugs occur between 4 and 5 m followed by plugs. In the test EU5-6 the calculation first shows an annular flow, than at 6 m the transition regime is reached. After 7.2 m slugs occur and after 9 m plugs.
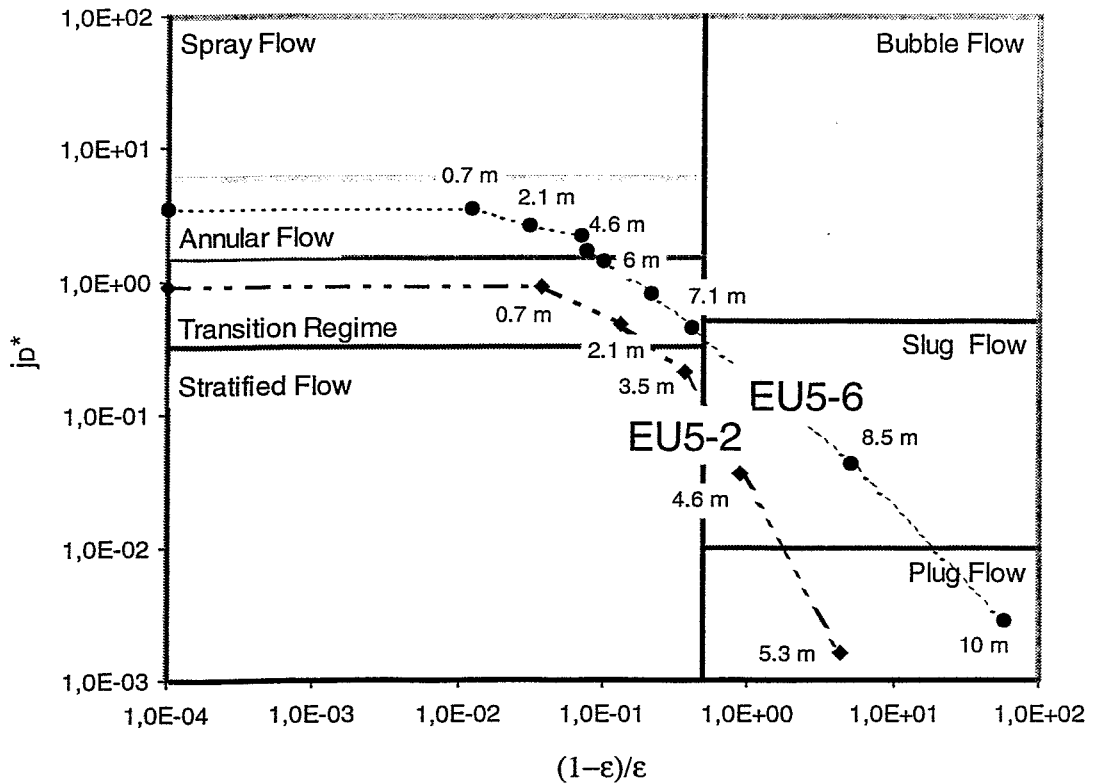


**Fig. 3.15:** Flow regimes inside the emergency condenser tubes for tests EU5-2 and EU5-6.

The Fig. 3.16 and 3.17 show the steam and condensate velocities of these experiments. The steam velocity at the tube inlet is in EU5-6 more than two times higher than in EU5-2. Therefore in EU5-6 the interfacial shear dominates towards the gravity and a symmetrical condensate film is formed. After a decrease of the steam velocity up to 5 m/s stratification occurs, and the condensate collects in the tube sump. Because the steam velocity at the entrance is too low in EU5-2 no annular flow adjusts.
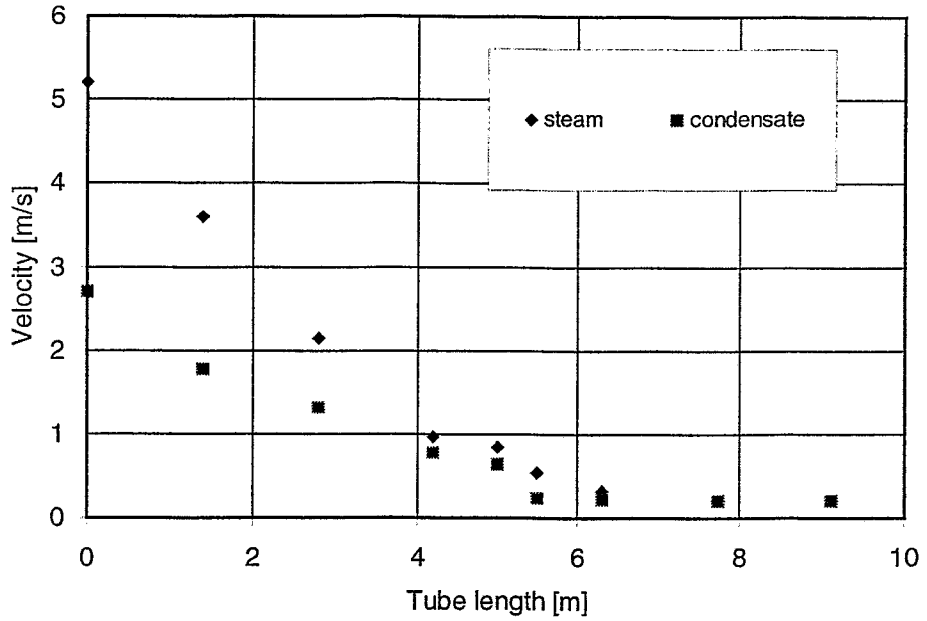
**Fig. 3.16:** Steam and condensate velocity inside the emergency condenser tube for EU5-2.
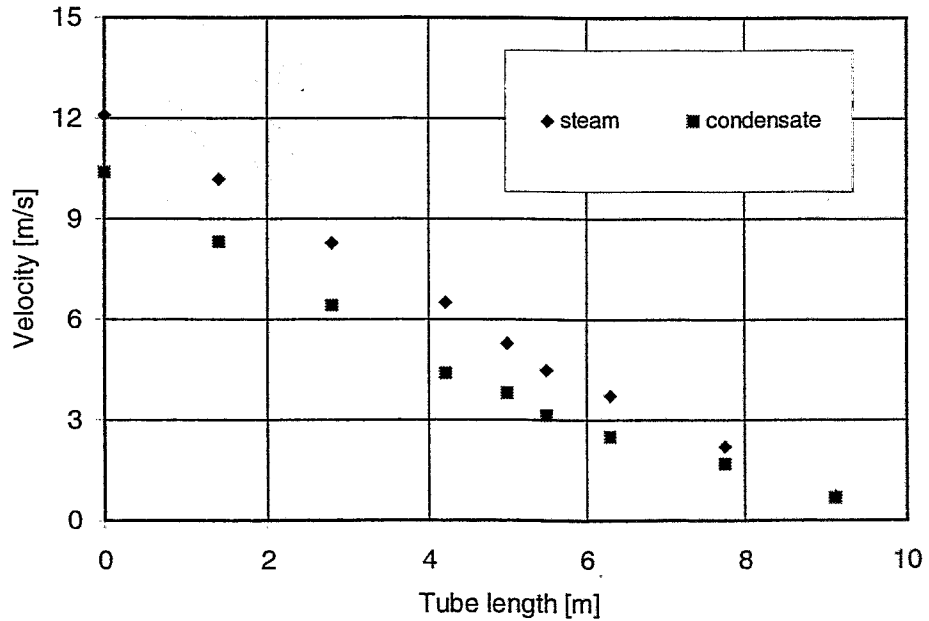


**Fig. 3.17:** Steam and condensate velocity inside the emergency condenser tube for EU5-6.

In Fig. 3.18 and 3.19 void and mass quality is plotted versus tube length. These Fig. show the different bundle uncovery (nearly 50% in EU5-2, nearly 100% in EU5-6). The uncovery is directly proportional the condensate mass flow rate and the driving temperature difference (compare Fig. 3.20 and Fig. 3.21).
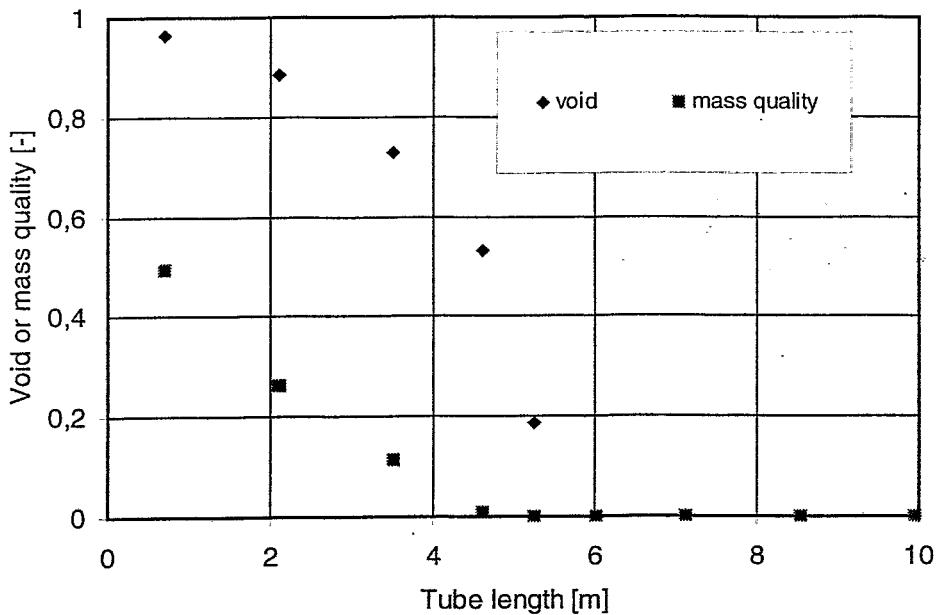


**Fig. 3.18:** Void and mass quality for EU5-2.
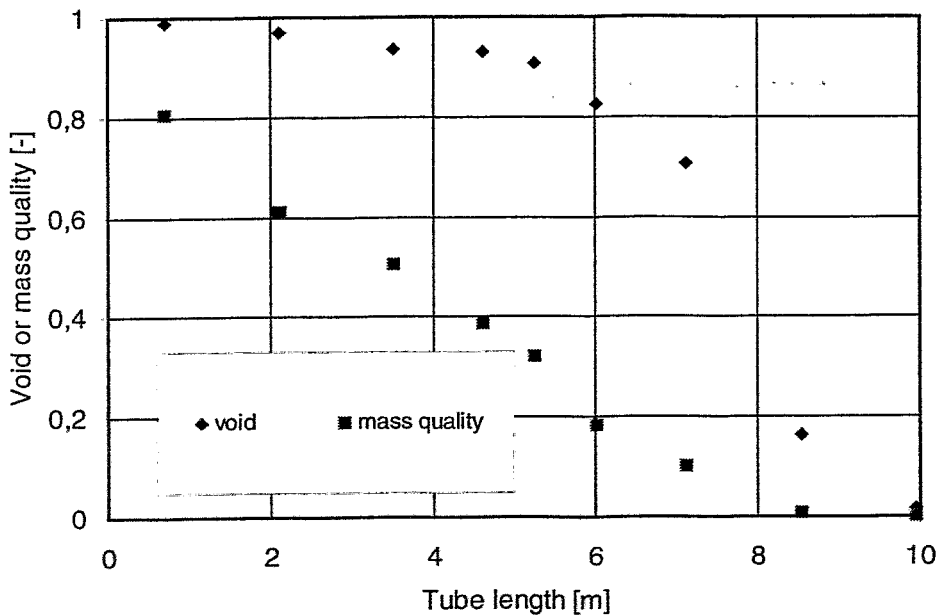


**Fig. 3.19:** Void and mass quality for EU5-6.

Fig. 3.20 and 3.21 show the temperature distribution in different cross section areas. It can be seen that the fluid temperature in the case of annular and stratified flow and in the transition regime is nearly constant. The wall temperature at the inner tube surface decreases with leaving the annular flow regime, because of the decrease of the heat transfer coefficients (compare Fig. 3.22 and 3.23).
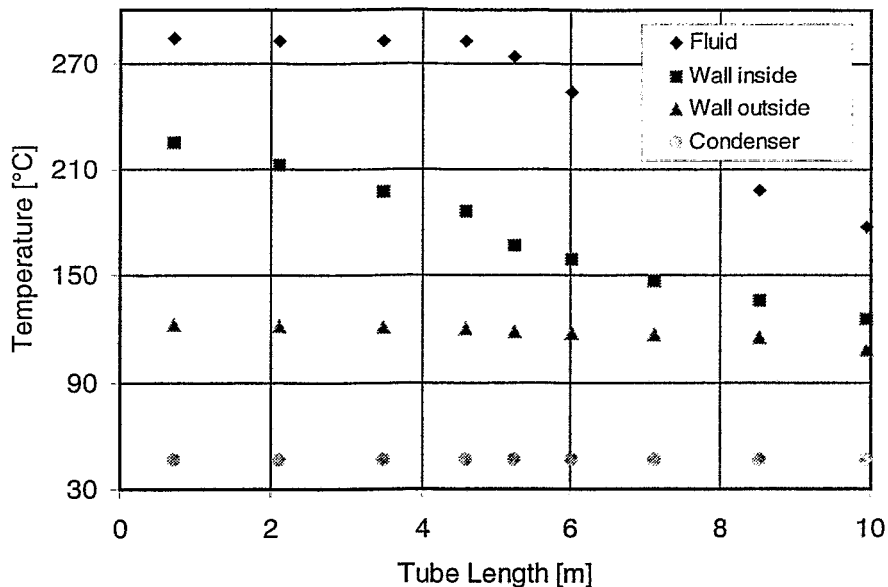


**Fig. 3.20:** Temperature distribution for EU5-2.

In the Fig. 3.22 and 3.23 the heat transfer coefficient at the inner and outer surface are plotted versus tube length. Additionally it has to be mentioned that the heat conduction coefficient of the tube is in a magnitude of 5200 W/m²K.

In EU5-2 the heat transfer coefficients at the outside surface indicate in the first region (nearly 5 m) a transition regime from boiling to free convection. Afterwards single phase free convection has adjusted. Inside the tube the heat transfer first decreases due to the accumulation of condensate in the cross sectional areas. After total condensation a single phase condensate establishes with a low heat transfer coefficient of nearly 1800 W/m²K, which is now the mean heat transfer resistance.
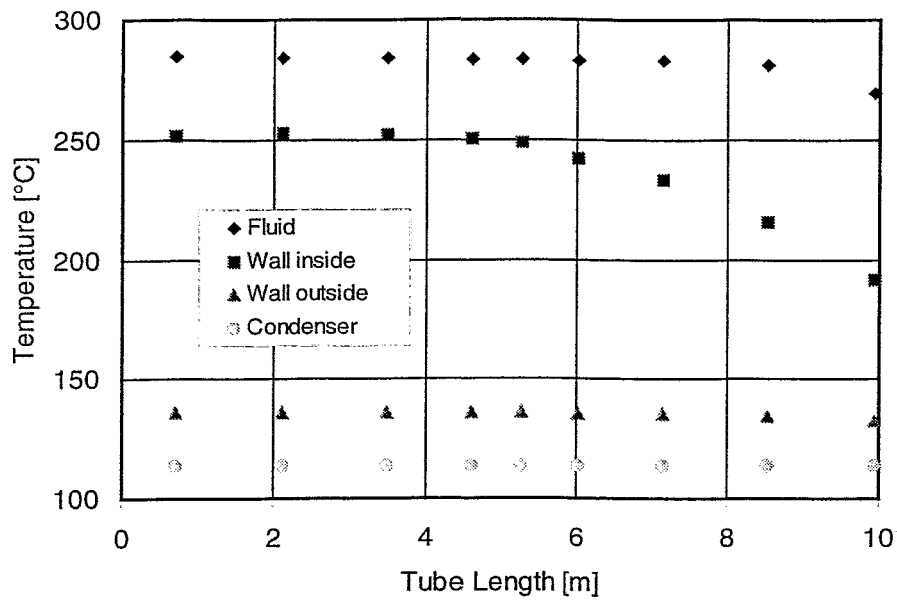
**Fig. 3.21:** Temperature distribution for EU5-6.
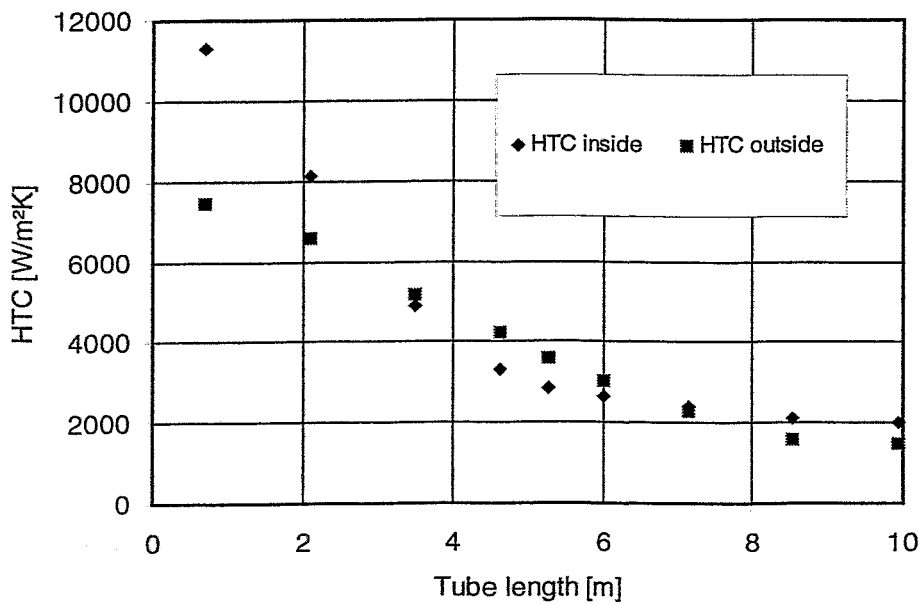


**Fig. 3.22:** Heat transfer coefficients for EU5-2.

The history of the heat transfer coefficients for EU5-6 is different from EU5-2. During the annular flow regime the heat transfer coefficients are nearly constant and negligible in comparison to the resistance of the wall. During the transition regime the inner heat transfer coefficient decreases. This decrease is continuing in the slug and plug flow regime. At the end of the tube the heat transfer coefficient inside the tube and the heat conduction coefficient of the wall are in the same magnitude. During all the time boiling occurs outside. The heat transfer decreases due to the decrease of the heat transfer resistance at the inner surface as described above.
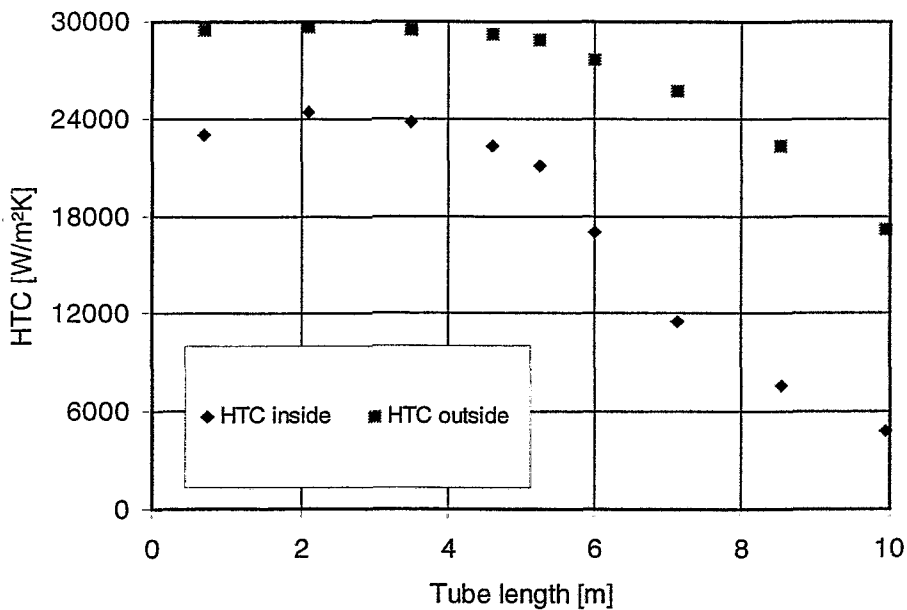


**Fig. 3.23:** Heat transfer coefficients for EU5-6.

The history of the heat flux density of EU5-2 and EU5-6 is evident from the history of the other parameters. In EU5-2 a continuous decrease of the heat flux density is observed due to the transition of the flow regimes. However the heat flux density in EU5-6 is nearly constant during annular flow (that means fully developed boiling outside). The decrease of the heat transfer coefficients starts with the transition to other flow regimes and the resulting decrease of the heat transfer coefficients.
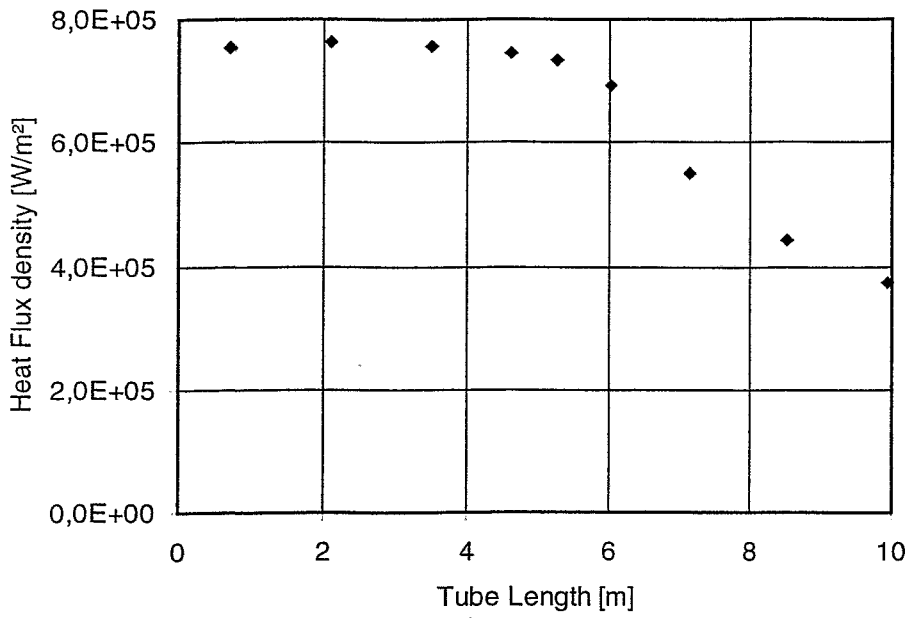
**Fig. 3.24:** Heat flux for EU5-2.
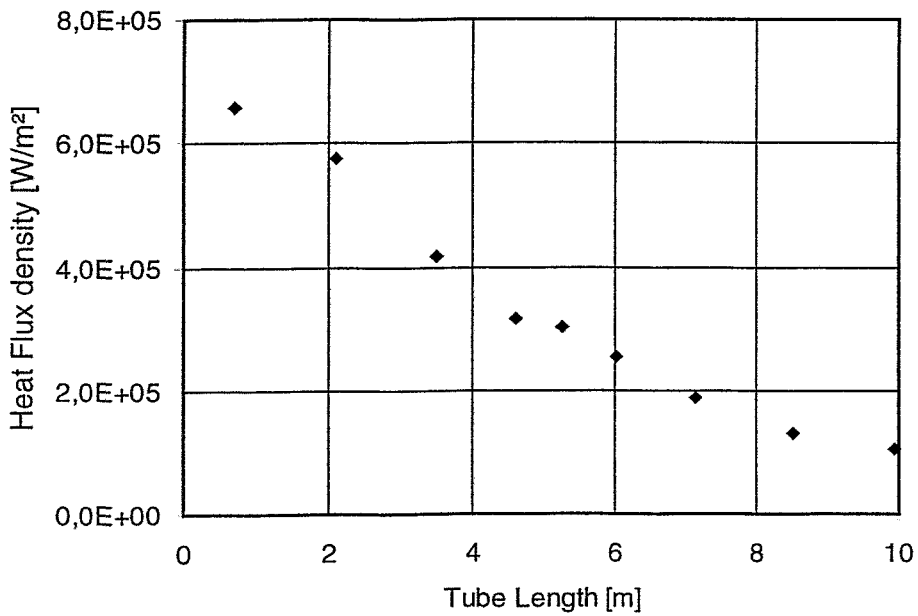


**Fig. 3.25:** Heat flux for EU5-6.

## 3.7    Blind Calculation

FZR has participated at a blind post calculation of a steady state emergency conden-
ser test. The selected test (B6-2) was performed within the German framework
"Emergency Condenser for medium Boiling Water Reactor – experiments to deter-
mine the Condenser performance", the data are available within the BWR Cluster
and the BWR/CA. The initial and boundary conditions of the test are given in [JAH-
97] as follows:

| | |
|---|---|
| pressure in pressure vessel | 1.05 MPa, |
| water level in pressure vessel | 2.5 m, |
| water level in condenser | 1.58 m, |
| water temperature in condenser | 132 °C |
| pressure in condenser | 0.3 MPa. |

The main measured values of the test are the mass flow $M_{NOKO}$, the temperature at
the outlet $T_{NOAB}$ and the capacity of the emergency condenser (see Fig. 3.11). The
capacity of the bundle is determined by three independent energy balances (balance
of the emergency condenser bundle $L_{NOKO,1}$, of the condenser $L_{NOKO,2}$ and of the
whole primary circuit containing the electrical heater loop, the pressure vessel and
the emergency condenser system $L_{NOKO,3}$). The evaluation of the blind experiment
was again performed with CASH-Graphics.

In the following the computational results of these parameters are presented and
compared with the experimental values. It has to be recognized that the ATHLET
calculations start with the opening of the valve in the condenser outlet line. Therefore
the computational data include the fluctuations before reaching the steady state con-
dition. These fluctuations are not stored for the experiments.

Fig. 3.26 and 3.27 show the mass flow in the inlet line of the emergency condenser.
After opening the valve in the outlet line the condensate flows out of the condenser
with a maximum value of 4.5 kg/s and steam is suck in. After nearly 200 seconds
steady state conditions are reached and inlet and outlet mass flow are equal. The
comparison between the computational and the experimental data shows an
excellent agreement.
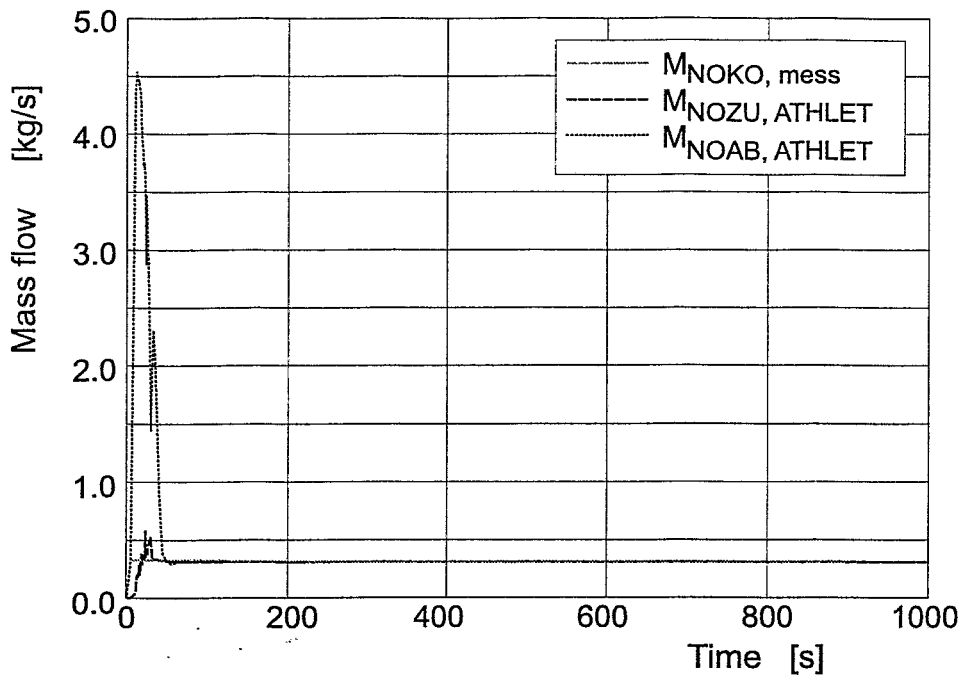
**Fig. 3.26:** Mass flow in the condenser inlet line and outlet line and comparison of the experimental and computational data for mass flow in the condenser inlet line.
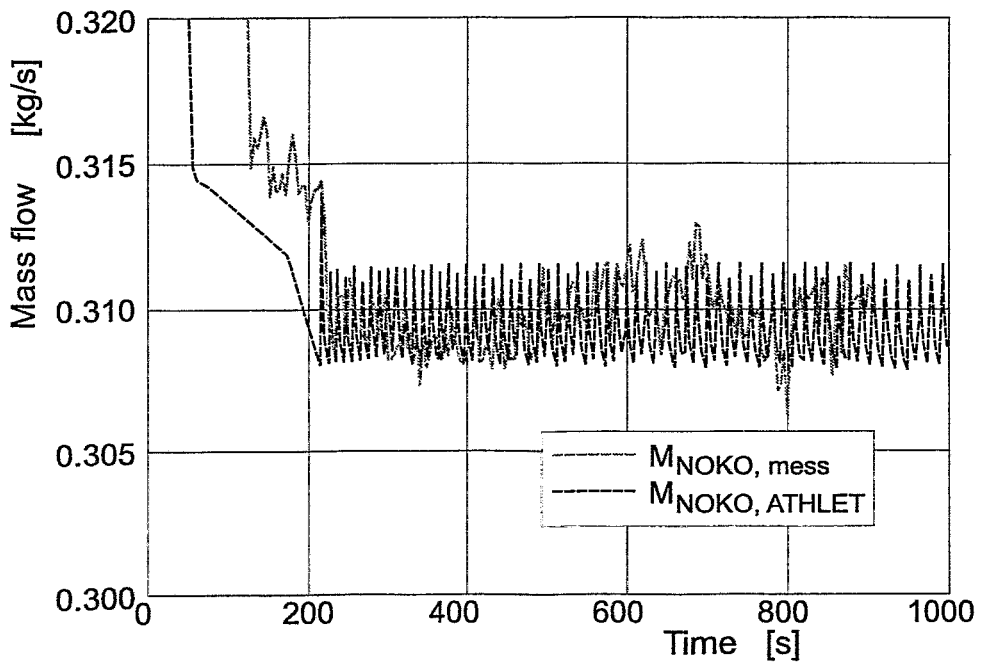


**Fig. 3.27:** Comparison of the experimental and computational data for mass flow in the condenser inlet line (detail viewing - zooming of the ordinate).

Fig. 3.28 shows the temperatures in the inlet and outlet line. The inlet line temperature is equal to the saturation temperature and therefore a boundary condition. Regarding to the operation conditions presented in [4] the outlet temperature depends on the surface area in the bundle which is available for subcooling and the driving temperatures for subcooling which are equal to the difference of the average condensate temperature and the water temperature in the condenser. Both, calculations and experiments show a small subcooling (0.3 K in the tests - 2.5 K in the calculation), the agreement is good. The deviation lay within the magnitude of the uncertainty of the temperature measurement (here 2.5 K).
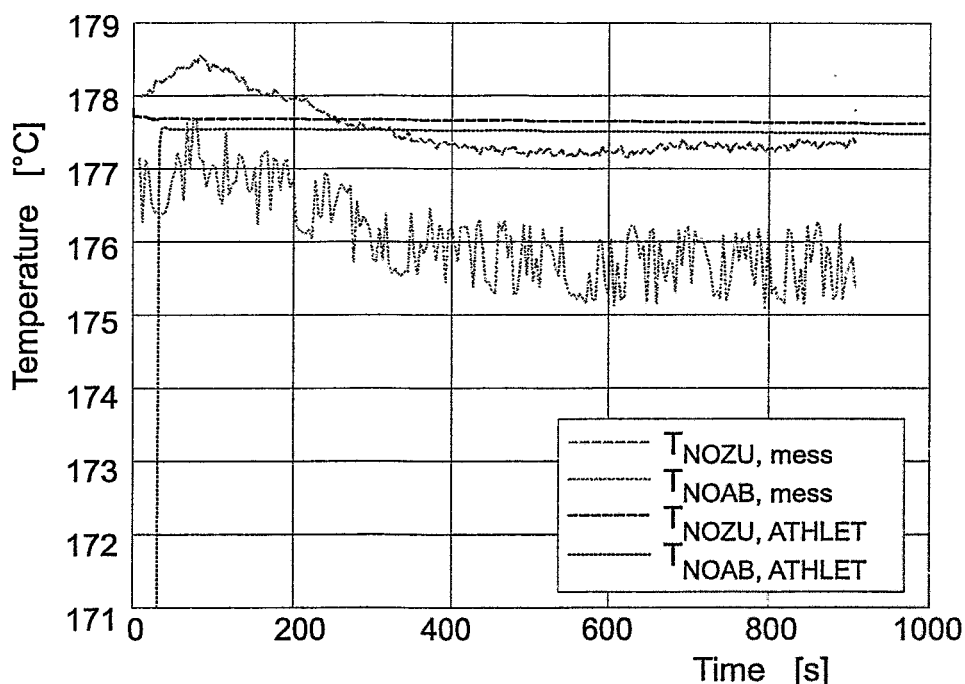


**Fig. 3.28:** Comparison of the experimental and computational data for temperatures in the condenser in- and outlet line.

In Fig. 3.29 the pressure drops in the emergency condenser system are compared with the measured values. In Fig. 3.29 $dp_{2\_2}$ is the pressure drop over the inlet line, $dp_{2\_3}$ over the bundle and $dp_{2\_4}$ over the outlet line. The deviations for the ATHLET calculations lay in the magnitude of 0.66 kPa for $dp_{2\_2}$, 0.27 kPa for $dp_{2\_3}$ and 1.3 kPa for $dp_{2\_4}$. Especially for $dp_{2\_4}$ this seems to be not satisfactory, but it has to recognized that no zero point deviations are available. For other tests these deviations lay in the magnitude of up to 0.6 kPa for $dp_{2\_2}$, up to 1.4 kPa for $dp_{2\_3}$ and up to
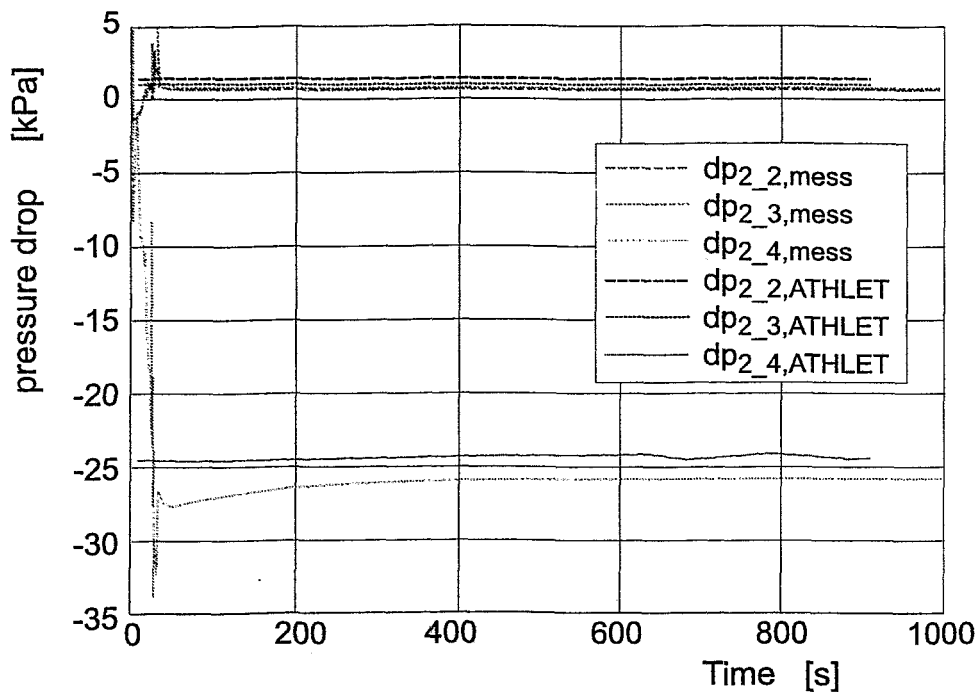
**Fig. 3.29:** Comparison of the experimental and computational data for pressure drops over the inlet line $dp_{2\_2}$, the bundle $dp_{2\_3}$ and the outlet line $dp_{2\_4}$.

1.9 kPa for $dp_{2\_4}$ as shown in [PRM-97]. Regarding the same deviations the calculated data are quite good .

As described in chapter 3.4 the emergency condenser capacity is determined by three independent energy balances. Fig. 3.30 and 3.31 show that the differences of the capacities lay in a magnitude of nearly 100 kW, which is nearly 15% of the measured value. Additionally for the second balance $L_{NOKO,2}$ some problems occur with the water level measurement, which is used for the determination of the inventory of the condenser. Therefore only the time period between 100 and 600 seconds is taken into account for the comparison. Fig. 3.30 and 3.31 show that the calculated capacities lay between the measured capacities and agree very well with the first balance.

The blind test calculation proves again, that the improved version of ATHLET (that means ATHLET coupled with KONWAR) is able to perform proper calculations.
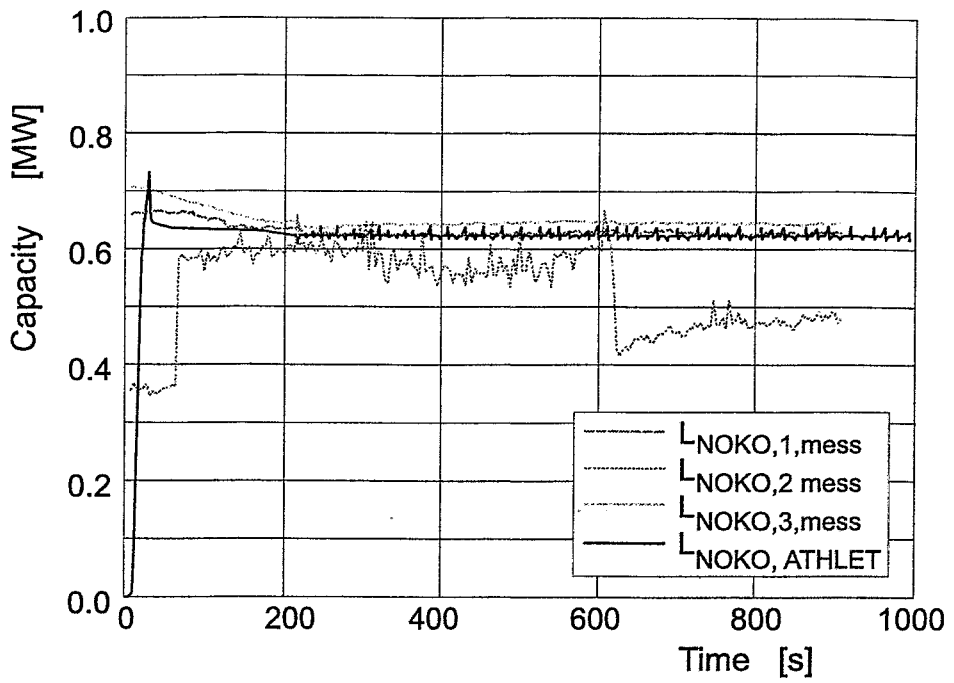
**Fig. 3.30:** Comparison of the experimental and computational data for emergency condenser capacity.
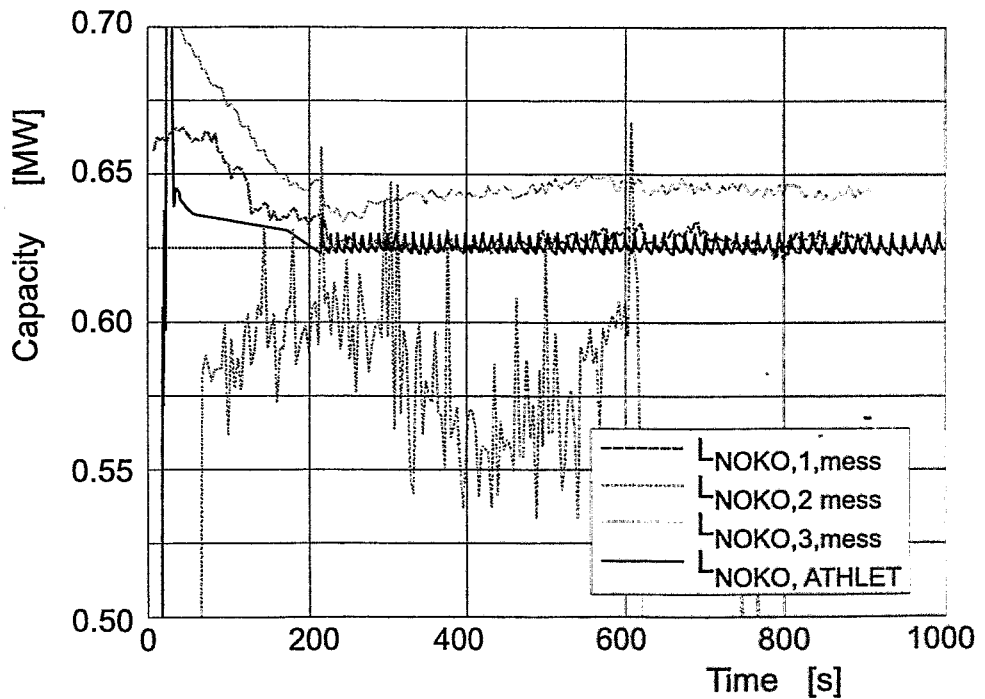


**Fig. 3.31:** Comparison of the experimental and computational data for emergency condenser capacity (detail viewing).

# 4 Optimization of the heat exchanger bundle

Chapter four starts with a review of existing emergency condensers. After a discussion of the main guidelines for an optimization a proposal for a new bundle is presented. A calculation for the suggested bundle was performed for the determination of its thermal hydraulic yield. Afterwards some general suggestions concerning non-condensable gases were added.

## 4.1 Review of the existing bundle design

The first bundle design of the SWR1000 was chosen on the basis of experimental results obtained at the NPP Gundremmingen unit A (compare Fig. 4.1) in test series from the 10th May 1975. In these tests, published in [PAC-75], a heat exchanger of 2 bundles with 52 tubes each was able to remove a thermal power of up to 70 MW (see Fig. 4.2). The intention for the SWR1000 was to obtain a total heat removal capacity of about 300 MW at nominal primary pressure. This was done by increasing the number of tubes from 104 in Gundremmingen to 4 x 104 = 416 tubes.

A bundle of 4 tubes of this kind was tested in the NOKO facility in Jülich. It has been found that the effectiveness is much higher than the value extrapolated from the Gundremmingen data. The lower heat removal capacity found in Gundremmingen can be explained by the specific operation mode, which leads to significant water losses on the secondary side during start-up. The reason for the deviation was discussed in [SCA-962]. Additionally it has to be mentioned that the experiments in Gundremmingen had to relay on the standard instrumentation, while the NOKO facility is extensively instrumented. The quantity of 416 tubes guarantees a thermal capacity of about 370 - 380 MW, if we relay on the NOKO data (Fig. 4.2), which predicts a power of about 0.9 MW per tube (primary pressure 7 MPa, secondary pressure 0.1 MPa) [SCA-962, HIE-97].
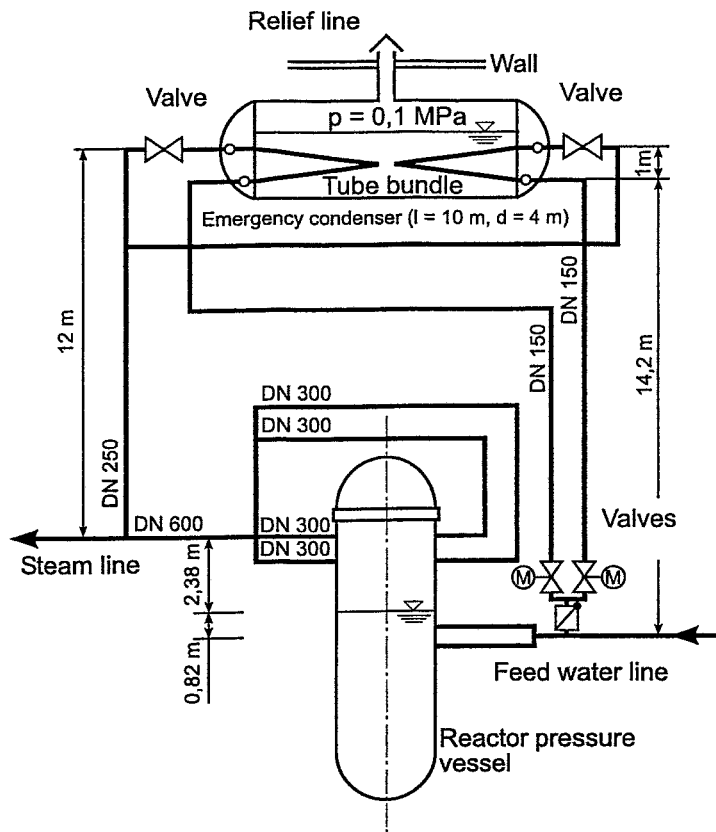
**Fig. 4.1:** Emergency condenser of the NPP Gundremmingen A [PAC-75].
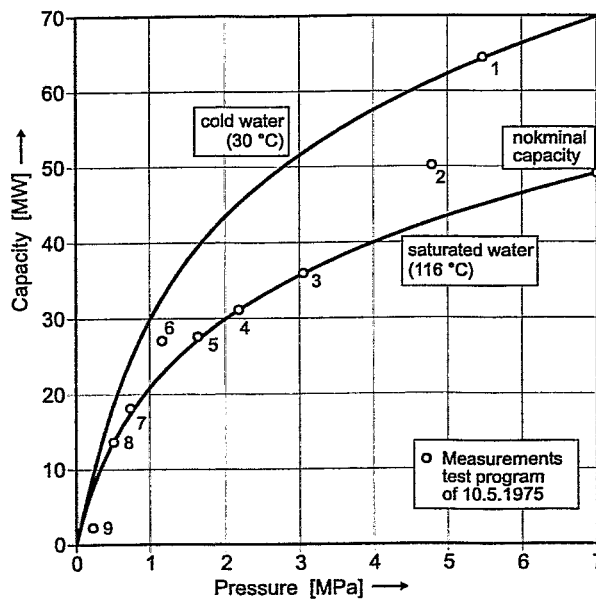


**Fig. 4.2:** Emergency condenser tests at the 10<sup>th</sup> May 1975 in NPP Gundremmingen A [PAC-75].
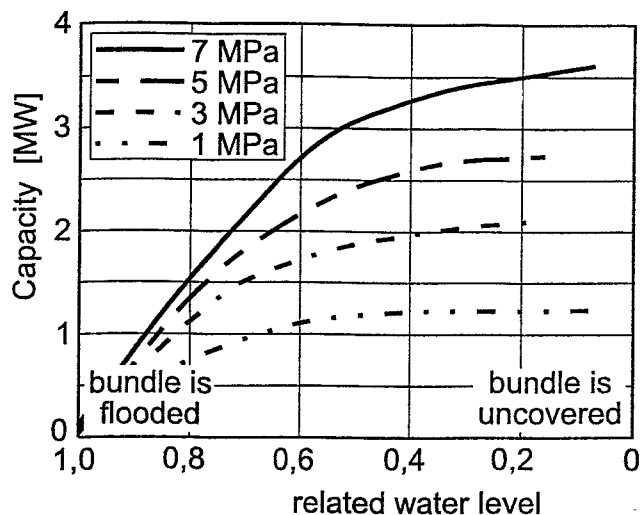
**Fig. 4.3:** Experimental results of the NOKO tests with a four tube test bundle [HIE-97].

## 4.2 Main guidelines for an optimization

This chapter contains possible and desirable measures to optimize the bundle of the emergency condenser. The main topics, which are discussed afterwards are: heat transfer, pressure losses and mechanical loads.

### 4.2.1 Heat Transfer

The increase of the heat transfer coefficient allows to decrease the number of heat exchanger tubes and/or to reduce the dimensions of the emergency condenser. This is desirable because the pressurized circuit of the BWR and the possibilities for leakages could be reduced.

The NOKO bundle operates in the condensation regime inside and subcooled or saturated boiling outside the bundle. The heat transfer of boiling and condensation is very effective. Therefore the resistance of the NOKO tubes is dominated by the thermal conductivity of the wall material. The options to reduce the thermal resistance of the wall are:

the reduction of the wall thickness

or

the use of materials with higher conductivity than the stainless steel 1.4301.

Due to the required corrosional stability stainless steel cannot be substituted. The search must go into the direction of steel with better mechanical properties. This would allow to reduce the wall thickness, which is bound to the requirements of mechanical integrity.

Another possibility would be to reduce the tube diameter (see e.g. Dodewaard), but this will lead to an increased number of tubes in the bundle and is contradicted to the aim of the optimization.

## 4.2.2  Pressure Losses

The uncovery of the NOKO bundle is set by the mixture level inside the pressure vessel and influenced by the pressure losses in the NOKO system (e.g. feed line, bundle and back line). The smaller the pressure drop, the earlier the uncovery takes place. Additionally the heat removal starts earlier.

The pressure drop can be decreased by:

increasing the diameter of the tubes,

increasing the number of the tubes

and

reducing the liquid inventory of the tubes by applying larger inclinations.

The individual possibilities particularly contradict the goals of the optimization of the heat transfer. The optimization has to be carried out commonly for both goals. Therefor a pay-off function has to be formulated. This pay-off function has to consider safety parameters, which have not been quantified up to now. Additionally the optimization must be accompained by accident simulation calculations.

## 4.2.3  Mechanical Loads

Deficiences of the present construction are

thermostresses in the inlet collector due to water level fluctuations during

normal plant operation,

bundle oscillations during NOKO operation

and

plastic deformations of the heat exchanger tubes due to the high temperature gradients combined with the inner pressure.

Improvements are contributions to the increase of the mechanical integrity of NOKO during normal operation and in the case of request. The proposed measures are therefore:

the increase of the elevation of the inlet collector,

the development and analysis of fixing constructions

and at least

the analysis of thermal stresses and conclusions concerning the necessary material and wall thickness.

## 4.3 Proposal for a new optimized bundle

General proposals have been discussed in chapter 4.2 to optimize the bundle of the emergency condenser of the SWR1000. Siemens has similar ideas and proposes to change the material of the NOKO tubing from the stainless steel X5CrNiMo1810 (1.4301) to Remanit 4462 (1.4462). Remanit disposes of a significantly higher strength than X5CrNiMo1810. In the following results of thermal hydraulic calculations carried out for a single tube made from the new material are presented. Further some additional proposals concerning the overall design of the emergency condenser are made.

A further opportunity to minimise the dimensions of the bundle is given by a less conservative approach. Without changing neither the material nor the geometry of the heat exchanger tubes the number of tubes can be reduced by approximately 20 %. The minimised design would be then able to remove 10 % of the nominal power,

which is still containing a safety factor of at least 1.5 in comparison to the maximum decay heat. For the further discussion, the NOKO results can be transferred to modified bundle designs by the help of the analytical model proposed in [SCA-962]. It is based on the thermal hydraulic code ATHLET extended by the module KONWAR calculating the heat transfer coefficients at the primary side. The model was verified against experimental data from the NOKO test facility.

## 4.3.1 Thermal hydraulic yield of the new material

The higher yield strength of Remanit 4462 allows to decrease the wall thickness of the heat exchanger tubes. According to an information from Siemens [MEJ-97], in the same time, additionally an increase of the diameter was proposed. The main parameters of the two bundles are given in Table 4.1.

**Table 4.1:**　Main parameters of the heat exchanger bundles.

| Parameter | Design | |
|---|---|---|
| | old bundle | new bundle |
| number of tubes | 4 x 104 | to be determined |
| material | 1.4301 | 1.4462 |
| inner diameter, mm | 38.7 | 51.1 |
| wall thickness, mm | 2.9 | 1.9 |
| total bundle surface, m$^2$ | 570 | to be determined |

On the basis of the design data presented in [MEJ-97] a steady state calculation of the new bundle was performed with the thermal hydraulic computer code ATHLET Mod 1.1 Cycle C coupled with KONWAR. The results were compared to calculations of the old bundle performed for the BWR/CA (compare Chap. 3). The thermal conductivity of Remanit 4462 used in the calculations is given in Table 4.2. It is slightly lower then that of the old material.

The calculations were carried out for a single heat exchanger tube of both kinds at nominal reactor pressure and with cold water at the secondary side of the emergency condenser. The tube was assumed to be completely depleted. The most important results are given in Table 4.3.

**Table 4.2:** Thermal conductivities of the steels 1.4301 and 1.4462.

| Steel | Temperature in deg. C | | | |
|---|---|---|---|---|
| | 20 | 100 | 200 | 300 |
| 1.4301 | 15 | 16 | 18 | 19 |
| 1.4462 | 14 | 15 | 17 | 18 |

**Table 4.3:** Thermal hydraulic parameters of a single tube of both designs.

| Parameter | Design | |
|---|---|---|
| | old tube | new tube |
| total power, MW | 0.9 | 1.4 |
| inlet velocity of steam, m/s | 15.5 | 12.0 |
| required number of tubes for 300 MW total | ≈330 | ≈210 |
| proposed bundle design | 4 x 84 = 336 | 4 x 52 = 208 |
| economy of total heat exchanger surface | ≈20 % | ≈38 % |

The effect of the proposed new tubing is clearly illustrated by the decrease of the heat exchanger surface and the reduction of the overall dimensions of the emergency condenser. Any decrease of the total surface is of great safety relevance, because the emergency condenser belongs to the primary circuit and the pressurized parts can be reduced. The possibility for leakages is minimized.

A second effect is given by the reduction of the steam velocity due to the larger diameter. In the result the pressure drop is decreased significantly, which improves the operation with partially uncovered tube bundle (e.g. during start-up). The uncovery of the bundle happens earlier, because the difference between the water levels in the reactor and in the primary side of the emergency condenser is decreased. The lower steam velocity causes a small decrease of the heat transfer coefficient at the primary side. This negative effect is overcompensated by the decrease of the thermal resistance of the wall. Further, the higher power leads to an higher heat transfer coefficient for the boiling at the secondary side. The heat transfer coefficients are plotted versus tube length in Fig. 4.4. In Fig. 4.5 the heat flux densities of both designs are compared.
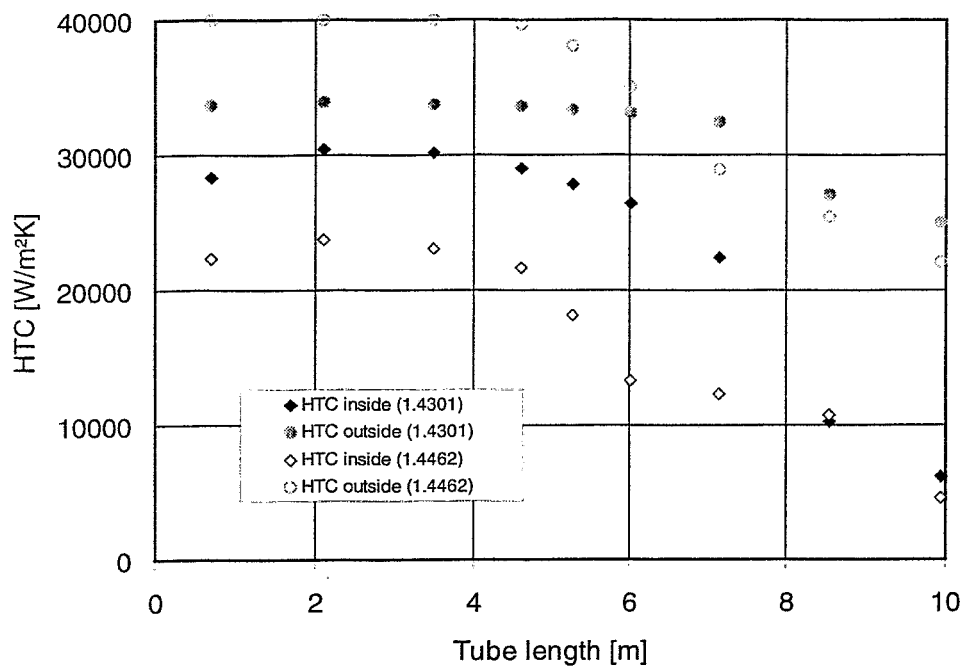
**Fig. 4.4:** Comparison of the heat transfer coefficients at the inner and outer tube surface for X5CrNiMo1810 (1.4301) and Remanit (1.4462).
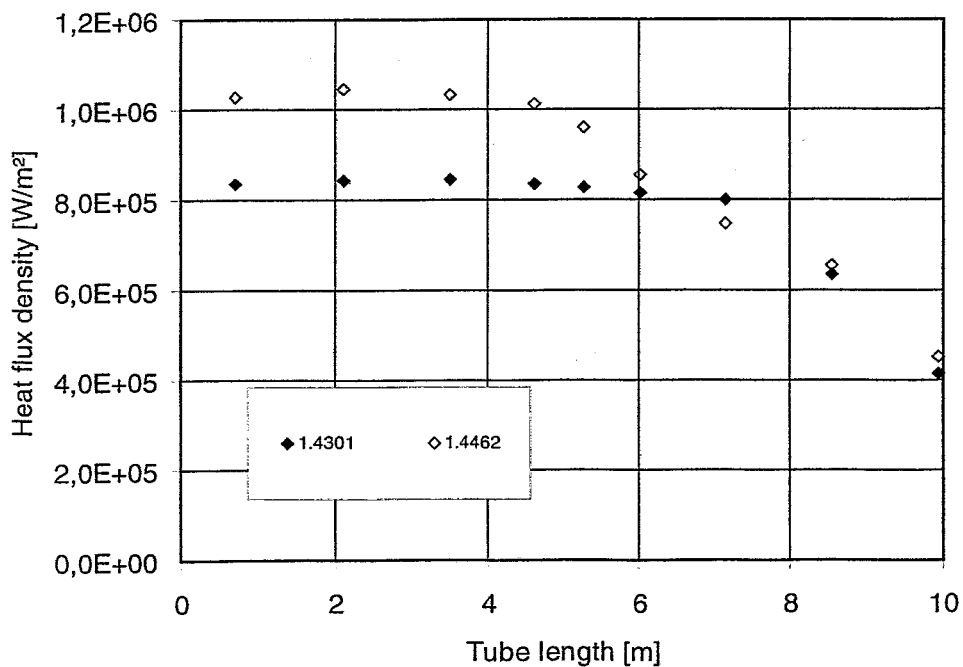


**Fig. 4.5:** Comparison of the heat flux densities of the tubes of X5CrNiMo1810 (1.4301) and Remanit (1.4462).

The lower steam velocity leads to a smaller momentum of the two-phase flow inside the heat exchanger tube. This is illustrated in Fig. 4.6, where the characteristic of the flow regimes over the tube length is plotted into the flow map of Tandon [TAT-82]. For each node of the ATHLET model the related steam velocity according to Wallis is plotted versus the fraction of liquid and void. The tube length is given as a parameter.

Due to the lower steam velocity the region of annular flow is less extended in the Remanit tube. Further, the flow map predicts lower probability for slugs and plugs. The region of stratified flow becomes more significant. This is the explanation for the lower heat transfer coefficient at the primary side (see Fig. 4.4).
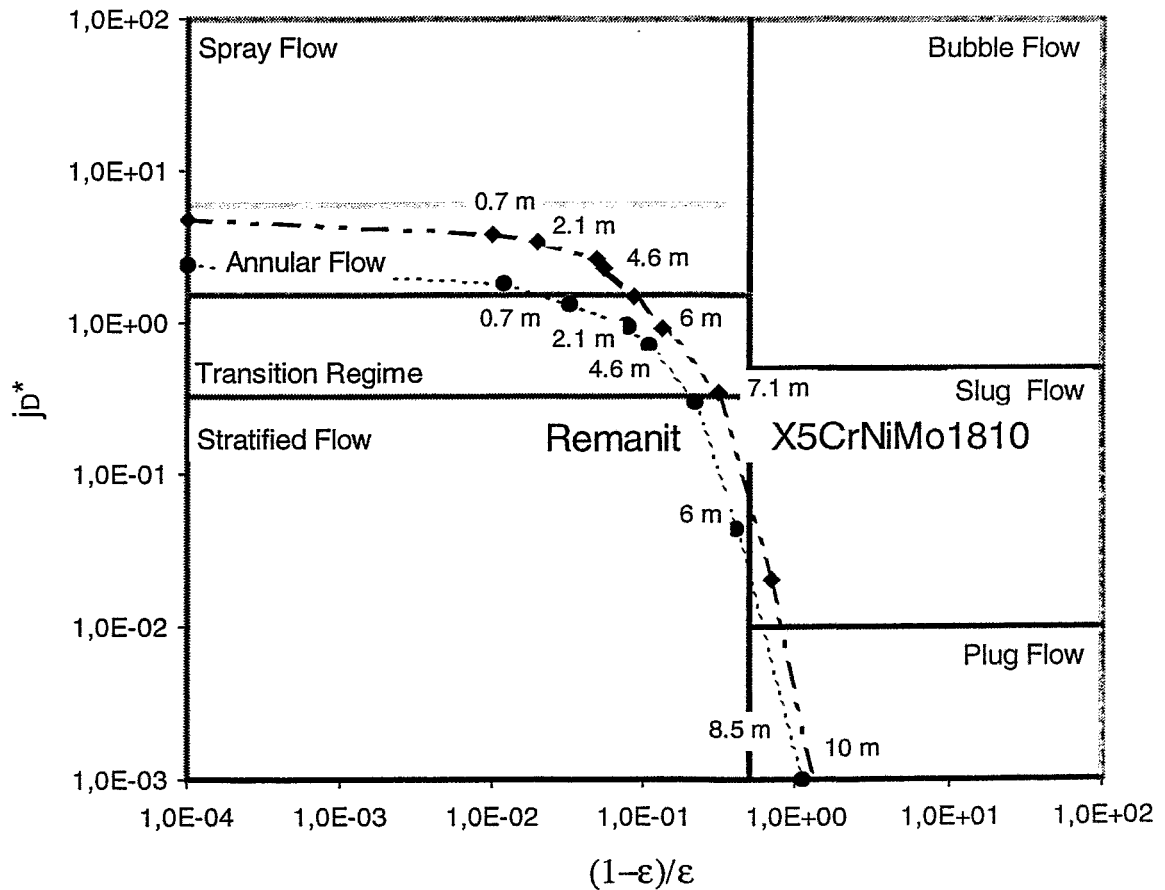


**Fig. 4.6:** Comparison of the flow regimes for the emergency condenser tubes consisting of the stainless steel X5CrNiMo1810 and Remanit.

## 4.3.2 Non-condensables

Up to now, the question of the role of the emergency condenser during severe accidents with high amounts of non-condensables is still under discussion. Other sources of significant amounts of non-condensables are not known, and most likely not existing. In the present construction of the NOKO-bundle low quantities (several ppm) of non-condensables are dissolved in the condensate. A danger of non-condensable concentration is not given. The capability of the heat exchanger bundle to remove non-condensables inherently is not finally investigated. Large quantities definitely lead to condensation blockage [PRM-97], and cannot be removed with the condensate because of the vertical orientation of the bends of the tubes.

Independently of the relevance of non-condensables, FZR prefers a bundle design with a slightly inclined orientation of the tube bends comparable to Dodewaard [SCA-962]. In this case, bubbles of non-condensable are transported to the outlet collector by the drag of the condensate flow. A similar effect was observed by needle probes during several NOKO single tube tests, when the water level was already behind the tube bend, but still above the lower probe assembly [PRM-97]. The water flow was carrying gas bubbles long before the level arrived at the probes.

Additional measures have to be taken to remove the gases from the collector, e.g. by an additional venting tube, connecting the top of the collector with the reactor vessel. This is still subject to further discussions.

# 5   Conclusions and Outlook

Within the Physics and Thermalhydraulics Complementary Actions to the BWR Cluster (BWR/CA) the Forschungszentrum Rossendorf (FZR) e.V. has performed extensive work on the theoretical support of the NOKO experiments. The work was divided into the three topics: Implementation of two phase flow instrumentation, ATHLET calculations of NOKO experiments and approach for the optimization of passive components.

FZR is developing special two phase instrumentation (needle probe, wire-mesh sensors), which was installed in several test facilities (e.g. PKL, ISB, PHDR, PMK, NOKO). The NOKO tests were performed to provide experimental data for the validation of the improved condensation model in ATHLET - especially the clarification of the changing of the flow regimes during condensation inside the emergency condenser tubes. During the experiments annular and stratified flows were detected in the expected geometric and temporary lengths, but no slugs and plugs could be proven. This can be explained by the accumulation of large amounts of non-condensables in front of the water level. Because of the missing shear stresses at the phase interface no slugs and plugs were formed. An additional reason is that the geometric length, in which the different flow regimes should occur, were predicted by using steady state flow regime maps. Maybe the characteristic length (here $L/D \approx 15$) is too small for the formation of slugs and plugs.

Therefore there is an additional need for further single tube experiments with an improved instrumentation. First the reason for the accumulation of the non-condensables must be clarified. These experiments should be performed with an improved instrumentation taken into account that the standard instrumentation of the NOKO facility is designed for bundle design. Therefore it doesn't fit the parameters of the single tube operation. The installation of additional two phase flow instrumentation provides new detailed insights into the NOKO tube (e.g. information about flow regimes, the distribution of non-condensables), which are important for code validation.

The post test calculations of the NOKO experiments presented in this report prove qualitatively and quantitatively the expected operation mode and the capacity of the emergency condenser. Additionally the blind calculation proves, that the improved version of ATHLET (ATHLET coupled with KONWAR) is able to perform proper calculations.

At least a suggestion for an optimization of the emergency condenser bundles has been made. The intention is to increase the heat transfer, which allows to decrease the number of heat exchanger tubes and the emergency condenser dimensions. This is desirable because it reduces the surface of the pressurized BWR circuit and the possibilities for leakages, which is a safety relevant task. The options to reduce the thermal resistance of the wall are e.g.:

- the reduction of the tube wall thickness,

or

- the use of materials with higher thermal conductivity.

For this a material with a higher mechanical parameters should be used. A possible candidate is the austenitic-ferritic duplex steel REMANIT. At the same time it is desirable to increase the inner diameter of the tube to limit the increase of the pressure losses caused by the higher mass flows. A further opportunity to minimize the dimensions of the bundle is given by a less conservative approach.

# Literature

[AUH-90]     H. Austregesilo. T. Voggenberger. *"The general control simulation mo-dule GCSM within the ATHLET code"*, GRS-A-1660, April 1990.

[BRW-961]    W. Brettschuh, K. Wagner. *"SWR1000 – Das innovative Siedewasser-reaktorkonzept"*, Atomwirtschaft-Atomtechnik 41 (1996), No. 4, p. 244 – 247.

[BRW-962]    W. Brettschuh, K. Wagner. *"SWR1000 – Konzept zur Beherrschung schwerer Störfälle"*, Proceedings of the Annual Meeting on Nuclear Technology, Topical Report „Reactor Safety", 21.-23.5.1996 in Mann-heim, p. 25 - 38.

[EZG-951]    G. Ezsöl, A. Guba, L. Perneczky, H.-M. Prasser, F. Schäfer, E. Krepper. *"1% cold leg breakexperiment on PMK-2 - Test results and computer code analysis."* Report Forschungszentrum Rossendorf, FZR-76, March 1995.

[EZG-952]    G. Ezsöl, A. Guba, H.-M. Prasser, F. Schäfer. *"Small cold leg break ex-periment on PMK-2."* Proceedings of the Annual Meeting on Nuclear Technology, 16.-18. Mai 1995 in Nürnberg, p. 123-126, ISSN 0720-9207.

[GAM-95]     M. P. Gashenko, A. P. Proshutinsky, H.-M. Prasser, W. Zippe. *"Hot leg break tests at the ISB-VVER integral test facility"*, Proceedings of the Annual Meeting on Nuclear Technology, 16.-18. Mai 1995 in Nürnberg, p. 123-126, ISSN 0720-9207.

[HIE-96]     E. F. Hicken, W. von Lensa. *"Innovative BWR R&D cluster for innovati-ve passive safety systems"*, Proceedings of the Annual Meeting on Nuc-lear Technology, 21.-23. Mai 1996 in Mannheim, p. 298 - 301, ISSN 0720-9207.

[HIE-97]     E. F. Hicken, H. Jaegers, A. Schaffrath. *"Experimentelle Ergebnisse mit der NOKO-Versuchsanlage"*, Proceedings of the Annual Meeting on

Nuclear Technology, 13.-15. Mai 1997 in Aachen, p. 128 - 131, ISSN 0720-9207.

[JAH-97]    H. Jaegers. *"NOKO Experiments for code validation"*, Forschungszentrum, Jülich, INNO-IPPS(97)-D-0, February 1997.

[LEG-96]    G. Lerchl, H. Austregesilo. *"ATHLET Mod. 1.1 Cycle C - User's Manual"*, Gesellschaft für Anlagen- und Reaktorsicherheit (GRS) mbH. GRS - P-1/Vol. 1, Oktober 1996.

[LUD-96]    D. Lucas, H.-M. Prasser. *"Schwankungen des Massenstroms bei Druckentlastungsvorgängen"*, Proceedings of 3. Fachtagung Anlagen-, Arbeits- und Umweltsicherheit, Köthen, 7.-8.11.1996, GVC VDI, p. 233-240.

[MEJ-97]    J. Meseth. *"Personal information: NOKO-Versuche 2. Bündel"*, 5. Februar 1997.

[PAC-75]    C. Palavecino. *"Personal information: Versuchsprotokoll des Notkondensatortestprogramms vom 10.05.1975"*, Dezember 1995.

[PRM-91]    H.-M. Prasser, R. Lotzmann, G. Uhlmann, L. Maroti, P. Windberg. *"Beobachtung des Loop-Seal-Clearings in der Integralanlage PMK-NVH des KFKI Budapest mit Nadelsonden"*, Kernenergie 34 (1991) 1, p. 21-24.

[PRM-921]   H.-M. Prasser, W. Zippe, D. Baldauf, L. Szabados, G. Ezsöl, G., Baranyai, I. Nagy. *"Two-phase flow behaviour during a medium size cold leg LOCA test on PMK-II (SPE-4)"*, Proceedings of the Annual Meeting on Nuclear Technology, 17.-19. Mai 1994 in Stuttgart, p. 77-80, ISSN 0720-9207.

[PRM-922]   H.-M. Prasser, L. Küppers, R. May. *"Conductivity probes for two-phase flow pattern determination during emergency cooling (ECC) injection Experiments at the COCO facility (PHDR)"*, Proceedings of the 1. OECD (NEA) CSNI - Specialist Meeting on Instrumentation to Manage

Severe Accidents, Cologne, Germany, July 1992, NEA/CSNI,R(92)11, p. 273-289.

[PRM-951]   H.-M. Prasser, H. Ringel. *"Gasgehaltsprofile in einer Blasenströmung bei erzwungener Konvektion"*, GVC-Fachausschuß "Mehrphasenströmungen", Magdeburg, 16.-17.2.1995.

[PRM-952]   H.-M. Prasser, H. Steinkamp, U. Rohde. *"Aufwallen und Austragen von zweiphasigen Gemischen"*, Proceedings of the DECHEMA-Jahrestagung 1995, 30.5.-1.6.1995 in Wiesbaden.

[PRM-953]   H.-M. Prasser, C. Schlenkrich. *"Void fraction measurements in transient bubble columns by needle-shaped conductivity probes"*, Proceedings 33rd European Two phase flow group meeting, 30.5-2.6.1995, 's Hertogenbosch, The Netherlands, Presentation F-2.

[PRM-96]   H.-M. Prasser, H. Steinkamp, G. Wehmeier. *"Dampfgehaltsmessungen bei der Druckentlastung von Ethanol"*, Vortrag auf 42. Sitzung des DECHEMA/GVC-Arbeitsausschusses "Sicherheitsgerechtes Auslehen von Chemieapparaten", 15.-15.10.1996 in Rossendorf.

[PRM-97]   H.-M. Prasser, A. Böttger, A. Schaffrath. *"Messungen zu Strömungsformen und Kondensationsvorgängen im Notkondensator-Versuchsstand"*, Mai 1997, Report Forschungszentrum Rossendorf e.V.

[PRP-95]   A. P. Proshutinsky, M. P. Gashenko, I. A. Lipatov, E.V. Stolyarov, B. I. Nigmatulin, V. A. Gashenko, I. V. Elkin, H.-M. Prasser, W. Zippe. *"Experimental investigations of accidental thermalhydraulic processes caused by circuit depressurization at the ISB-VVER integral test facility"*, Proceedings of Symposium on Two-Phase Flow Modelling and Experimentation, Rome 1995, Volume 1, p. 537-544.

[REN-96]   N. Reinecke, M. Boddem, G. Petritsch, D. Mewes. *"Tomographisches Messen der relativen Phasenanteile in zweiphasigen Strömungen fluider Phasen"*, Chem. Ing. Tech. 68 (1996) 11, p. 1404-1412.

[SCA-961]   A. Schaffrath, H. Jaegers. *"Allgemeine Beschreibung des NOKO-Versuchsstandes"*, Report Forschungszentrum Jülich, No. 3167, ISSN 0944-2952, Januar 1996.

[SCA-962]   A. Schaffrath. *"Experimentelle und analytische Untersuchungen zur Wirksamkeit des Notkondensators des SWR600/1000"*, Report Forschungszentrum Jülich, No. 3326, ISSN 0944 – 2952, December 1996.

[SCA-971]   A. Schaffrath. *"KONWAR - eine Erweiterung von ATHLET zur Berechnung der Kondensation in waagerechten Rohren"*, Report Forschungszentrum Jülich, No. 3343, Januar 1997.

[STK-80]    K. Stephan, M. Abdelsalam. "Heat transfer correlations for natural convection boiling", Int. J. Heat Mass Transfer 23 (12980), p. 73-87.

[TEV-88]    V. Teschendorf, J. Miro, G. Lerchl. *"ATHLET ein fortschrittlicher Systemcode zur Analyse thermohydraulischer Prozesse"*, 12. GRS-Fachgespräch "Forschung zur Erhöhung der Reaktorsicherheit", Köln, 3.-4. November 1988.

[TAT-82]    T. N. Tandon, H. K. Varma, C. P. Gupta. *"A new flow regimes map for condensation inside horizontal tubes"*, Journal of Heat Transfer 104 (1982), p. 763 – 768.

[WEP-94]    P. Weber, S. Kusch, H.-M. Prasser. *"Analysis of two-phase flow phenomena with conductivity probes in integral reactor safety experiments"*, Proceedings European Two-Phase Flow Group Meeting, Piacenza, Italy, 6.-8. June, 1994, Paper I1.

[ZIL-93]    L. Zipser. *"Akustische Gassensoren für die Prozeßmeßtechnik"*, Berichte und Informationen aus Forschung, Lehre und Praxis, Hochschule für Technik und Wirtschaft, Dresden (FH), 1 (1993), p. 148-152, ISSN 0942-8240.

# Appendix A: Evaluation of EU NOKO experiments

Test Series EU01

Test Series EU02

Test Series EU03

Test Series EU04

Test Series EU05

Test Series EU06

The measured data of the NOKO experiments are stored on the DEC workstation cluster of the Institute or Safety Research and Reactor Technology (ISR) of the Forschungszentrum Jülich GmbH. By access the data can be transferred via Internet. In the following tables the values averaged over the measured time period are given. The abbreviations have the following meanings:

| | |
|---|---|
| Nr. | experiment in the actual test series |
| P2_1 | pressure in pressure vessel in MPa |
| MNOKO | mass flow in emergency condenser system in kg/s |
| MRDB | steam mass flow (measured in steam line) in kg/s |
| TNOAB | temperature in outlet line in °C |
| DHNOKO | enthalpy difference between in- and outlet line |
| LNOKO1 | capacity determined by the first energy balance in kW |
| LNOKO1,K | capacity due to condensation in kW |
| LNOKO1,U | capacity due to subcooling in kW |
| LNOKO1,K/LNOKO1 | capacity due to condensation normalized to the total capacity |
| UMAX LNOKO1 absolut | maximum of the uncertainty of LNOKO1 in kW |
| UMAX LNOKO1 proz. | percentage maximum of the uncertainty of LNOKO1 |
| U-Anteil MNOKO | percentage maximum of the uncertainty of LNOKO1 due the uncertainty of MNOKO |
| U-Anteil DHNOKO | percentage maximum of the uncertainty of LNOKO1 due |

to the uncertainty of DHNOKO

UWAHR LNOKO1 abs.    possible total uncertainty of LNOKO1 in kW

UWAHR LNOKO1 proz.   percentage possible total uncertainty of LNOKO1


P3_1                 pressure in condenser in MPa

T3MMG                averaged temperature in condenser (smoothed) in °C

MWASSER              water inventory in condenser in kg

HKON                 water level in condenser in m

MND                  blow off mass flow of condenser in kJ/kg

DHND                 enthalpy difference between the blow off mass flow and
                     the water in the condenser in kg/s (only determined for the
                     blow off phase - compare Chap. 4)

LWVER,2              heat losses of the condenser


LNOKO2              capacity determined by the second energy balance in kW

UMAX LNOKO2 absolut  maximum of the uncertainty of LNOKO2 in kW

UMAX LNOKO2 proz.   percentage maximum of LNOKO2

U-Anteil MND         percentage maximum of the uncertainty of LNOKO2 due
                     to the uncertainty of MND (only determined for the blow off
                     phase)

U-Anteil DHND        percentage maximum of uncertainty of LNOKO2 due to
                     the uncertainty of DHND (only determined for the blow off
                     phase)

U-Anteil LKON        percentage maximum of the uncertainty of LNOKO2 due

to the uncertainty of LWVER,2 (only mentioned for the blow off phase)

UWAHR LNOKO2 abs.    possible uncertainty of LNOKO2 in kW (only determined for the blow off phase)

UWAHR LNOKO2 proz.    percentage possible uncertainty of LNOKO2 (only determined for the blow off phase)

HDRUCK    water level in pressure vessel in m

RHODRU    averaged density of the water in the pressure vessel in $kg/m^3$

PEL    capacity of the heater in MW

MSPW    feed water mass flow in kg/s

LSPW    capacity of MSPW in kW

MHD    blow off mass flow of the primary system in kg/s

LHD    capacity of MHD in kW

LNOKO3    capacity determined by the third energy balance in kW

UMAX LNOKO3 absolut    maximum of the uncertainty of LNOKO3 in kW

UMAX LNOKO3 proz.    percentage maximum of LNOKO3

UWAHR LNOKO3 abs.    possible uncertainty LNOKO3 in kW

UWAHR LNOKO3 proz.    percentage maximum of LNOKO3

U-Anteil EK    percentage maximum of the uncertainty of LNOKO3 due

to the uncertainty of PEL

U-Anteil UWP              percentage maximum of the uncertainty of LNOKO3 due
                          to UWP

U-Anteil WPRI             percentage maximum of the uncertainty of LNOKO3 due
                          to the uncertainty of the heat losses of the primary system

U-Anteil MHD              percentage maximum of the uncertainty of LNOKO3 due
                          to MHD

U-Anteil DHHD             percentage maximum of the uncertainty of LNOKO3 due
                          to uncertainty of the enthalpy of the blow off mass flow of
                          the primary system DHHD

U-Anteil MSPW             percentage maximum of the uncertainty of LNOKO3 due
                          to MSPW

U-Anteil HSPW             percentage maximum of the uncertainty of LNOKO3 due
                          to uncertainty of the enthalpy of the feed water mass flow
                          HSPW

# Test Series EU01

First Energy Balance (Measured Values)

| NR. | P2_1 [MPa] | MNOKO [kg/s] | MRDB [kg/s] | TNOAB [Grad C] | DHNOKO [kJ/kg] |
|---|---|---|---|---|---|
| 1 | 1.00 | .06 | .00 | 22.9 | 2680.0 |
| 2 | .95 | .29 | .35 | 82.1 | 2413.2 |
| 3 | .98 | .42 | .36 | 122.7 | 2251.5 |
| 4 | 1.00 | .50 | .49 | 157.6 | 2104.8 |
| 5 | .98 | .49 | .48 | 160.8 | 2091.7 |

First Energy Balance (Evaluation)

| NR. | LNOKO1 [kW] | LNOKO1,K [kW] | LNOKO1,U [kW] | LNOKO1,K/ LNOKO1 [%] |
|---|---|---|---|---|
| 1 | 171.5 | 129.0 | 42.6 | 75.2 |
| 2 | 705.6 | 590.0 | 115.6 | 83.6 |
| 3 | 943.9 | 846.4 | 97.5 | 89.7 |
| 4 | 1060.1 | 1014.9 | 45.2 | 95.7 |
| 5 | 1023.6 | 987.6 | 36.0 | 96.5 |

First Energy Balance (Uncertainty Analysis)

| NR. | LNOKO1 [kW] | UMAX LNOKO1 absolut [kW] | UMAX LNOKO1 prozent [%] | U-Anteil infolge MNOKO [%] | U-Anteil infolge Enthalpie [%] | UWAHR LNOKO1 absolut [kW] | UWAHR LNOKO1 prozent [%] |
|---|---|---|---|---|---|---|---|
| 1 | 171.5 | 172.6 | 97.9 | 97.3 | .6 | 171.6 | 97.3 |
| 2 | 705.6 | 168.9 | 31.0 | 30.3 | .7 | 164.1 | 30.3 |
| 3 | 943.9 | 125.3 | 13.3 | 12.6 | .7 | 118.4 | 12.6 |
| 4 | 1060.1 | 103.4 | 9.9 | 9.0 | .8 | 95.1 | 9.1 |
| 5 | 1023.6 | 102.9 | 10.1 | 9.2 | .8 | 94.7 | 9.3 |

Second Energy Balance (Measured Values)

| NR. | P3_1 [MPa] | T3MMG [Grad C] | MWASSER [kg] | HKON [m] | MND,AB [kg/s] | DHNDAB [kJ/kg] | LWVER,2 [kW] |
|---|---|---|---|---|---|---|---|
| 1 | .10 | 24.6 | 13895. | 1.31 | .00 | .0 | 1.9 |
| 2 | .11 | 34.2 | 13890. | 1.31 | .00 | .0 | 5.7 |
| 3 | .11 | 66.1 | 13854. | 1.33 | .00 | .0 | 18.4 |
| 4 | .11 | 88.0 | 13803. | 1.35 | .00 | .0 | 27.2 |
| 5 | .11 | 100.4 | 13813. | 1.36 | .07 | 1289.6 | 32.2 |

Second Energy Balance (Evaluation and Uncertainty Analysis)

| NR. | LNOKO2 [kW] | UMAX LNOKO2 abs. [kW] | UMAX LNOKO2 proz. [%] | U-Anteil infolge MND [%] | U-Anteil infolge DHV,ND [%] | U-Anteil infolge LKON [%] | UWAHR LNOKO2 abs. [kW] | UWAHR LNOKO2 proz. [%] |
|---|---|---|---|---|---|---|---|---|
| 1 | 2.1 | .0 | .0 | .0 | .0 | .0 | .0 | .0 |
| 2 | 813.2 | .0 | .0 | .0 | .0 | .0 | .0 | .0 |
| 3 | 879.1 | .0 | .0 | .0 | .0 | .0 | .0 | .0 |
| 4 | 1607.9 | .0 | .0 | .0 | .0 | .0 | .0 | .0 |
| 5 | 677.0 | 242.5 | 36.3 | 34.6 | .2 | 1.5 | 231.1 | 34.6 |

Third Energy Balance (Measured Values)

| NR. | HDRUCK [m] | RHODRU [kg/m3] | PEL [MW] | MSPW [kg/s] | LSPW [kW] | MHD [kg/s] | LHD [kW] |
|---|---|---|---|---|---|---|---|
| 1 | 5.94 | 916.9 | .73 | .24 | 30.4 | .27 | 756.1 |
| 2 | 4.79 | 904.6 | .88 | .07 | 9.3 | .08 | 222.8 |
| 3 | 3.66 | 898.5 | 1.15 | .10 | 12.7 | .09 | 255.7 |
| 4 | 2.49 | 896.0 | 1.31 | .09 | 10.8 | .08 | 224.2 |
| 5 | 1.31 | 893.3 | 1.31 | .13 | 16.4 | .10 | 272.2 |

Third Energy Balance (Evaluation and Uncertainty Analysis)

| NR. | LNOKO3 [kW] | UMAX LNOKO3 absolut [kW] | UMAX LNOKO3 prozent [%] | UWAHR LNOKO3 absolut [kW] | UWAHR LNOKO3 prozent [%] |
|---|---|---|---|---|---|
| 1 | 77.2 | 294.8 | 387.9 | 241.5 | 317.8 |
| 2 | 715.7 | 307.6 | 7.5 | 243.0 | 6.7 |
| 3 | 946.5 | 318.2 | 33.7 | 243.6 | 25.8 |
| 4 | 1140.6 | 324.1 | 28.4 | 244.3 | 21.4 |
| 5 | 1073.6 | 311.2 | 29.0 | 242.9 | 22.6 |

Third Energy Balance (Uncertainty Analysis - Continuation)

| NR. | U-Anteil infolge EK [%] | UWP [%] | WPRI [%] | MHD [%] | DHV,HD [%] | MSPW [%] | HSPW [%] |
|---|---|---|---|---|---|---|---|
| 1 | 315.8 | 6.6 | 26.3 | 15.8 | 2.0 | 15.2 | 6.2 |
| 2 | 6.8 | .1 | .6 | -.6 | .0 | .8 | -.3 |
| 3 | 25.4 | .5 | 2.1 | 2.5 | .1 | 2.9 | .2 |
| 4 | 21.0 | .4 | 1.8 | 2.2 | .0 | 2.8 | .1 |
| 5 | 22.4 | .5 | 1.9 | 1.9 | .1 | 2.1 | .2 |

A-7

# Test Series EU02

First Energy Balance (Measured Values)

| NR. | P2_1 [MPa] | MNOKO [kg/s] | MRDB [kg/s] | TNOAB [Grad C] | DHNOKO [kJ/kg] |
|-----|-----|-----|-----|-----|-----|
| 1 | 1.01 | .07 | .00 | 44.7 | 2599.5 |
| 2 | 1.01 | .33 | .31 | 102.4 | 2334.3 |
| 3 | 1.00 | .43 | .48 | 148.5 | 2144.6 |
| 4 | .99 | .52 | .50 | 173.7 | 2033.7 |
| 5 | .99 | .54 | .51 | 175.4 | 2027.4 |

First Energy Balance (Evaluation)

| NR. | LNOKO1 [kW] | LNOKO1,K [kW] | LNOKO1,U [kW] | LNOKO1,K/ LNOKO1 [%] |
|-----|-----|-----|-----|-----|
| 1 | 188.2 | 145.8 | 42.4 | 77.5 |
| 2 | 762.7 | 658.1 | 104.6 | 86.3 |
| 3 | 922.2 | 866.5 | 55.8 | 94.0 |
| 4 | 1049.7 | 1041.1 | 8.5 | 99.2 |
| 5 | 1090.8 | 1085.4 | 5.4 | 99.5 |

First Energy Balance (Uncertainty Analysis)

| NR. | LNOKO1 [kW] | UMAX LNOKO1 absolut [kW] | UMAX LNOKO1 prozent [%] | U-Anteil infolge MNOKO [%] | U-Anteil infolge Enthalpie [%] | UWAHR LNOKO1 absolut [kW] | UWAHR LNOKO1 prozent [%] |
|-----|-----|-----|-----|-----|-----|-----|-----|
| 1 | 188.2 | 189.4 | 100.6 | 100.0 | .6 | 188.2 | 100.0 |
| 2 | 762.7 | 165.8 | 21.7 | 21.0 | .7 | 160.3 | 21.0 |
| 3 | 922.2 | 119.6 | 13.1 | 12.3 | .8 | 112.4 | 12.3 |
| 4 | 1049.7 | 97.2 | 9.3 | 8.4 | .9 | 88.4 | 8.4 |
| 5 | 1090.8 | 94.2 | 8.7 | 7.8 | .9 | 85.0 | 7.9 |

Second Energy Balance (Measured Values)

| NR. | P3_1 [MPa] | T3MMG [Grad C] | MWASSER [kg] | HKON [m] | MND,AB [kg/s] | DHNDAB [kJ/kg] | LWVER,2 [kW] |
|-----|-----|-----|-----|-----|-----|-----|-----|
| 1 | .10 | 68.1 | 14168. | 1.37 | .00 | .0 | 19.3 |
| 2 | .11 | 77.8 | 14136. | 1.38 | .00 | .0 | 23.1 |
| 3 | .11 | 103.0 | 13971. | 1.38 | .28 | 2248.7 | 33.2 |
| 4 | .12 | 104.8 | 13497. | 1.33 | .43 | 2245.4 | 33.9 |
| 5 | .12 | 105.1 | 12974. | 1.27 | .44 | 2244.5 | 34.1 |

Second Energy Balance (Evaluation and Uncertainty Analysis)

| NR. | LNOKO2 [kW] | UMAX LNOKO2 abs. [kW] | UMAX LNOKO2 proz. [%] | U-Anteil infolge MND [%] | U-Anteil infolge DHV,ND [%] | U-Anteil infolge LKON [%] | UWAHR LNOKO2 abs. [kW] | UWAHR LNOKO2 proz. [%] |
|-----|-----|-----|-----|-----|-----|-----|-----|-----|
| 1 | 5.3 | .0 | .0 | .0 | .0 | .0 | .0 | .0 |
| 2 | 672.9 | .0 | .0 | .0 | .0 | .0 | .0 | .0 |
| 3 | 755.2 | 230.8 | 31.2 | 29.4 | .5 | 1.3 | 217.6 | 29.5 |
| 4 | 866.3 | 159.1 | 18.6 | 16.3 | .6 | 1.2 | 144.2 | 16.8 |
| 5 | 910.6 | 154.2 | 17.1 | 15.4 | .6 | 1.1 | 139.1 | 15.4 |

Third Energy Balance (Measured Values)

| NR. | HDRUCK [m] | RHODRU [kg/m3] | PEL [MW] | MSPW [kg/s] | LSPW [kW] | MHD [kg/s] | LHD [kW] |
|-----|--------|--------|------|------|------|------|------|
| 1 | 6.00 | 905.4 | .74 | .24 | 30.5 | .27 | 756.9 |
| 2 | 4.83 | 897.9 | .92 | .05 | 6.3 | .07 | 191.5 |
| 3 | 3.66 | 895.8 | 1.34 | .12 | 15.2 | .09 | 241.1 |
| 4 | 2.52 | 893.4 | 1.33 | .12 | 15.2 | .07 | 202.4 |
| 5 | 1.31 | 890.9 | 1.33 | .14 | 18.2 | .07 | 202.4 |

Third Energy Balance (Evaluation and Uncertainty Analysis)

| NR. | LNOKO3 [kW] | UMAX LNOKO3 absolut [kW] | UMAX LNOKO3 prozent [%] | UWAHR LNOKO3 absolut [kW] | UWAHR LNOKO3 prozent [%] |
|-----|--------|--------|--------|--------|--------|
| 1 | 82.0 | 294.7 | 360.8 | 241.5 | 295.6 |
| 2 | 792.4 | 326.2 | 41.2 | 244.7 | 30.9 |
| 3 | 1135.0 | 313.6 | 27.6 | 243.1 | 21.4 |
| 4 | 1152.7 | 317.5 | 27.5 | 243.5 | 21.1 |
| 5 | 1135.0 | 314.4 | 27.7 | 243.2 | 21.4 |

Third Energy Balance (Uncertainty Analysis - Continuation)

| NR. | U-Anteil infolge EK [%] | UWP [%] | WPRI [%] | MHD [%] | DHV,HD [%] | MSPW [%] | HSPW [%] |
|-----|--------|--------|--------|--------|--------|--------|--------|
| 1 | 293.8 | 6.1 | 24.5 | 14.7 | 1.8 | 14.1 | 5.7 |
| 2 | 30.3 | .6 | 2.5 | 3.5 | .0 | 4.0 | .1 |
| 3 | 21.1 | .4 | 1.8 | 2.0 | .0 | 2.0 | .2 |
| 4 | 20.8 | .4 | 1.7 | 2.3 | .0 | 2.0 | .2 |
| 5 | 21.1 | .4 | 1.8 | 2.4 | .0 | 1.7 | .2 |

# Test Series EU03

First Energy Balance (Measured Values)

| NR. | P2_1 [MPa] | MNOKO [kg/s] | MRDB [kg/s] | TNOAB [Grad C] | DHNOKO [kJ/kg] |
|---|---|---|---|---|---|
| 1 | 3.02 | .32 | .41 | 72.9 | 2470.8 |
| 2 | 3.02 | .69 | .70 | 143.9 | 2183.3 |
| 3 | 3.01 | 1.01 | 1.00 | 188.3 | 1993.5 |
| 4 | 3.01 | 1.17 | 1.17 | 225.2 | 1826.5 |
| 5 | 3.00 | 1.17 | 1.14 | 231.8 | 1798.4 |

First Energy Balance (Evaluation)

| NR. | LNOKO1 [kW] | LNOKO1,K [kW] | LNOKO1,U [kW] | LNOKO1,K/ LNOKO1 [%] |
|---|---|---|---|---|
| 1 | 791.8 | 573.9 | 217.9 | 72.5 |
| 2 | 1505.0 | 1236.3 | 268.7 | 82.1 |
| 3 | 2008.4 | 1807.3 | 201.1 | 90.0 |
| 4 | 2139.5 | 2101.4 | 38.1 | 98.2 |
| 5 | 2100.2 | 2096.3 | 3.9 | 99.8 |

First Energy Balance (Uncertainty Analysis)

| NR. | LNOKO1 [kW] | UMAX LNOKO1 absolut [kW] | UMAX LNOKO1 prozent [%] | U-Anteil infolge MNOKO [%] | U-Anteil infolge Enthalpie [%] | UWAHR LNOKO1 absolut [kW] | UWAHR LNOKO1 prozent [%] |
|---|---|---|---|---|---|---|---|
| 1 | 791.8 | 514.6 | 66.5 | 65.8 | .8 | 508.7 | 65.8 |
| 2 | 1505.0 | 220.9 | 14.7 | 13.8 | .9 | 208.0 | 13.8 |
| 3 | 2008.4 | 152.0 | 7.6 | 6.6 | 1.0 | 133.4 | 6.6 |
| 4 | 2139.5 | 130.3 | 6.1 | 5.0 | 1.1 | 108.3 | 5.1 |
| 5 | 2100.2 | 128.7 | 6.1 | 5.0 | 1.1 | 106.7 | 5.1 |

Second Energy Balance (Measured Data)

| NR. | P3_1 [MPa] | T3MMG [Grad C] | MWASSER [kg] | HKON [m] | MND,AB [kg/s] | DHNDAB [kJ/kg] | LWVER,2 [kW] |
|---|---|---|---|---|---|---|---|
| 1 | .11 | 39.0 | 14483. | 1.38 | .00 | .0 | 7.6 |
| 2 | .11 | 63.2 | 14453. | 1.40 | .00 | .0 | 17.3 |
| 3 | .11 | 101.7 | 14391. | 1.43 | .25 | 1497.1 | 32.7 |
| 4 | .14 | 111.0 | 13745. | 1.37 | .82 | 2231.0 | 36.4 |
| 5 | .15 | 113.4 | 12891. | 1.27 | .95 | 2225.6 | 37.4 |

Second Energy Balance (Evaluation)

| NR. | LNOKO2 [kW] | UMAX LNOKO2 abs. [kW] | UMAX LNOKO2 proz. [%] | U-Anteil infolge MND [%] | U-Anteil infolge DHV,ND [%] | U-Anteil infolge LKON [%] | UWAHR LNOKO2 abs. [kW] | UWAHR LNOKO2 proz. [%] |
|---|---|---|---|---|---|---|---|---|
| 1 | 1092.1 | .0 | .0 | .0 | .0 | .0 | .0 | .0 |
| 2 | 1434.3 | .0 | .0 | .0 | .0 | .0 | .0 | .0 |
| 3 | 1412.9 | 178.0 | 11.4 | 10.5 | .3 | .6 | 163.4 | 10.5 |
| 4 | 1758.1 | 104.9 | 6.0 | 4.8 | .6 | .6 | 85.3 | 4.9 |
| 5 | 1897.1 | 100.1 | 5.3 | 4.2 | .6 | .5 | 79.0 | 4.2 |

Third Energy Balance (Measured Values)

| NR. | HDRUCK [m] | RHODRU [kg/m3] | PEL [MW] | MSPW [kg/s] | LSPW [kW] | MHD [kg/s] | LHD [kW] |
|-----|-----------|----------------|----------|-------------|-----------|------------|----------|
| 1 | 5.98 | 835.1 | 1.40 | .16 | 20.0 | .21 | 570.4 |
| 2 | 4.83 | 834.9 | 1.73 | .05 | 5.9 | .06 | 166.0 |
| 3 | 3.64 | 835.0 | 2.46 | .13 | 16.5 | .17 | 482.5 |
| 4 | 2.47 | 832.5 | 2.44 | .15 | 18.8 | .08 | 226.4 |
| 5 | 1.33 | 825.9 | 2.40 | .18 | 22.7 | .07 | 187.1 |

Third Energy Balance (Evaluation and Uncertainty Analysis)

| NR. | LNOKO3 [kW] | UMAX LNOKO3 absolut [kW] | UMAX LNOKO3 prozent [%] | UWAHR LNOKO3 absolut [kW] | UWAHR LNOKO3 prozent [%] |
|-----|-------------|-------------------------|-------------------------|---------------------------|--------------------------|
| 1 | 909.3 | 304.9 | 33.7 | 242.6 | 26.8 |
| 2 | 1599.7 | 335.8 | 21.0 | 246.3 | 15.4 |
| 3 | 2051.7 | 307.8 | 15.0 | 242.9 | 11.8 |
| 4 | 2184.3 | 315.9 | 14.5 | 243.4 | 11.1 |
| 5 | 2140.0 | 316.4 | 14.8 | 243.3 | 11.4 |

Third Energy Balance (Uncertainty Analysis - Continuation)

| NR. | U-Anteil infolge EK [%] | UWP [%] | WPRI [%] | MHD [%] | DHV,HD [%] | MSPW [%] | HSPW [%] |
|-----|------------------------|---------|----------|---------|------------|----------|----------|
| 1 | 26.5 | .6 | 2.2 | 1.3 | .1 | 2.8 | .3 |
| 2 | 15.0 | .3 | 1.3 | 1.8 | .0 | 2.6 | .0 |
| 3 | 11.7 | .2 | 1.0 | .6 | .0 | 1.4 | .1 |
| 4 | 11.0 | .2 | .9 | 1.0 | .0 | 1.2 | .1 |
| 5 | 11.2 | .2 | .9 | 1.3 | .0 | 1.0 | .1 |

# Test Series EU04

First Energy Balance (Measured Values)

| NR. | P2_1 [MPa] | MNOKO [kg/s] | MRDB [kg/s] | TNOAB [Grad C] | DHNOKO [kJ/kg] |
|-----|------|-------|------|--------|---------|
| 1 | 3.01 | .65 | .64 | 154.0 | 2147.0 |
| 2 | 3.01 | .03 | .00 | 115.6 | 2331.1 |
| 3 | 3.01 | 1.01 | 1.00 | 188.3 | 1993.5 |
| 4 | 3.01 | 1.17 | 1.17 | 225.2 | 1826.5 |
| 5 | 3.00 | 1.17 | 1.14 | 231.8 | 1798.4 |

First Energy Balance (Evaluation)

| NR. | LNOKO1 [kW] | LNOKO1,K [kW] | LNOKO1,U [kW] | LNOKO1,K/ LNOKO1 [%] |
|-----|--------|---------|--------|---------|
| 1 | 1394.3 | 1165.2 | 229.1 | 83.6 |
| 2 | 79.6 | 60.9 | 18.8 | 76.4 |
| 3 | 2008.4 | 1807.3 | 201.1 | 90.0 |
| 4 | 2139.5 | 2101.4 | 38.1 | 98.2 |
| 5 | 2100.2 | 2096.3 | 3.9 | 99.8 |

First Energy Balance (Uncertainty Analysis)

| NR. | LNOKO1 [kW] | UMAX LNOKO1 absolut [kW] | UMAX LNOKO1 prozent [%] | U-Anteil infolge MNOKO [%] | U-Anteil infolge Enthalpie [%] | UWAHR LNOKO1 absolut [kW] | UWAHR LNOKO1 prozent [%] |
|-----|--------|--------|-------|------|------|--------|-------|
| 1 | 1394.3 | 228.6 | 16.5 | 15.6 | .9 | 216.6 | 15.6 |
| 2 | 79.6 | 80.2 | 39.0 | 38.8 | .3 | 79.6 | 38.8 |
| 3 | 2008.4 | 152.0 | 7.6 | 6.6 | 1.0 | 133.4 | 6.6 |
| 4 | 2139.5 | 130.3 | 6.1 | 5.0 | 1.1 | 108.3 | 5.1 |
| 5 | 2100.2 | 128.7 | 6.1 | 5.0 | 1.1 | 106.7 | 5.1 |

Second Energy Balance (Measured Values)

| NR. | P3_1 [MPa] | T3MMG [Grad C] | MWASSER [kg] | HKON [m] | MND,AB [kg/s] | DHNDAB [kJ/kg] | LWVER,2 [kW] |
|-----|------|-------|--------|------|------|--------|------|
| 1 | .12 | 105.1 | 14154. | 1.41 | .46 | 2244.6 | 34.0 |
| 2 | .11 | 101.8 | 13647. | 1.35 | .16 | 2253.2 | 32.7 |
| 3 | .11 | 101.7 | 14391. | 1.43 | .25 | 1497.1 | 32.7 |
| 4 | .14 | 111.0 | 13745. | 1.37 | .82 | 2231.0 | 36.4 |
| 5 | .15 | 113.4 | 12891. | 1.27 | .95 | 2225.6 | 37.4 |

Second Energy Balance (Evaluation)

| NR. | LNOKO2 [kW] | UMAX LNOKO2 abs. [kW] | UMAX LNOKO2 proz. [%] | U-Anteil infolge MND [%] | U-Anteil infolge DHV,ND [%] | U-Anteil infolge LKON [%] | UWAHR LNOKO2 abs. [kW] | UWAHR LNOKO2 proz. [%] |
|-----|--------|-------|------|------|------|------|-------|------|
| 1 | 1290.7 | 154.9 | 12.0 | 10.7 | .4 | .8 | 139.5 | 10.8 |
| 2 | 360.8 | 328.3 | 93.7 | 90.2 | .5 | 2.9 | 316.4 | 90.3 |
| 3 | 1412.9 | 178.0 | 11.4 | 10.5 | .3 | .6 | 163.4 | 10.5 |
| 4 | 1758.1 | 104.9 | 6.0 | 4.8 | .6 | .6 | 85.3 | 4.9 |
| 5 | 1897.1 | 100.1 | 5.3 | 4.2 | .6 | .5 | 79.0 | 4.2 |

Third Energy Balance (Measured Values)

| NR. | HDRUCK [m] | RHODRU [kg/m3] | PEL [MW] | MSPW [kg/s] | LSPW [kW] | MHD [kg/s] | LHD [kW] |
|-----|------------|----------------|----------|-------------|-----------|------------|----------|
| 1 | 4.85 | 831.7 | 2.14 | .23 | 29.6 | .29 | 815.5 |
| 2 | 6.04 | 833.7 | 1.37 | .39 | 49.1 | .37 | 1024.9 |
| 3 | 3.64 | 835.0 | 2.46 | .13 | 16.5 | .17 | 482.5 |
| 4 | 2.47 | 832.5 | 2.44 | .15 | 18.8 | .08 | 226.4 |
| 5 | 1.33 | 825.9 | 2.40 | .18 | 22.7 | .07 | 187.1 |

Third Energy Balance (Evaluation and Uncertainty Analysis)

| NR. | LNOKO3 [kW] | UMAX LNOKO3 absolut [kW] | UMAX LNOKO3 prozent [%] | UWAHR LNOKO3 absolut [kW] | UWAHR LNOKO3 prozent [%] |
|-----|-------------|----------|---------|----------|---------|
| 1 | 1429.4 | 296.7 | 20.8 | 241.7 | 16.9 |
| 2 | 390.3 | 293.4 | 63.0 | 241.4 | 51.8 |
| 3 | 2051.7 | 307.8 | 15.0 | 242.9 | 11.8 |
| 4 | 2184.3 | 315.9 | 14.5 | 243.4 | 11.1 |
| 5 | 2140.0 | 316.4 | 14.8 | 243.3 | 11.4 |

Third Energy Balance (Uncertainty Analysis - Continuation)

| NR. | EK [%] | UWP [%] | WPRI [%] | MHD [%] | DHV,HD [%] | MSPW [%] | HSPW [%] |
|-----|--------|---------|----------|---------|------------|----------|----------|
| 1 | 16.8 | .3 | 1.4 | .7 | .1 | 1.2 | .3 |
| 2 | 51.5 | 1.1 | 4.3 | 2.3 | .2 | 2.3 | 1.3 |
| 3 | 11.7 | .2 | 1.0 | .6 | .0 | 1.4 | .1 |
| 4 | 11.0 | .2 | .9 | 1.0 | .0 | 1.2 | .1 |
| 5 | 11.2 | .2 | .9 | 1.3 | .0 | 1.0 | .1 |

# Test Series EU05

First Energy Balance (Measured Data)

| NR. | P2_1 [MPa] | MNOKO [kg/s] | MRDB [kg/s] | TNOAB [Grad C] | DHNOKO [kJ/kg] |
|-----|------|--------|-------|---------|---------|
| 1 | 7.08 | .00 | .00 | 22.8 | 2641.8 |
| 2 | 7.07 | .78 | .80 | 143.4 | 2147.6 |
| 3 | 7.07 | 1.24 | 1.22 | 192.4 | 1936.9 |
| 4 | 7.07 | 1.60 | 1.60 | 231.0 | 1762.9 |
| 5 | 7.06 | 1.85 | 1.81 | 261.1 | 1620.2 |
| 6 | 7.06 | 2.08 | 2.08 | 280.1 | 1523.8 |

First Energy Balance (Evaluation)

| NR. | LNOKO1 [kW] | LNOKO1,K [kW] | LNOKO1,U [kW] | LNOKO1,K/ LNOKO1 [%] |
|-----|--------|--------|-------|------|
| 1 | .0 | .0 | .0 | .0 |
| 2 | 1679.7 | 1173.5 | 506.2 | 69.9 |
| 3 | 2406.5 | 1864.8 | 541.6 | 77.5 |
| 4 | 2823.3 | 2403.1 | 420.1 | 85.1 |
| 5 | 2996.6 | 2776.6 | 220.0 | 92.7 |
| 6 | 3164.0 | 3117.5 | 46.5 | 98.5 |

First Energy Balance (Uncertainty Analysis)

| NR. | LNOKO1 [kW] | UMAX LNOKO1 absolut [kW] | UMAX LNOKO1 prozent [%] | U-Anteil infolge MNOKO [%] | U-Anteil infolge Enthalpie [%] | UWAHR LNOKO1 absolut [kW] | UWAHR LNOKO1 prozent [%] |
|-----|--------|--------|------|------|------|--------|------|
| 1 | .0 | .0 | .0 | .0 | .0 | .0 | .0 |
| 2 | 1679.7 | 458.4 | 27.3 | 26.1 | 1.2 | 439.0 | 26.2 |
| 3 | 2406.5 | 283.7 | 11.8 | 10.5 | 1.3 | 252.8 | 10.5 |
| 4 | 2823.3 | 224.7 | 8.0 | 6.5 | 1.5 | 185.0 | 6.6 |
| 5 | 2996.6 | 198.7 | 6.6 | 5.0 | 1.6 | 153.6 | 5.1 |
| 6 | 3164.0 | 187.1 | 5.9 | 4.1 | 1.8 | 136.5 | 4.3 |

Second Energy Balance (Measured Data)

| NR. | P3_1 [MPa] | T3MMG [Grad C] | MWASSER [kg] | HKON [m] | MND,AB [kg/s] | DHNDAB [kJ/kg] | LWVER,2 [kW] |
|-----|------|-------|--------|------|------|--------|------|
| 1 | .10 | 22.4 | 14389. | 1.36 | .00 | .0 | .9 |
| 2 | .11 | 44.6 | 14365. | 1.37 | .00 | .0 | 9.8 |
| 3 | .11 | 84.1 | 14299. | 1.40 | .00 | .0 | 25.6 |
| 4 | .14 | 111.0 | 13971. | 1.39 | .82 | 2230.7 | 36.4 |
| 5 | .18 | 119.2 | 12749. | 1.26 | 1.30 | 2210.9 | 39.7 |
| 6 | .17 | 117.0 | 13470. | 1.34 | 1.20 | 2215.5 | 38.8 |

Second Energy Balance (Evaluation and Uncertainty Analysis)

| NR. | LNOKO2 [kW] | UMAX LNOKO2 abs. [kW] | UMAX LNOKO2 proz. [%] | U-Anteil infolge MND [%] | U-Anteil infolge DHV,ND [%] | U-Anteil infolge LKON [%] | UWAHR LNOKO2 abs. [kW] | UWAHR LNOKO2 proz. [%] |
|---|---|---|---|---|---|---|---|---|
| 1 | 32.0 | .0 | .0 | .0 | .0 | .0 | .0 | .0 |
| 2 | 2317.7 | .0 | .0 | .0 | .0 | .0 | .0 | .0 |
| 3 | 2660.2 | .0 | .0 | .0 | .0 | .0 | .0 | .0 |
| 4 | 2168.4 | 108.8 | 5.0 | 4.1 | .4 | .5 | 89.3 | 4.1 |
| 5 | 2683.1 | 97.5 | 3.6 | 2.7 | .6 | .4 | 72.0 | 2.7 |
| 6 | 2804.0 | 97.5 | 3.5 | 2.6 | .5 | .4 | 73.3 | 2.6 |

Third Energy Balance (Measured Values)

| NR. | HDRUCK [m] | RHODRU [kg/m3] | PEL [MW] | MSPW [kg/s] | LSPW [kW] | MHD [kg/s] | LHD [kW] |
|---|---|---|---|---|---|---|---|
| 1 | 7.26 | 761.4 | 1.35 | .42 | 53.0 | .46 | 1255.3 |
| 2 | 5.89 | 761.2 | 2.08 | .11 | 14.3 | .07 | 197.2 |
| 3 | 4.73 | 760.0 | 2.71 | .10 | 12.9 | .10 | 271.5 |
| 4 | 3.58 | 760.0 | 3.06 | .10 | 12.7 | .10 | 290.6 |
| 5 | 2.41 | 763.9 | 3.59 | .23 | 29.0 | .28 | 776.3 |
| 6 | 1.29 | 748.9 | 3.62 | .17 | 20.8 | .23 | 644.8 |

Third Energy Balance (Evaluation and Uncertainty Analysis)

| NR. | LNOKO3 [kW] | UMAX LNOKO3 absolut [kW] | UMAX LNOKO3 prozent [%] | UWAHR LNOKO3 absolut [kW] | UWAHR LNOKO3 prozent [%] |
|---|---|---|---|---|---|
| 1 | 129.8 | .0 | .0 | .0 | .0 |
| 2 | 1790.0 | 331.8 | 18.5 | 245.9 | 13.7 |
| 3 | 2385.9 | 331.1 | 13.9 | 246.3 | 10.3 |
| 4 | 2736.1 | 332.1 | 12.1 | 246.4 | 9.0 |
| 5 | 2846.2 | 300.1 | 10.5 | 242.1 | 8.5 |
| 6 | 3028.5 | 308.2 | 10.2 | 243.0 | 8.0 |

Third Energy Blanace (Uncertainty Analysis - Continuation)

| NR. | U-Anteil infolge EK [%] | UWP [%] | WPRI [%] | MHD [%] | DHV,HD [%] | MSPW [%] | HSPW [%] |
|---|---|---|---|---|---|---|---|
| 1 | .0 | .0 | .0 | .0 | .0 | .0 | .0 |
| 2 | 13.4 | .3 | 1.1 | 1.2 | .0 | 2.4 | .1 |
| 3 | 10.1 | .2 | .8 | .7 | .0 | 2.0 | .1 |
| 4 | 8.8 | .2 | .7 | .6 | .0 | 1.8 | .1 |
| 5 | 8.4 | .2 | .7 | .3 | .0 | .8 | .1 |
| 6 | 7.9 | .2 | .7 | .3 | .0 | 1.0 | .1 |

# Test Series EU06

First Energy Balance (Measured Values)

| NR. | P2_1 [MPa] | MNOKO [kg/s] | MRDB [kg/s] | TNOAB [Grad C] | DHNOKO [kJ/kg] |
|-----|------|-------|-------|--------|--------|
| 1 | 7.07 | .75 | .73 | 157.1 | 2095.2 |
| 2 | 7.07 | 1.19 | 1.13 | 200.2 | 1904.3 |
| 3 | 7.07 | 1.24 | 1.22 | 192.4 | 1936.9 |
| 4 | 7.07 | 1.60 | 1.60 | 231.0 | 1762.9 |
| 5 | 7.06 | 1.85 | 1.81 | 261.1 | 1620.2 |
| 6 | 7.06 | 2.08 | 2.08 | 280.1 | 1523.8 |

First Energy Balance (Evaluation)

| NR. | LNOKO1 [kW] | LNOKO1,K [kW] | LNOKO1,U [kW] | LNOKO1,K/ LNOKO1 [%] |
|-----|--------|--------|-------|------|
| 1 | 1569.9 | 1124.3 | 445.6 | 71.6 |
| 2 | 2275.4 | 1793.5 | 481.9 | 78.8 |
| 3 | 2406.5 | 1864.8 | 541.6 | 77.5 |
| 4 | 2823.3 | 2403.1 | 420.1 | 85.1 |
| 5 | 2996.6 | 2776.6 | 220.0 | 92.7 |
| 6 | 3164.0 | 3117.5 | 46.5 | 98.5 |

First Energy Balance (Uncertainty Analysis)

| NR. | LNOKO1 [kW] | UMAX LNOKO1 absolut [kW] | UMAX LNOKO1 prozent [%] | U-Anteil infolge MNOKO [%] | U-Anteil infolge Enthalpie [%] | UWAHR LNOKO1 absolut [kW] | UWAHR LNOKO1 prozent [%] |
|-----|--------|------|------|------|-----|------|------|
| 1 | 1569.9 | 465.0 | 29.6 | 28.5 | 1.2 | 446.7 | 28.5 |
| 2 | 2275.4 | 286.9 | 12.6 | 11.3 | 1.3 | 257.7 | 11.3 |
| 3 | 2406.5 | 283.7 | 11.8 | 10.5 | 1.3 | 252.8 | 10.5 |
| 4 | 2823.3 | 224.7 | 8.0 | 6.5 | 1.5 | 185.0 | 6.6 |
| 5 | 2996.6 | 198.7 | 6.6 | 5.0 | 1.6 | 153.6 | 5.1 |
| 6 | 3164.0 | 187.1 | 5.9 | 4.1 | 1.8 | 136.5 | 4.3 |

Second Energy Balance (Measured Data)

| NR. | P3_1 [MPa] | T3MMG [Grad C] | MWASSER [kg] | HKON [m] | MND,AB [kg/s] | DHNDAB [kJ/kg] | LWVER,2 [kW] |
|-----|------|-------|--------|------|------|--------|------|
| 1 | .13 | 108.3 | 14695. | 1.47 | .67 | 2238.3 | 35.3 |
| 2 | .15 | 113.5 | 13780. | 1.38 | .96 | 2225.4 | 37.4 |
| 3 | .11 | 84.1 | 14299. | 1.40 | .00 | .0 | 25.6 |
| 4 | .14 | 111.0 | 13971. | 1.39 | .82 | 2230.7 | 36.4 |
| 5 | .18 | 119.2 | 12749. | 1.26 | 1.30 | 2210.9 | 39.7 |
| 6 | .17 | 117.0 | 13470. | 1.34 | 1.20 | 2215.5 | 38.8 |

Second Energy Balance (Evaluation and Uncertainty Analysis)

| NR. | LNOKO2 [kW] | UMAX LNOKO2 abs. [kW] | UMAX LNOKO2 proz. [%] | U-Anteil infolge MND [%] | U-Anteil infolge DHV,ND [%] | LKON [%] | UWAHR LNOKO2 abs. [kW] | UWAHR LNOKO2 proz. [%] |
|---|---|---|---|---|---|---|---|---|
| 1 | 1422.4 | 113.8 | 8.0 | 6.7 | .6 | .7 | 96.0 | 6.8 |
| 2 | 1987.7 | 99.5 | 5.0 | 3.9 | .6 | .5 | 78.2 | 3.9 |
| 3 | 2658.0 | .0 | .0 | .0 | .0 | .0 | .0 | .0 |
| 4 | 2168.8 | 108.8 | 5.0 | 4.1 | .4 | .5 | 89.3 | 4.1 |
| 5 | 2683.2 | 97.5 | 3.6 | 2.7 | .6 | .4 | 72.0 | 2.7 |
| 6 | 2804.7 | 97.5 | 3.5 | 2.6 | .5 | .4 | 73.3 | 2.6 |

Third Energy Balance (Measured Values)

| NR. | HDRUCK [m] | RHODRU [kg/m3] | PEL [MW] | MSPW [kg/s] | LSPW [kW] | MHD [kg/s] | LHD [kW] |
|---|---|---|---|---|---|---|---|
| 1 | 5.44 | 815.9 | 2.09 | .14 | 17.3 | .16 | 433.6 |
| 2 | 4.40 | 809.4 | 2.70 | .13 | 16.5 | .13 | 362.4 |
| 3 | 4.73 | 760.0 | 2.71 | .10 | 12.9 | .10 | 271.5 |
| 4 | 3.58 | 760.0 | 3.06 | .10 | 12.7 | .10 | 290.6 |
| 5 | 2.41 | 763.9 | 3.59 | .23 | 29.0 | .28 | 776.3 |
| 6 | 1.29 | 748.9 | 3.62 | .17 | 20.8 | .23 | 644.8 |

Third Energy Balance (Evaluation and Uncertainty Analysis)

| NR. | LNOKO3 [kW] | UMAX LNOKO3 absolut [kW] | UMAX LNOKO3 prozent [%] | UWAHR LNOKO3 absolut [kW] | UWAHR LNOKO3 prozent [%] |
|---|---|---|---|---|---|
| 1 | 1641.5 | 317.7 | 19.4 | 244.2 | 14.9 |
| 2 | 2294.9 | 318.2 | 13.9 | 244.2 | 10.6 |
| 3 | 2385.9 | 331.1 | 13.9 | 246.3 | 10.3 |
| 4 | 2736.1 | 332.1 | 12.1 | 246.4 | 9.0 |
| 5 | 2846.2 | 300.1 | 10.5 | 242.1 | 8.5 |
| 6 | 3028.5 | 308.2 | 10.2 | 243.0 | 8.0 |

Third Energy Balance (Uncertainty Analysis - Continuation)

| NR. | U-Anteil infolge EK [%] | UWP [%] | WPRI [%] | MHD [%] | DHV,HD [%] | MSPW [%] | HSPW [%] |
|---|---|---|---|---|---|---|---|
| 1 | 14.6 | .3 | 1.2 | .8 | .0 | 2.2 | .1 |
| 2 | 10.5 | .2 | .9 | .6 | .0 | 1.7 | .1 |
| 3 | 10.1 | .2 | .8 | .7 | .0 | 2.0 | .1 |
| 4 | 8.8 | .2 | .7 | .6 | .0 | 1.8 | .1 |
| 5 | 8.4 | .2 | .7 | .3 | .0 | .8 | .1 |
| 6 | 7.9 | .2 | .7 | .3 | .0 | 1.0 | .1 |